



LUND UNIVERSITY

Unifying first-principles and model approaches for strongly correlated materials

Interplay between long- and short-range correlations

Nilsson, Fredrik

2019

Document Version:

Publisher's PDF, also known as Version of record

[Link to publication](#)

Citation for published version (APA):

Nilsson, F. (2019). *Unifying first-principles and model approaches for strongly correlated materials: Interplay between long- and short-range correlations*. [Doctoral Thesis (compilation), Department of Physics]. Lund University.

Total number of authors:

1

General rights

Unless other specific re-use rights are stated the following general rights apply:

Copyright and moral rights for the publications made accessible in the public portal are retained by the authors and/or other copyright owners and it is a condition of accessing publications that users recognise and abide by the legal requirements associated with these rights.

- Users may download and print one copy of any publication from the public portal for the purpose of private study or research.
- You may not further distribute the material or use it for any profit-making activity or commercial gain
- You may freely distribute the URL identifying the publication in the public portal

Read more about Creative commons licenses: <https://creativecommons.org/licenses/>

Take down policy

If you believe that this document breaches copyright please contact us providing details, and we will remove access to the work immediately and investigate your claim.

LUND UNIVERSITY

PO Box 117
221 00 Lund
+46 46-222 00 00



Unifying first-principles and model approaches for strongly correlated materials

Interplay between long- and short-range correlations

FREDRIK NILSSON | DEPARTMENT OF PHYSICS | LUND UNIVERSITY 2019



Unifying first-principles and model approaches for strongly
correlated materials

Unifying first-principles and model approaches for strongly correlated materials

Interplay between long- and short-range correlations

by Fredrik Nilsson



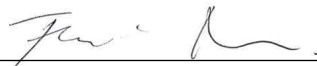
LUND
UNIVERSITY

Thesis for the degree of Doctor of Philosophy
Thesis advisors: Prof. Ferdi Aryasetiawan, Prof. Krister Karlsson
Faculty opponent: Prof. Rex Godby

To be presented, with the permission of the Faculty of Science of Lund University, for public criticism in the Rydberg lecture hall at the Department of Physics on Wednesday, the 30th of January 2019 at 09:00.

Organization LUND UNIVERSITY	Document name DOCTORAL DISSERTATION	
Department of Physics Box 118 SE-221 00 LUND Sweden	Date of issue 2019-01-30	
Author(s) Fredrik Nilsson	Sponsoring organization	
Title and subtitle Unifying first-principles and model approaches for strongly correlated materials: Interplay between long and short ranged correlations		
Abstract <p>In materials with open $3d$ and $4f$ shells the valence electrons are relatively localized around the atoms which leads to large electron-electron correlations. These, so called strongly correlated materials, exhibit many intriguing properties such as high T_c superconductivity, colossal magneto-resistance and heavy fermion behaviour. The strong electron-electron correlations make these materials extremely difficult to describe theoretically since mean-field and perturbative treatments break down. In so called Local Density Approximation+Dynamical Mean-Field Theory (LDA+DMFT) the strong local correlations are treated to all orders but the nonlocal correlations are omitted. In this thesis we use and develop methods that can treat both the long-range and strong local correlations from first principles. We show that a proper treatment of the long-range correlations is essential to get a correct description of the satellite features in the spectral function for a number of transition metal compounds. We also investigate and analyze trends in the effective Coulomb interaction for lanthanide and cuprate compounds. The first part of the thesis provides an introduction to the theory as well as a discussion of the most important results and conclusions and the second part consists of the papers. In Paper I and VI we compute and analyse the effective Coulomb interaction for a number of lanthanides and cuprates using the constrained random-phase approximation (cRPA). In Paper II we compute the spectral function of La_2CuO_4, the parent compound of the cuprate high T_c superconductor, using LDA+DMFT with a dynamical effective Coulomb interaction calculated with the cRPA. In Paper III-IV we develop a multitier combination of GW and DMFT and apply it to the cubic perovskites SrVO_3 and SrMoO_3 as well as stretched sodium and Paper V is a review of first-principle methods for computing the electronic structure of correlated materials.</p>		
Key words first-principle methods, strongly correlated materials, GW approximation, cRPA, random-phase approximation, dynamical mean-field theory, GW+DMFT, downfolding		
Classification system and/or index terms (if any)		
Supplementary bibliographical information		Language English
ISSN and key title		ISBN 978-91-7753-918-6 (print) 978-91-7753-919-3 (pdf)
Recipient's notes	Number of pages 236	Price
	Security classification	

I, the undersigned, being the copyright owner of the abstract of the above-mentioned dissertation, hereby grant to all reference sources permission to publish and disseminate the abstract of the above-mentioned dissertation.

Signature  Date 20181217

Unifying first-principles and model approaches for strongly correlated materials

Interplay between long- and short-range
correlations

by Fredrik Nilsson



LUND
UNIVERSITY

A doctoral thesis at a university in Sweden takes either the form of a single, cohesive research study (monograph) or a summary of research papers (compilation thesis), which the doctoral student has written alone or together with one or several other author(s).

In the latter case the thesis consists of two parts. An introductory text puts the research work into context and summarizes the main points of the papers. Then, the research publications themselves are reproduced, together with a description of the individual contributions of the authors. The research papers may either have been already published or are manuscripts at various stages (in press, submitted, or in draft).

Cover illustration: ©Julia Stenberg, <https://juliastenberg.com/>

Funding information: The thesis work was financially supported by The Swedish Research Council (VR).

© Fredrik Nilsson 2019

Paper I © 2013 by the American Physical Society

Paper II © 2015 by the American Physical Society

Paper III © 2016 by the American Physical Society

Paper IV © 2017 by the American Physical Society

Paper V Published by MDPI under Open Access License 2018

Paper VI © 2018 by the authors

Faculty of Science, Department of Physics

ISBN: 978-91-7753-918-6 (print)

ISBN: 978-91-7753-919-3 (pdf)

Printed in Sweden by Media-Tryck, Lund University, Lund 2019



*To my children
Tore, Mio, Knut and Holger*

Contents

Acknowledgements	iii
Populärvetenskaplig sammanfattning	v
List of publications and author's contributions	viii
I Theoretical Background and Main Results	I
1 Introduction	3
1 Units	8
2 Role of first-principle calculations	8
3 Density functional theory	9
4 Probing the electronic structure: Photoemission, inverse photoemission and relation to the Green's function	13
5 The self-energy and the Dyson equation	16
6 Finite temperature formalism	17
2 The GW approximation	21
1 Conventions	21
2 The Hedin equations	22
3 Implementations	27
4 Matrix representation	28
5 The screened interaction and the self-energy	29
3 The constrained Random-Phase Approximation (cRPA)	33
1 Defining a low-energy model	33
2 Keeping only the onsite interaction: The Hubbard model	35
3 Effective Coulomb interaction	37
4 cRPA for entangled bands	38
5 Results from Paper I: cRPA for the early lanthanides	40
6 Results from Paper VI: cRPA for the cuprates	43
4 Dynamical Mean-Field Theory	47

1	Self-consistent Anderson impurity model	47
2	Hubbard bands: The physics of local correlations	51
3	Hubbard bands versus plasmons	55
4	Results from Paper II: LDA+DMFT for La_2CuO_4	56
5	GW+EDMFT	61
1	Basic theory	61
2	The multitier approach	67
3	Implementation	69
4	Real Materials: A discussion of Paper III-V	70
5	Comparison with related methods	77
6	Summary and Outlook	85
1	References	89
II	The Papers	109
	Paper I: <i>Ab initio</i> calculations of the Hubbard U for the early lan- thanides using the constrained random-phase approximation . . .	111
	Paper II: Dynamical screening in La_2CuO_4	127
	Paper III: When strong correlations become weak: Consistent merging of <i>GW</i> and DMFT	139
	Paper IV: Multitier Self-Consistent <i>GW</i> + EDMFT	147
	Paper V: Recent Progress in First-Principles Methods for Computing the Electronic Structure of Correlated Materials	169
	Paper VI: Dynamically screened Coulomb interaction in the parent compounds of hole-doped cuprates, trends and exceptions . . .	205

Acknowledgements

I owe my deepest gratitude to my supervisor, Ferdi Aryasetiawan. Thank you for guiding me through my PhD-studies and for all inspiring discussions. You have taught me so much, both about physics and how to conduct research. Your view on physics and research in general will always remain an inspiration to me.

I would also like to thank the past and present members of our group, especially Rei Sakuma for introducing me to the codes in the beginning of my PhD and Tor Sjöstrand for all our heated discussions. A special thanks also goes to my co-supervisor Krister Karlsson. Thank you for inspiring discussions, good collaborations and also your careful feedback on this thesis.

I would like to thank Philipp Werner and his group for taking such good care of me during my visits in Fribourg and for a fruitful collaboration. I would especially like to thank Lewin Boehnke, my close collaborator for paper III-IV. I would also like to thank Ole Krogh Andersen for his visits to Lund and for the insightful discussions and comments related to Paper VI. It was a pleasure to visit Alexander Lichtenstein's group in Hamburg and I learned a lot from our discussions. Finally I would like to thank Christoph Friedrich for providing us with his FLAPW-code SPEX and for taking time to discuss and help out with various problems.

The division of Mathematical Physics has been an inspiring place to do my PhD especially due to all the great people working here, thank you all. A special thanks goes to Katarina. Thank you for always taking time to guide me through the administrative jungle and for all fun discussions in the lunch room, this division would not be the same without you.

The open and friendly climate at the teaching department at the natural science faculty (UDIF) during my bachelor and master studies really spurred my interest in physics. Thank you Tomas, Carl-Erik and Per-Olof for the great education and open atmosphere.

A special thanks goes to my close friends Jon, Johannes, David, Sanna and Martin who have followed me throughout my education. Physics would not be half as fun without you. I would also like to thank Linus that I lived, climbed and traveled with during my years as a student. The awesome cover illustration was made by

Julia Stenberg, thank you for that. Finally, I would like to thank my parents Ulla and Claes and my sister Marika for their support and encouragement throughout my life.

Last but absolutely not least I would like to thank Marta. Thank you for supporting me but also helping me to figure out and prioritize the important things in life. Thank you for all the love and energy you give me and our children and for being such an extraordinary and inspiring person. I am so happy to share my life with you.

Populärvetenskaplig sammanfattning

Fysik handlar om att försöka förstå hur världen omkring oss fungerar utifrån vissa grundläggande principer. Fasta tillståndets fysik fokuserar på de fasta material vi har omkring oss. Dessa material har olika strukturer beroende på vilka grundämnen de är uppbyggda av och hur de har bildats. Om en gas av atomer kyls ner långsamt tenderar atomerna att ordna sig i specifika regelbundna mönster, så kallade kristaller. Kristallstrukturen påverkar till stor del materialets egenskaper. De stora skillnaderna mellan grafit och diamant, som båda är uppbyggda av kolatomer men har väldigt olika egenskaper, utgör ett tydligt exempel på detta. I diamant är kolatomerna hårt bundna och varje kolatom delar en negativt laddad elektron med fyra andra kolatomer, vilket gör diamanter väldigt hållbara och hårda. Kristallstrukturen påverkar även vilka energitillstånd elektronerna kan befinna sig i och därmed materialens optiska egenskaper. I diamant kostar det mycket energi för att excitera elektronerna till tillstånd med högre energi, vilket gör att materialet inte absorberar synligt ljus och därför har de blänkande egenskaper som vi normalt associerar med diamanter. Grafit består av löst sammanhållna lager av kolatomer. På grund av den annorlunda strukturen kan grafit absorbera ljus i hela det synliga spektrumet vilket gör att materialet uppfattas som svart. Den svarta färgen, eller mer korrekt avsaknaden av färg, samt det faktum att de löst sammansatta lagrerna lätt faller sönder, gör att grafit är ett bra material att tillverka blyertspennor av men knappast kan användas till sågklingor och smyckestillverkning som diamanter.

För att beskriva elektronernas tillstånd kan man inte använda den klassiska mekaniken som vi är vana vid att beskriva den makroskopiska världen med. Istället måste man använda en teori som kallas kvantmekanik. Den kvantmekaniska världen skiljer sig mycket från vår alldagliga värld. Ett klassiskt exempel på en ointuitiv kvantmekanisk effekt är att det är omöjligt att veta både hastigheten och positionen för en elektron samtidigt. När man mäter elektronens position blir dess hastighet helt obestämd. Med detta menas att en senare mätning av elektronens hastighet kan ge vilket värde som helt, det är helt enkelt på ett fundamentalt plan omöjligt att förutse resultatet av hastighetsmätningen. Om man sedan faktiskt mäter hastigheten för samma elektron så får elektronen en välbestämd hastighet, men till priset av att elektronens position blir helt obestämd. Det vi uppfattar i den makroskopiska världen är medelpositionen och medelhastigheten hos en väldigt stor mängd kvantmekaniska partiklar. Dessa makroskopiska objekt rör sig då enligt den klassiska mekaniken även om de partiklar som bygger upp dem beskrivs

kvantmekaniskt.

Kvantmekaniska system beskrivs med den så kallade Schrödingerekvationen. Denna ekvation kan lösas exakt för få antal partiklar men antalet elektroner i fasta ämnen är väldigt många, storleksordningen 10^{23} stycken per cm^3 och därför behöver man använda olika approximationer för att beskriva dessa system. Vilka approximationer som är relevanta beror på hur stark växelverkan mellan elektronerna i materialet är.

I denna avhandling används och utvecklas metoder för att beskriva så kallade starkt korrelerade material. Ett material sägs vara starkt korrelerat om elektronernas växelverkan med varandra är så pass stark att varje elektrons tillstånd specifikt beror på vilka tillstånd de övriga elektronerna befinner sig i. Den starka växelverkan mellan elektronerna ger upphov till en uppsjö av intressanta egenskaper, till exempel så tillhör de kopparbaserade hög-temperatur supraledarna denna kategori av material, men den starka växelverkan gör också att de approximationer som används för att beskriva andra, mindre starkt korrelerade material, inte fungerar. Därför förlitar man sig ofta på förenklade modeller som är tänkta att fånga de viktigaste aspekterna av de verkliga systemen. Modellerna har ofta input-parametrar som man gissar för att få resultat som överensstämmer med experimenten eller uppskattar teoretiskt med olika metoder. Ett alternativt tillvägagångssätt är att försöka beskriva materialen från grundläggande fysikaliska principer, med så kallade *ab initio*-metoder. I en *ab initio*-beräkning anger man enbart vilka atomer som bygger upp materialet och hur dessa är arrangerade och sedan löser man ekvationerna som beskriver systemet numeriskt, det vill säga med hjälp av datorer och avancerade datorprogram, genom att göra olika approximationer. Modellberäkningar har ofta enklare reducerade ekvationer vilket gör att man behöver färre approximationer för att lösa dem medan *ab initio*-metoder har mer kompletta ekvationer men då behövs grövre approximationer för att lösa dem. De approximationer som behöver göras i *ab initio*-metoder är i många fall för grova för att kunna ge korrekta beskrivningar av starkt korrelerade material. Å andra sidan är materialen som vi vill beskriva väldigt komplexa så det finns en risk att man missar viktiga delar av fysiken när man reducerar beräkningarna till enklare modeller. Då modellerna beror på vilka parametrar man har som input och vilka aspekter av systemet man väljer att fokusera på har även modellberäkningar en begränsad kapacitet att förutspå nya material och materialegenskaper. Målet med denna avhandling är att förena *ab initio*-metoder med modellberäkningar för att kunna dra nytta av styrkan hos båda metoderna.

Man kan tänka sig kristallen som en periodisk uppsättning av positioner i ett tredimensionellt gitter som elektronerna kan hoppa mellan. Interaktionen och korrelationen mellan elektroner på samma position är större än interaktionen och korrelationen mellan elektroner på olika positioner i gittret i och med att den elektriska repulsionen mellan två negativt laddade elektroner är större om de är nära varandra. I modellberäkningar av starkt korrelerade material reducerar man antalet tillstånd och elektroner i modellen till ett minimum och bortser oftast från interaktioner och korrelationer mellan elektroner som befinner sig på olika positioner i gittret. De elektroner och excitationer som inte tas med explicit i modellen kan inkluderas implicit genom att ta hänsyn till att de skärmar, och därmed reducerar, interaktionerna mellan elektronerna i modellen. I artikel I och VI beräknar vi de effektiva interaktionerna mellan elektronerna med *ab initio* metoder som tar hänsyn till skärmingen som inte är inkluderad i modellerna för ett antal olika lanthanider och kuprater. Dessa interaktioner kan sedan användas i modellberäkningar av materialen. I artikel II-IV går vi ett steg längre och utvecklar en metod för att systematiskt reducera den kompletta beskrivningen av materialet till en väldefinierad modell utan odefinierade input-parametrar. Våra beräkningar tar även hänsyn till korrelationer och interaktioner mellan elektroner på olika positioner i gittret. Vi visar att det för många material är viktigt att ta hänsyn till dessa icke-lokala korrelationer för att kunna beskriva elektronernas tillstånd och möjliga excitationer.

List of publications and author's contributions

This thesis is based on the following publications, referred to by their Roman numerals:

I *Ab initio* calculations of the Hubbard U for the early lanthanides using the constrained random-phase approximation

F. Nilsson, R. Sakuma, and F. Aryasetiawan
Physical Review B **88**, 125123 (2013)

Lanthanide materials exhibit many intriguing properties such as magnetism, heavy fermion behaviour and superconductivity with a wide range of industrial applications. In this paper we compute the effective Coulomb interaction U for the early lanthanides (Ce - Gd) using the constrained random-phase approximation. Our result compares well with experimental estimations and can be used as *ab-initio* input for model calculations using e.g. LDA+DMFT for the early lanthanides and related compounds. We also analyse the frequency dependence of U and identified the origin of the different subplasmonic modes.

Contributions: I performed all calculations, produced all figures and wrote the first draft of the article.

II Dynamical screening in La_2CuO_4

P. Werner, R. Sakuma, F. Nilsson, and F. Aryasetiawan
Physical Review B **91**, 125142 (2015)

In this paper we investigate the spectral function of La_2CuO_4 , the parent compound of the prototypical cuprate high T_c superconductor. The parent compounds of the cuprate superconductors are Mott-insulators due to the strong onsite Coulomb repulsion U . In this paper we compute and analyse the spectral function using LDA+DMFT, with a dynamically screened Coulomb interaction $U(\omega)$ derived from the LDA bandstructure, using the cRPA. We consider both the commonly used one and three band models. We show that the frequency dependence is essential to open up a gap in the spectral function in both models although the gap is too small in the one-band model. We also show that the feature below the Oxygen p states

in the PES spectra, commonly identified as the lower Hubbard band, in fact is a plasmon satellite due to the strong p - d screening mode in $U(\omega)$. The Hubbard band is located in the same energy range as the p -states.

Contributions: I performed a large part of the cRPA-calculations, took an active part in discussing the setup of the full calculations, including the form of the Hartree shift in the three-band calculations, as well as analysing and interpreting the results. I also wrote section IIA of the first draft.

III When strong correlations become weak: Consistent merging of GW and DMFT

L. Boehnke, F. Nilsson, F. Aryasetiawan, and P. Werner
Physical Review **B** 94, 201106(R) (2016)

In this paper we present the first fully self-consistent GW +EDMFT calculations for real materials using a newly developed multitier implementation. We apply the scheme to the cubic perovskite SrVO_3 and show that the nonlocal screening included in the method yields a new interpretation of the satellite features as plasmons rather than Hubbard bands.

This paper was published as **Rapid Communications** and selected as *Editor's Suggestion*.

Contributions: I wrote all code handling \mathbf{k} -dependent quantities in the self-consistency cycle, this includes a costume finite-temperature self-consistent GW -code that was interfaced with the ALPS impurity solver by L. B. within the TRIQS framework. Together with L. B. I was a driving force in the multitier formulation of GW +EDMFT. I performed all cRPA and G^0W^0 calculations and took an active part in discussing the setup of the full calculations. I also took an active part in analysing the results and wrote a small part of the first draft. I am joint first author with L. B.

IV Multitier Self-Consistent GW + EDMFT

F. Nilsson, L. Boehnke, P. Werner and F. Aryasetiawan
Phys. Rev. Materials **1** (4), 043803 (2017)

In this paper we present the details of the multitier GW +EDMFT implementation developed in Paper III and apply it to new materials, the cubic perovskite SrMoO_3 and stretched sodium. We show that, contrary to LDA+DMFT that cannot describe the satellite structures of SrMoO_3 , GW +EDMFT provides a coherent description of the two cubic perovskites SrVO_3 and SrMoO_3 as moderately correlated materials with plasmonic satellites. For stretched sodium we show that the nonlocal screening included in our approach is essential to capture the physically expected trend in the effective impurity interaction and that the GW +EDMFT approach correctly describes a Mott transition for a large stretching. We also investigate the causality properties of the effective impurity interaction and analyse the effect of a local approximation to the polarization and self-energy, using the electron gas as an example. From a method perspective it has been known that self-consistent GW alone yields a poor spectra. In this paper we show that the local vertex corrections from EDMFT in GW +EDMFT improves the results substantially in the moderately to strongly correlated regime but are not sufficient in the very weakly correlated regime.

This paper was selected as *Editor's Suggestion* and *Featured in Physics* with a synopsis written by Matteo Rini at <https://physics.aps.org/synopsis-for/10.1103/PhysRevMaterials.1.043803>.

Contributions: In this paper we use the code that was developed by me and L.B for Paper III. I performed all calculations in section IIB and all cRPA and G^0W^0 calculations for the remaining materials. I wrote the first draft for Sections I, IIA, IIC-D, IIIA, IIIC and IV. I am joint first author with L. B.

v **Recent Progress in First-Principles Methods for Computing the Electronic Structure of Correlated Materials**

F. Nilsson and F. Aryasetiawan

Computation 6 (1), 26 (2018)

This paper is a review of modern *ab-initio* electronic structure methods starting from Density Functional Theory and ending with $GW+EDMFT$. We also provide a comparison of different recent implementations of $GW+EDMFT$, with different levels of self-consistency, using $SrVO_3$ as an example. This article belongs to the Special Issue In Memory of Walter Kohn—Advances in Density Functional Theory.

Contributions: I produced all new figures and wrote the first draft for section 3.3-3.5.

vi **Dynamically screened Coulomb interaction in the parent compounds of hole-doped cuprates, trends and exceptions**

F. Nilsson, K. Karlsson and F. Aryasetiawan

Draft

In this paper we compute the effective Coulomb interaction (Hubbard U), in the one-band model for the parent compounds of a number of hole-doped cuprates, using the constrained random-phase approximation. We show that, apart from La_2CuO_4 , both U and U/t , where t is the nearest neighbour hopping, follow increasing trends with $T_{c\max}$. These results suggest that superconductivity in the cuprates may be favoured by a large on-site Coulomb repulsion. However, the fact that La_2CuO_4 does not follow the trend implies that a large U cannot be the only important parameter to achieve high T_c superconductivity in the cuprates. We also investigate the frequency dependence of U and analyse the contribution from the different screening channels to the trend.

Contributions: I performed half of the calculations, wrote the first draft and produced all figures.

All papers are reproduced with permission of their respective publishers.

Publications not included in this thesis

Electronic structure of strongly correlated materials: from one-particle to many-body theory

F. Nilsson and F. Aryasetiawan

Materials Research Express 4, 034001 (2017)

Part I

Theoretical Background and Main Results

1

Introduction

Quantitative theoretical descriptions of strongly correlated materials remain one of the great challenges of modern condensed matter theory. Materials that exhibit strong electron-electron correlations include high- T_c superconductors, materials with colossal magneto-resistance, spintronic materials and heavy fermion materials. Common to these materials is that the valence electrons originate from partially filled $3d$ or $4f$ shells and are relatively localized around the atomic sites. This leads to strong electron-electron correlation effects due to the strong Coulomb repulsion between electrons on the same site. The strong local correlations make these materials notoriously difficult to describe theoretically, since mean-field or perturbative treatments break down. One general recipe is to focus on the important degrees of freedom and solve the problem in a small subspace more accurately. This is the idea behind the Hubbard model [77], that describes a lattice with nearest-neighbour hopping and onsite interaction only. However, in order to be predictive we do not only need to solve the simplified models (which in itself is highly nontrivial), but also make sure that these models are close to reality. This involves a systematic downfolding of the full many-body Hamiltonian onto a low-energy problem and making sure that the approximations done when solving the low-energy problem do not throw away any important physical processes. This thesis both investigates the downfolding procedure and also different ways to solve the low-energy problem.

However, before describing our theoretical approach I will begin with a short discussion of what is meant by "strongly correlated", which materials that typically exhibit strong correlation effects and why these materials are interesting.

A quantum mechanical system is described by the Hamiltonian H through the

Schrödinger equation:

$$i\hbar \frac{\partial}{\partial t} |\Psi(t)\rangle = H |\Psi(t)\rangle. \quad (1.1)$$

The complete Hamiltonian for the solid is (in atomic units with \hbar , the electron mass and electron charge set to 1) given by

$$H = \underbrace{-\sum_{\alpha} \frac{\nabla_{\alpha}^2}{2m_{\alpha}} + \frac{1}{2} \sum_{\alpha \neq \beta} \frac{Z_{\alpha} Z_{\beta}}{|\mathbf{R}_{\alpha} - \mathbf{R}_{\beta}|}}_{\text{nucleon}} \underbrace{-\sum_i \frac{\nabla_i^2}{2} + \frac{1}{2} \sum_{i \neq j} \frac{1}{|\mathbf{r}_i - \mathbf{r}_j|}}_{\text{electron}} - \underbrace{\sum_{\alpha, i} \frac{Z_{\alpha}}{|\mathbf{R}_{\alpha} - \mathbf{r}_i|}}_{\text{electron-nucleon}} + H_{\text{Rel}}, \quad (1.2)$$

where H_{Rel} includes all relativistic effects. In this thesis I will not consider relativistic effects and will therefore put $H_{\text{Rel}} = 0$. Further on, I will neglect lattice vibrations and hence the nucleon part of the Hamiltonian vanishes and the electron-nucleon part reduces to an external periodic potential for the electrons, henceforth referred to as the crystal potential V_{crys} . With these approximations the Hamiltonian (1.2) reduces to

$$H = \sum_i \left(-\frac{\nabla_i^2}{2} + V_{\text{crys}}(\mathbf{r}_i) \right) + \frac{1}{2} \sum_{i \neq j} \frac{1}{|\mathbf{r}_i - \mathbf{r}_j|}. \quad (1.3)$$

An exact solution for the eigenvalues and eigenvectors of the Hamiltonian in Eq. 1.3 would, apart from relativistic effects and lattice vibrations, yield an exact description of the stationary states in the solid. However, since the solid contains the order of 10^{23} electrons the electron-electron interaction (last term in Eq. 1.3) makes this an infeasible task. For practical calculations we therefore need to resort to different approximations. Which approximations that are suitable are determined by the strength of the electron-electron interaction in the solid which to a large extent is determined by the valence electrons of the atoms constituting the solid.

To understand what we mean by "strongly correlated" it is instructive to consider the dimer model depicted in Fig. 1.1. In this model we have two sites with one single-particle energy level on each site corresponding to the states $|1\rangle$ and $|2\rangle$. The

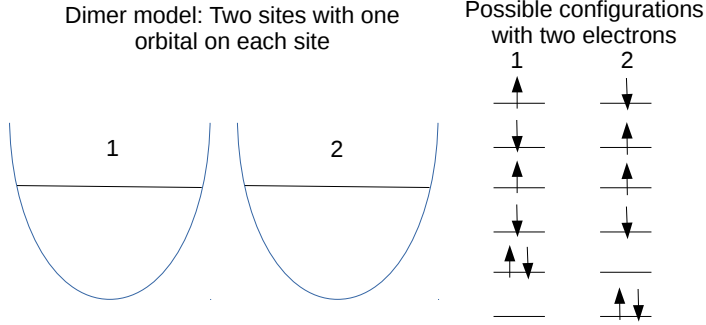


Figure 1.1: Schematic figure of a two site (dimer) model with one orbital per site. The different possible two-electron configurations are shown to the right.

Coulomb repulsion between two electrons on the same site is U and, for a large separation between the sites, the Coulomb repulsion between electrons localized on different sites is negligible. With a single electron in the system there is no Coulomb repulsion term and the two energy eigenfunctions are given by

$$|\psi_g\rangle = \frac{1}{\sqrt{2}}(|1\rangle + |2\rangle) \quad (1.4)$$

$$|\psi_u\rangle = \frac{1}{\sqrt{2}}(|1\rangle - |2\rangle). \quad (1.5)$$

Since the kinetic energy depends on the curvature of the wavefunction it is minimized if the wavefunctions are smooth and extended over the two sites. Therefore the even state $|\psi_g\rangle$ will be lower in energy than $|\psi_u\rangle$.

We now consider what happens if we add a second electron to the system. If we assume that the electron-electron interaction U is small compared to the kinetic energy it is justified to treat this term in a mean-field approximation, i.e. replace the interaction term with a single-particle potential that includes the average effect of the interaction, such as the Hartree approximation. The two-particle problem is then reduced to an effective single-particle problem and the many-body eigenstates are single Slater determinants of the single-particle eigenstates of the effective problem. On the other hand, if U is large, configurations with two electrons on the same site will not be energetically favourable. Hence, given an electron on one of the sites there is a high probability that the other electron is found on the other site, in other words, the two electrons are strongly correlated. The kinetic

energy is higher if the electrons are confined and the hopping between the sites is suppressed by the Pauli principle if the two electrons have the same spin. Thus, in the large U limit, the lowest energy eigenstate will be the linear combination of the two first configurations shown in Fig. 1.1 corresponding to the singlet

$$|\Psi\rangle = \frac{1}{\sqrt{2}}(|1 \uparrow\rangle|2 \downarrow\rangle - |1 \downarrow\rangle|2 \uparrow\rangle). \quad (1.6)$$

This state cannot be written as a single Slater determinant. The triplet will be higher in energy since it has an antisymmetric spacial wavefunction and hence a larger kinetic energy.

In simple metals and semiconductors where the valence states are of s or p character the electrons are relatively delocalized in the solid. This means that they are described by extended wave-functions and hence the electron-electron interaction term is small compared to the kinetic term and crystal potential. These solids are therefore called weakly correlated and their electronic structure is typically well described with a mean-field treatment in bandstructure calculations using Density Functional Theory (DFT) [71, 88] with the Local Density Approximation (LDA) [88, 148, 149, 150] or perturbatively within the GW approximation [64].

The lanthanides occupy a special place at the bottom of the periodic table. These materials have $4f$ valence electrons that are extremely localized around the atomic core. When forming a solid these materials therefore retain a large part of their atomic properties and exhibit strong correlation effects. On the other hand, the correlation effects are mainly local around the atoms and long-range correlations between electrons at different atomic sites are small. These materials can therefore be described within dynamical mean field theory (DMFT) [52, 53, 112] combined with the local density approximation (LDA+DMFT) [6, 103, 90, 67] that gives a nonperturbative treatment of local onsite correlations but neglects long-range correlations [106]. Relativistic effects can also be large for the $4f$ and $5f$ materials and a proper description of these effects is indeed a challenging task.

Apart from Paper I that deals with the lanthanides this thesis is mainly concerned with transition metal compounds. Examples of such compounds are FeSe as well as cuprate high- T_c superconductors. A proper description of these compounds is therefore essential to understand the mechanisms behind high- T_c superconductivity. Another class of interesting transition metal based compounds are the perovskites. Transition metal oxides in perovskite structure exhibit many interesting properties including colossal magneto-resistance, spin-state transitions, multifer-

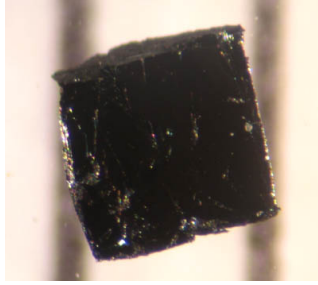


Figure 1.2: Image of a sample of the high-temperature superconductor BSCCO-2223. Taken from Ref. [151].
Credit: James Slezak

roics and multifunctional catalytic properties [94]. In this thesis we consider the cubic perovskites SrVO_3 and SrMoO_3 , the former is considered a prototype of a strongly correlated metal and is therefore often used to benchmark new electronic structure methods. However, SrVO_3 is also interesting from an industrial point of view with applications as electrode material for functional perovskite oxides [117], transparent conductors used in photovoltaics [43] and in Mott-transistors [194].

The early transition metals with $3d$ valence electrons are somewhere in between the sp -compounds with long-range weak correlations and the f -compounds with short-range strong correlations. On the one hand valence states for many of these compounds are sufficiently localized so that the local correlations are too strong to be treated using the GW approximation, on the other hand the valence states are sufficiently delocalized so that the DMFT-assumption of only retaining local correlations becomes questionable. The typical approach to most of these materials is to use LDA+DMFT with parameters adapted to fit the experimental data or computed from the LDA bandstructure. This yields an interpretation of the spectra in terms of renormalized quasiparticle peaks and Hubbard bands due to strong local correlations. One of the major topics of this thesis is devoted to showing that this interpretation is not always correct for the transition metal compounds. For these compounds the long-range correlations are important and can drastically change the physical interpretation of the spectra:

Satellite features in the spectral function previously interpreted as Hubbard bands arising from local atomic like excitations should in fact be interpreted as plasmons originating from long-range collective charge excitations.

In the following chapters I outline our theoretical approach starting from the basic

constituents, density functional theory, the GW approximation and dynamical mean-field theory. I do not aim to give any rigorous proofs, rather I try to present my understanding of the theory in a more physically intuitive way, that I hope could serve as a compliment to the standard text-books in the subject.

1 Units

In the remainder of this thesis I will, unless otherwise specified, use atomic units in which $\hbar = \frac{e^2}{4\pi\epsilon_0} = m_e = 1$, where m_e is the electron mass.

2 Role of first-principle calculations

A common and powerful way to understand the different physical phenomena observed in condensed matter systems is to construct models that focus on different aspects of the system and takes input parameters that are either estimated from experiment, or adjusted to yield physically reasonable results that agree with experiment. Since this makes it possible to focus on certain mechanisms that are thought to be important and also solve the models for a wide range of input parameters it is a powerful way to understand the system under study and different emergent phenomena. However, solid-state systems are extremely complex and therefore models with adjustable parameters often lack predictive power. A model that is suitable for one material does not have to be suitable for another material and the input parameters can also be very different.

First-principle calculations on the other hand do not make use of adjustable parameters. Instead the starting point is the Hamiltonian in Eq. 1.3. To solve this Hamiltonian the only input needed is the charge and position of the different atoms in the solid. This makes it possible to predict the equilibrium crystal structure of different solids and also their electronic structure. Using first-principle approaches it is therefore, in principle, possible both to understand and describe existing materials and to predict new materials that have not yet been synthesized experimentally, with different intriguing properties. However, the challenge in first-principle calculations is to find suitable approximations that makes the system described by the Hamiltonian numerically solvable and still provides an accurate description of the important physical processes in the solid. In this thesis I use,

develop and discuss different first-principle methods and to which materials they are applicable.

3 Density functional theory

A solution of the complete many-body problem defined by the Hamiltonian in Eq. 1.3 is, as discussed in the previous section, an infeasible task even for moderately large systems. The complete solution of the N -particle many-body problem requires the knowledge of the full many-body wave functions, complex quantities with $3N$ -coordinates. However, usually one is only interested in certain quantities, such as total ground-state energies and densities, excitation spectra and magnetic properties. Although the values of these quantities can be derived from the many-body wavefunctions, the complete wavefunctions include a lot of redundant information that one is typically not interested in. The idea behind DFT is to reduce the problem so that one can still compute the interesting quantities without having to find the exact many-body wave functions. The basis of DFT relies on the two Hohnberg-Kohn (HK) theorems that were originally derived for non-degenerate systems in Ref. [71] and later extended to degenerate systems by Levi and Lieb [100, 101, 104, 105].

The first theorem states that the ground-state densities of two systems with external potentials that differ by more than a constant will always be different. This means that the Hamiltonian, and therefore also the complete many-body wave functions, are completely determined by the ground-state density. Thus, given only the ground-state density, all properties of the system are determined. It should be noted that, while for non-degenerate systems this implies that there is a one-to-one correspondence between the ground-state density and the external potential, for degenerate systems there can be more than one ground-state density that corresponds to the same external potential. However, a given ground-state density uniquely determines the external potential.

The second theorem states that for each system with a given external potential $V_{\text{crys}}(\mathbf{r}_i)$ there exist a unique functional of the density $E_{\text{HK}}[n(\mathbf{r})]$ whose minimum gives the ground-state energy of the system,

$$E_{\text{HK}}[n(\mathbf{r})] = F_{\text{HK}}[n(\mathbf{r})] + \int d^3r V_{\text{crys}}(\mathbf{r})n(\mathbf{r}) + E_{\text{II}}, \quad (\text{I.7})$$

where $F_{\text{HK}}[n(\mathbf{r})] = T[n(\mathbf{r})] + E_{\text{int}}[n(\mathbf{r})]$ includes all internal energies (kinetic and interaction energies) and E_{II} is the interaction energy of the nuclei. The functional $F_{\text{HK}}[n(\mathbf{r})]$ has to be universal since it does not contain any system specific constituents. It should be noted that, while the functional $E_{\text{HK}}[n(\mathbf{r})]$ is sufficient to determine the ground-state density and energy of the system, it does not provide any information about excited states.

As mentioned above the Hohenberg-Kohn theorems were originally only proven for non-degenerate systems. Furthermore, the Hohenberg-Kohn functional is only defined for densities that can be generated by an external potential (V -representability). V -representability has been proven for lattice systems [36, 87] (for relatively mild restrictions on the densities) but the general conditions for V -representable densities are not known.

The formulation of DFT by Levy and Lieb (LL) circumvents these problems through a constrained search formulation. Similar to the HK-formulation the LL-formulation defines an energy functional $E_{\text{LL}}[n(\mathbf{r})]$ whose minimum gives the ground-state energy of the system.

$$E_{\text{LL}}[n(\mathbf{r})] = F_{\text{LL}}[n(\mathbf{r})] + \int d^3r V_{\text{crys}}(\mathbf{r})n(\mathbf{r}) + E_{\text{II}}. \quad (1.8)$$

However, the functional $F_{\text{LL}}[n(\mathbf{r})]$ is defined through a two-step procedure: First the internal energy F_{LL} is written as an expectation value in terms of the energy eigenstates or wavefunctions. Then the energy is minimized with respect to all wavefunctions that correspond to a given density $n(\mathbf{r})$,

$$F_{\text{LL}}[n(\mathbf{r})] = \min_{\Psi \rightarrow n(\mathbf{r})} \langle \Psi | \hat{T} + \hat{V}_{\text{int}} | \Psi \rangle. \quad (1.9)$$

This formulation is valid also for degenerate systems and the functional $F_{\text{LL}}[n(\mathbf{r})]$ is defined for any density that can be derived from a many-body wave-function (N -representability). Any density satisfying simple conditions can be shown to be N -representable [54].

3.1 The Kohn-Sham approach

Although HK and LL formulations of DFT are interesting from a fundamental point of view they do not provide any guidance on how to construct the total energy functionals or how to compute physical properties of a many-electron

system. However, for the ground-state total energy this is solved in the Kohn-Sham approach to DFT [88]. The Kohn-Sham approach to DFT relies on the mapping of the full interacting many-body problem to an auxiliary noninteracting problem that can be solved numerically. The auxiliary system is assumed to have the same ground-state density as the full interacting system (non-interacting V -representability or $V0$ -representability) and all the complicated effects of the many-body terms are included in an exchange-correlation functional $E_{xc}[n(\mathbf{r})]$ of the electron density. The non-interacting V -representability is an ansatz in the Kohn-Sham formulation which can be proven for the homogeneous electron gas and small deviations from it [88] as well as lattice systems [36], but has not been proven in general cases. In Ref. [170] the problem of $V0$ -representability is discussed in detail, and it is shown that it is always possible to set up a Kohn-Sham scheme that produces any interacting V -representable density.

With these definitions the problem is reformulated into finding physically motivated approximations to $E_{xc}[n(\mathbf{r})]$.

The auxiliary Hamiltonian is chosen to have a local effective potential $V_{KS}(\mathbf{r})$. The Schrödinger equation for the auxiliary system is given by

$$\left(-\frac{1}{2}\nabla^2 + V_{KS}^\sigma(\mathbf{r})\right) \psi_i^\sigma(\mathbf{r}) = \epsilon_i^\sigma \psi_i^\sigma(\mathbf{r}) \quad (1.10)$$

and the density by

$$n(\mathbf{r}) = \sum_{\sigma} \sum_{i=1}^{N_{\sigma}} |\psi_i^\sigma(\mathbf{r})|^2. \quad (1.11)$$

The Kohn-Sham expression for the ground-state energy is then given by

$$E_{KS}[n(\mathbf{r})] = T_s[n(\mathbf{r})] + \int d^3r V_{\text{ext}}(\mathbf{r})n(\mathbf{r}) + E_H[n(\mathbf{r})] + E_{II} + E_{xc}[n(\mathbf{r})], \quad (1.12)$$

where T_s is the kinetic energy of the *independent* particles described by the wavefunctions $\psi_i^\sigma(\mathbf{r})$

$$T_s = -\frac{1}{2} \sum_{\sigma} \sum_{i=1}^{N_{\sigma}} \langle \psi_i^\sigma | \nabla^2 | \psi_i^\sigma \rangle \quad (1.13)$$

and E_H the Hartree energy. From the second HK-theorem requiring $\frac{\delta E_{KS}}{\delta n(\mathbf{r})} = 0$ yields the Kohn-Sham potential

$$V_{KS}^\sigma(\mathbf{r}) = V_{\text{ext}}(\mathbf{r}) + V_H(\mathbf{r}) + V_{xc}^\sigma(\mathbf{r}), \quad (1.14)$$

where $V_H(\mathbf{r})$ is the usual Hartree potential

$$V_H(\mathbf{r}) = \int d^3r' \frac{n(\mathbf{r}')}{|\mathbf{r} - \mathbf{r}'|} \quad (1.15)$$

and the exchange-correlation potential is defined as

$$V_{xc}^\sigma(\mathbf{r}) = \frac{\delta E_{xc}}{\delta n(\mathbf{r}, \sigma)}. \quad (1.16)$$

For a given approximation of $E_{xc}[n(\mathbf{r})]$ and starting from an initial guess of the density (or single particle wave-functions) Eq. 1.10-1.14 can be iterated until self-consistency is reached. Hence, the Kohn-Sham formulation presents a practical scheme how to compute the ground-state total energy. What is left is to find an approximation of the exchange-correlation energy functional.

One of the most widely used approximations, and also the one used in this thesis, is the Local Density Approximation (LDA) [88], or for spin-polarized systems local spin density approximation (LSDA) [176]. In this approximation the exchange-correlation energy density is locally assumed to be the same as the exchange-correlation energy density of the homogeneous electron gas with the same density

$$E_{xc}^{LSDA}[n^\uparrow(\mathbf{r}), n^\downarrow(\mathbf{r})] = \int d^3r n(\mathbf{r}) \epsilon_{xc}^{\text{hom}}(n^\uparrow(\mathbf{r}), n^\downarrow(\mathbf{r})). \quad (1.17)$$

3.2 Bandstructure: DFT as a mean-field approach

While, according to the basic theorems of DFT, all quantities of the system can be computed from the ground-state density, the Kohn-Sham approach only yields the correct total ground-state energies as well as the energy of the highest occupied state [102]. Nevertheless the Kohn-Sham orbitals and eigenenergies (depicted in a bandstructure plot) are conventionally, and with great success, interpreted as corresponding to the quasiparticle energies of the system in the photoemission (PES)

and inverse photoemission (IPES) spectra. The fact that the DFT-bandstructure corresponds relatively well to the PES/IPES spectra for weakly to moderately correlated materials implies that the exchange-correlation potential, evaluated for the self-consistent electron density in the Kohn-Sham auxiliary Hamiltonian (Eq. 1.10), provides a good mean-field approximation to the system. However, there are no rigid proofs why this has to be the case. In this sense DFT bandstructure calculations correspond to mean-field calculations with the Kohn-Sham potential acting as the mean-field. Time-dependent DFT [135] can give information about excited states, but this is outside the scope of this thesis.

4 Probing the electronic structure: Photoemission, inverse photoemission and relation to the Green's function

In order to investigate the physical properties of a system one has to probe or interact with it in some way. In photoemission spectroscopy (PES) the binding energies of the electrons are probed by shining monochromatic light onto the sample. The kinetic energies of the emitted electrons after absorption of a single photon with energy ν are, from the conservation of energy, given by

$$E_k = \nu - E_B - \Phi_0, \quad (1.18)$$

where E_B is the binding energy of the electron and Φ_0 is the work function, i.e. the minimum energy needed to remove an electron from the sample to the vacuum. In angle-resolved PES (ARPES) it is also possible to measure the momenta of the emitted electrons which are related to the crystal momenta of the electrons in the solid (Fig. 1.3). However, the momentum perpendicular to the surface is not conserved. Therefore, to get complete information of the crystal momentum of the electrons one usually has to rely on certain assumptions of the final states in the photoemission process [145].

Inverse photoemission (IPES), also called Bremsstrahlung Isochromate Spectroscopy (BIS) gives information about the unoccupied electronic structure in the solid. IPES relies on the opposite process compared to PES. A collimated beam of electrons is directed onto the sample. The electrons are absorbed in high lying energy eigenstates that later decay to lower energy eigenstates. The energies of the emitted photons gives information about the unoccupied part of the spectra.

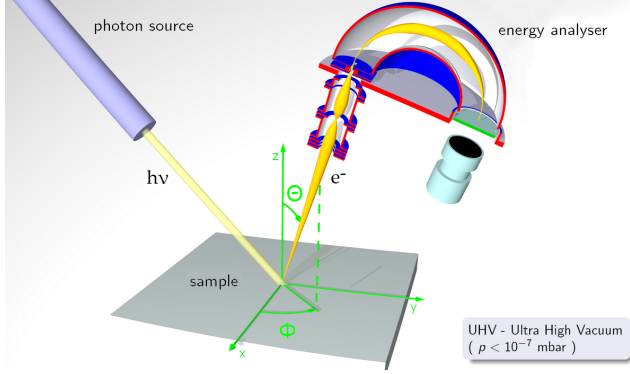


Figure 1.3: Schematic figure of ARPES setup. Taken from Ref. [7].

In order to interpret and predict the results of PES and IPES experiments we need a way to describe these processes theoretically. This can conveniently be done using the Green's function formalism. Below I give a brief review of the Green's function formalism following Refs. [8, 46, 158].

The time-ordered Green's function is defined as

$$iG(1, 2) = \frac{\langle \Psi_0^N | \hat{T} [\hat{\psi}(1) \hat{\psi}^\dagger(2)] | \Psi_0^N \rangle}{\langle \Psi_0^N | \Psi_0^N \rangle}, \quad (\text{I.19})$$

here 1 and 2 are generalized indices including both spacial, spin and time variables

$$1 = (r_1, t_1), \quad (\text{I.20})$$

$$r_1 = (\mathbf{r}_1, \sigma_1), \quad (\text{I.21})$$

$|\Psi_0^N\rangle$ is the many-body ground state of the N -particle system, $\hat{\psi}^\dagger(1)$ is a Heisenberg field operator that creates an electron with spin σ_1 at position \mathbf{r}_1 and time t_1 and \hat{T} the time ordering operator:

$$\hat{T} [\hat{\psi}(1) \hat{\psi}^\dagger(2)] = \theta(t_1 - t_2) \hat{\psi}(1) \hat{\psi}^\dagger(2) - \theta(t_2 - t_1) \hat{\psi}^\dagger(2) \hat{\psi}(1). \quad (\text{I.22})$$

Hence, for $t_1 > t_2$ the Green's function describes the probability amplitude for an electron created at 2 to propagate to 1 and similarly for $t_1 < t_2$ it describes the probability amplitude for a hole created at 1 to propagate to 2.

By making use of the completeness relation, $\sum_{N,i} |\Psi_i^N\rangle\langle\Psi_i^N| = \hat{1}$ the Green's function for a time-independent Hamiltonian can be written in terms of the quasi-particle amplitudes

$$\begin{aligned} f_i(r) &= \langle\Psi_i^{N-1}|\hat{\psi}(r)|\Psi_0^N\rangle, \\ g_i(r) &= \langle\Psi_0^N|\hat{\psi}(r)|\Psi_i^{N+1}\rangle : \end{aligned}$$

$$\begin{aligned} iG(1, 2) &= \theta(t_1 - t_2) \sum_i \exp(i(E_0^N - E_i^{N+1})(t_1 - t_2)) g_i(r_1) g_i^*(r_2) \\ &\quad - \theta(t_2 - t_1) \sum_i \exp(i(E_i^{N-1} - E_0^N)(t_1 - t_2)) f_i(r_1) f_i^*(r_2), \quad (1.23) \end{aligned}$$

where it becomes apparent that the Green's function for a system in equilibrium (with a time-independent Hamiltonian) only depends on the time-difference $t_1 - t_2$.

From the Green's function one can compute the ground-state expectation value of any single-particle operator, the ground-state energy as well as the spectrum of the system, i.e. the information experimentally obtained through PES and IPES. The relation between the Green's function and the PES/IPES spectra can be seen by considering the Fourier transform of $G(1, 2)$ in Eq. 1.23:

$$G(r_1, r_2; \omega) = \sum_i \frac{g_i(r_1) g_i^*(r_2)}{\omega - (E_i^{N+1} - E_0^N) + i\delta} + \sum_i \frac{f_i(r_1) f_i^*(r_2)}{\omega + (E_i^{N-1} - E_0^N) - i\delta}. \quad (1.24)$$

The poles of the Green's function correspond to the excitation energies of adding or removing a single electron from the ground state.

The relationship to the PES/IPES spectra becomes even more apparent by expressing the Green's function in terms of its spectral function $A(r_1, r_2, \omega)$

$$G(r_1, r_2; \omega) = \int_{-\infty}^{\mu} d\omega' \frac{A(r_1, r_2, \omega')}{\omega - \omega' - i\delta} + \int_{\mu}^{\infty} d\omega' \frac{A(r_1, r_2, \omega')}{\omega - \omega' + i\delta}, \quad (1.25)$$

where μ is the chemical potential.

Within the sudden approximation (see e. g. Ref. [66]) the spectral function, $A(r_1, r_2, \omega)$, is the quantity that is measured in PES/IPES experiments and is related to the imaginary part of the Green's function

$$A(r_1, r_2, \omega) = \sum_i [f_i(r_1)f_i^*(r_2)\delta(\omega - \mu + e_i^{N-1}) + g_i(r_1)g_i^*(r_2)\delta(\omega - \mu - e_i^{N+1})] - \frac{1}{\pi} \text{Im} G(r_1, r_2, \omega) \text{sgn}(\omega - \mu), \quad (1.26)$$

where $e_i^{N\pm 1} = E_i^{N\pm 1} - E_0^N$.

5 The self-energy and the Dyson equation

From the equation of motion of the field operators

$$i \frac{\partial}{\partial t} \hat{\psi}(1) = [\hat{\psi}(1), \hat{H}] \quad (1.27)$$

it follows that the Green's function obeys [8]

$$\left(i \frac{\partial}{\partial t} - b_0(\mathbf{r}) \right) G(1, 2) - \int d1' \Sigma(1, 1') G(1', 2) = \delta(1 - 2), \quad (1.28)$$

where the self-energy Σ is defined as

$$\begin{aligned} \int d1' \Sigma(1, 1') G(1', 2) = \\ - i \int d1' v(1 - 1') \langle \Psi_0^N | \hat{T} [\hat{\psi}^\dagger(1') \hat{\psi}(1') \hat{\psi}(1) \hat{\psi}^\dagger(2)] | \Psi_0^N \rangle \end{aligned} \quad (1.29)$$

and b_0 is the first term in Eq. 1.3. Here

$$v(1 - 2) = \frac{1}{|\mathbf{r}_1 - \mathbf{r}_2|} \delta(t_1 - t_2) \quad (1.30)$$

is the instantaneous bare Coulomb interaction.

The bare Green's function G^0 is defined as the solution to Eq. 1.28, but with the self-energy set to zero:

$$\left(i \frac{\partial}{\partial t} - b_0(\mathbf{r}) \right) G^0(1, 2) = \delta(1 - 2). \quad (1.31)$$

Inserting this definition into Eq. 1.28 and multiplying with $(i\frac{\partial}{\partial t} - h_0(\mathbf{r}))^{-1}$ on both sides we obtain, after some minor manipulations, the Dyson equation:

$$G(1, 2) = G^0(1, 2) + \int d1' d2' G^0(1, 1') \Sigma(1', 2') G(2', 2). \quad (1.32)$$

By introducing a basis and Fourier transforming Eq. 1.32 to frequency space the Dyson equation can be mapped to a matrix equation

$$G(\omega) = G^0(\omega) + G^0(\omega) \Sigma(\omega) G(\omega). \quad (1.33)$$

For practical applications one needs a way to evaluate the self-energy matrix in Eq. 1.33. By making use of Wick's theorem the interacting Green's function G , or equivalently the self-energy Σ , can be expanded in a perturbation series in terms of the non-interacting Green's function and the Coulomb interaction. This expansion, conveniently expressed through diagrams, is discussed in detail in Refs. [46, 158], and the reader is referred to these references for further reading. Alternatively one can also use the Schwinger functional derivative technique described in Chapter 2.2. This approach circumvents the use of Wick's theorem.

6 Finite temperature formalism

The equations in the preceding sections are defined for zero-temperature. In order to be able to explore finite temperature effects, such as transition temperatures for magnetic materials, and also to be able to use quantum Monte-Carlo methods, the concepts introduced in the preceding sections need to be extended to finite temperatures. Below I very briefly define and discuss the finite-temperature Green's function following Refs. [46, 158].

To describe finite temperature properties it is convenient to use the grand canonical ensemble, that allows for a variable particle number. The grand canonical partition function is defined as

$$Z = e^{-\beta\Omega} = \text{Tr} e^{-\beta\hat{K}}. \quad (1.34)$$

Here Ω is the thermodynamic potential, $\beta = 1/k_B T$ where k_B is the Boltzmann constant and T the temperature. \hat{K} is the grand canonical Hamiltonian defined as

$$\hat{K} = \hat{H} - \mu\hat{N}. \quad (1.35)$$

In the modified Heisenberg picture the field operators obey

$$\hat{\psi}(r, \tau) = e^{\hat{K}\tau} \hat{\psi}(r) e^{-\hat{K}\tau}, \quad (1.36)$$

$$\hat{\psi}^\dagger(r, \tau) = e^{\hat{K}\tau} \hat{\psi}^\dagger(r) e^{-\hat{K}\tau}. \quad (1.37)$$

While $\hat{\psi}^\dagger(r, \tau)$ is not the adjoint of $\hat{\psi}(r, \tau)$ when τ is real, if τ is interpreted as a purely imaginary time this is the case. Hence, for $\tau = it$ the finite temperature Heisenberg picture is identical to the zero-temperature relation with the substitution $\hat{H} \rightarrow \hat{K}$.

With these definitions the finite-temperature Green's function is defined as

$$G(r\tau, r'\tau') = \frac{1}{Z} \text{Tr} \left(e^{-\beta \hat{K}} \hat{T} \left[\hat{\psi}(r, \tau) \hat{\psi}^\dagger(r', \tau') \right] \right). \quad (1.38)$$

For a time independent Hamiltonian the Green's function only depends on the difference $\tau' - \tau$ and can therefore be denoted as $G(r, r', \tau)$.

The Fourier transform and its inverse are defined as

$$G(i\nu_n) = \int_0^\beta d\tau e^{i\nu_n \tau} G(\tau) \quad (1.39)$$

$$G(\tau) = \frac{1}{\beta} \sum_n e^{-i\nu_n \tau} G(i\nu_n), \quad (1.40)$$

where the Matsubara frequencies are

$$\nu_n = \frac{2n+1}{\beta} \pi \quad (1.41)$$

and n is an integer. The odd frequencies follow from the fermionic anti-periodic boundary conditions

$$G(r, r', \tau - \beta) = -G(r, r', \tau). \quad (1.42)$$

The bosonic quantities, such as the polarization and screened interaction (See Chapter 2) follow periodic boundary conditions and are therefore defined for even frequencies

$$\omega_n = \frac{2n\pi}{\beta}. \quad (1.43)$$

6.1 The problem with analytic continuation

In order to interpret the results of finite temperature calculations on the Matsubara axis it is necessary to extract the real-frequency or real-time results from the Matsubara data. One can easily compute the Matsubara Green's function from the spectral function on the real frequency axis by using the Hilbert transform

$$G(i\nu_n) = \int d\omega A(\omega) \underbrace{\frac{1}{i\nu_n - \omega}}_{K(i\nu_n, \omega)}, \quad (1.44)$$

or equivalently for the imaginary time Green's function

$$G(\tau) = \int d\omega A(\omega) \underbrace{\frac{e^{-\tau\omega}}{1 + e^{-\beta\omega}}}_{K(\tau, \omega)}. \quad (1.45)$$

However, these equations are not easily inverted, there are infinitely many $A(\omega)$ that will produce, within some error, the same $G(i\nu_n)$. In practice this means that if G and A are approximated as vectors and K by a square matrix the determinant of K is exponentially small, which means that the inverse is ill-defined. For clean data without noise it is possible to use the Padé-approximant method [175], where $G(i\nu_n)$ is fit to a rational function which is the ratio of two polynomials. The imaginary frequency data can then be directly continued to the real axis by substituting $i\nu_n \rightarrow \omega + i\delta$. However, in this thesis we make use of quantum Monte-Carlo methods, and hence our data will be noisy. For such cases the Padé method does not work very well. The standard method is instead the Maximum Entropy Method (MaxEnt) [28, 57]. Below I give a very brief introduction of the concepts behind MaxEnt loosely following Ref. [82].

MaxEnt is based on Bayes' theorem which states that the joint probability $P(a, b)$ for two events a and b is equal to the conditional probability for a given b $P(a|b)$ times the probability for b $P(b)$

$$P(a, b) = P(a|b)P(b) = P(b|a)P(a). \quad (1.46)$$

Since the physical spectra is normalizable and positive definite $A(\omega)$ can be treated as a probability distribution. Eq. 1.46 can then be inverted to yield

$$P(A|\tilde{G}) = P(\tilde{G}|A)P(A)/P(\tilde{G}), \quad (1.47)$$

where \tilde{G} is the measured, noisy, finite temperature Green's function. The problem is then reformulated to finding the spectral function A that maximizes $P(A|\tilde{G})$, which is the conditional probability of A given the data \tilde{G} . $P(\tilde{G}|A)$ is usually called the likelihood function, $P(A)$ the prior probability and for a given set of data $P(\tilde{G})$ is a constant, which can be ignored.

Using the principle of maximum entropy the prior probability is proportional to $\exp(\alpha S)$, where S is the entropy, which is defined relative a default model (positive definite function) $m(\omega)$ [147]

$$S = \int d\omega (A(\omega) - m(\omega) - A(\omega) \ln(A(\omega)/m(\omega))). \quad (1.48)$$

The likelihood function, which is related to the difference between the measured \tilde{G} and the Matsubara Green's function corresponding to A , can be determined using the central limit theorem.

In this thesis we use Bryan's algorithm [28] as implemented in Ref. [26]. I will not go into the details of this algorithm here, but the reader is referred to the original papers [28, 57] as well as the review in Ref. [83] for further details.

2

The GW approximation

The interaction between an added negative test charge at point (\mathbf{r}_1, t_1) with an electron at point (\mathbf{r}_2, t_2) in the solid is very different from the instantaneous bare Coulomb interaction, $v(1, 2) = 1/|\mathbf{r}_1 - \mathbf{r}_2|\delta(t_1 - t_2)$, due to the response of the surrounding electrons. The added test charge will repel the neighbouring electrons creating screening holes around the test charge that effectively reduce the interaction. If the self-energy is expressed in terms of the bare Coulomb interaction between the electrons the screening is taken into account through the different higher order diagrams in the self-energy expansion. An alternative route, suggested by Hedin in 1965 [64] in the so called Hedin equations, is to express the self-energy in terms of the screened Coulomb interaction W instead. The first order self-energy diagram in the screened interaction will already contain an infinite series of diagrams in the bare Coulomb interaction, therefore this formally exact rewriting provides a convenient starting point for different approximations. Before deriving the Hedin equations using the functional derivative technique I will begin by stating the Hedin equations one by one and briefly discuss them from a physical point of view.

I Conventions

In this chapter I will use the generalized notation introduced in Eqs. 1.20-1.21 with the additional convention that repeated spin indices are summed over. For

the total density operator this implies the notation

$$\begin{aligned}\hat{\rho}(1) &= \sum_{\sigma_1} \hat{\psi}^\dagger(\mathbf{r}_1, \sigma_1, t_1) \hat{\psi}(\mathbf{r}_1, \sigma_1, t_1) = \underbrace{\hat{\psi}^\dagger(\mathbf{r}_1, \sigma_1, t_1) \hat{\psi}(\mathbf{r}_1, \sigma_1, t_1)}_{\text{implicit sum}} \\ &= \hat{\psi}^\dagger(1) \hat{\psi}(1)\end{aligned}\tag{2.1}$$

2 The Hedin equations

To understand the origin of the screened interaction we will consider what happens when we apply an arbitrary external perturbation $V_{ext}(\mathbf{r}, t)$ to the system. The density ρ_{ind} induced by the perturbation is, in linear response theory, given by

$$\rho_{ind}(1) = - \int d2 \chi(1, 2) V_{ext}(2).\tag{2.2}$$

Here χ is the density-density response function

$$\chi(1, 2) = i \langle \hat{T}(\hat{\rho}'(1) \hat{\rho}'(2)) \rangle\tag{2.3}$$

and $\hat{\rho}'(1) = \hat{\psi}^\dagger(1) \hat{\psi}(1) - \langle \hat{\psi}^\dagger(1) \hat{\psi}(1) \rangle$.

The potential generated by the induced density is

$$V_{ind}(1) = \int d2 v(1 - 2) \rho_{ind}(2) = - \int d(23) v(1, 2) \chi(2, 3) V_{ext}(3).\tag{2.4}$$

The generated potential screens the external perturbation which yields the total screened potential

$$\begin{aligned}V_{scr}(1) &= V_{ext}(1) + V_{ind}(1) \\ &= V_{ext}(1) - \int d(23) v(1, 2) \chi(2, 3) V_{ext}(3).\end{aligned}\tag{2.5}$$

Now, to compute the effective Coulomb interaction between the electrons in the solid we consider the bare, instantaneous Coulomb interaction $v(1, 2)$ as the external perturbation. The screening is a dynamical and in general non-isotropic

process and hence the effective interaction will be a time-dependent function of two spacial coordinates [76, 64]

$$W(1, 2) = v(1, 2) - \int d(34) v(1, 3) \chi(3, 4) v(4, 2). \quad (2.6)$$

It should be noted that both the bare interaction v and the screened interaction W are independent of spin.

Instead of working with the response function χ it is convenient to express W in terms of the polarization Π :

$$W(1, 2) = v(1, 2) + \int d(34) v(1, 3) \Pi(3, 4) W(4, 2). \quad (2.7)$$

The polarization can be expressed as a functional of the Green's function where the first order term is equivalent to the Random Phase Approximation (RPA) [126],

$$\begin{aligned} \Pi(1, 2) &= -i \int d(34) G(1, 3) \Gamma(3, 4, 2) G(4, 1^+) \\ &= \underbrace{-i G(1, 2) G(2, 1^+)}_{\Pi^{\text{RPA}}} + \int d(34) G(1, 3) G(4, 1) W(3, 4) G(2, 4) G(3, 2) + \dots \end{aligned} \quad (2.8)$$

The three-point vertex function Γ in Eq. 2.8 is defined as

$$\begin{aligned} \Gamma(1, 2, 3) &= -\frac{\delta G^{-1}(1, 2)}{\delta V(3)} = \delta(1 - 2) \delta(2 - 3) + \frac{\delta \Sigma(1, 2)}{\delta V(3)} \\ &= \delta(1 - 2) \delta(2 - 3) + \int d(4567) \frac{\delta \Sigma(1, 2)}{\delta G(4, 5)} G(4, 6) G(7, 5) \Gamma(6, 7, 3), \end{aligned} \quad (2.9)$$

where V is the total (external and Hartree) potential. Finally the exchange and correlation part of the self-energy, $\Sigma^{xc} = \Sigma - V_H$ where V_H is the Hartree potential, can be written in terms of W and Γ as

$$\Sigma^{xc}(1, 2) = i \int d(34) G(1, 3^+) W(1, 4) \Gamma(3, 2, 4). \quad (2.10)$$

Together with the Dyson equation (Eq. 1.33) this set of coupled differential equations (Eqs. 2.7-2.10) are known as the Hedin equations. Although they are in

principle exact they are iterative in nature and for practical calculations one has to resort to different approximations. The suggestion by Hedin was to approximate the vertex function by its first order term, $\Gamma(1, 2, 3) \approx \delta(1 - 2)\delta(2 - 3)$, which yields the well known GW approximation for the self-energy:

$$\Sigma_{GW}^{xc}(1, 2) = iG(1, 2^+)W(1, 2), \quad (2.11)$$

and the RPA for the polarization

$$\Pi^{\text{RPA}}(1, 2) = -iG(1, 2)G(2, 1^+). \quad (2.12)$$

The self-energy diagram in Eq. 2.11 is similar in structure to the Fock exchange diagram but with the bare Coulomb interaction replaced by the screened interaction W . Hence all correlation effects are contained in the screening of the Coulomb interaction. To include the strong local correlations that e.g. drive the Mott Hubbard metal to insulator transition, one has to consider higher order self-energy diagrams, as will be discussed in Chapter 4.

2.1 Derivation

In this section I will derive the Hedin equations using the functional derivative technique following Refs. [8, 64, 10]. As a mathematical tool we will add a time dependent field $\phi(\mathbf{r}, t)$ to the Hamiltonian in Eq. 1.3; $H_p = H + \phi$. In the interaction picture the time-dependence of the field operators is the same as for the Heisenberg operators in the unperturbed ($\phi = 0$) case

$$\hat{\psi}_I(r, t) = e^{\hat{H}(t-t_0)} \hat{\psi}(r, t_0) e^{-i\hat{H}(t-t_0)}, \quad (2.13)$$

and the time-evolution of the state kets are given by

$$|\psi_I(t)\rangle = \underbrace{\hat{T} \exp \left[-i \int_{t_0}^t dt' \hat{\Phi}(t') \right]}_{\hat{U}(t, t_0)} |\psi_I(t_0)\rangle \quad (2.14)$$

where

$$\hat{\Phi}(t) = \int d\mathbf{r} \phi(\mathbf{r}, t) \hat{\psi}_I^\dagger(r, t) \hat{\psi}_I(r, t). \quad (2.15)$$

The Green's function is then given by

$$iG(1, 2) = \frac{\langle \Psi_0^N | \hat{T} \left[\hat{S} \hat{\psi}_I(1) \hat{\psi}_I^\dagger(2) \right] | \Psi_0^N \rangle}{\langle \Psi_0^N | \hat{S} | \Psi_0^N \rangle} \quad (2.16)$$

where

$$\hat{S} = \hat{U}(\infty, -\infty). \quad (2.17)$$

The beauty of using the interaction picture is that the all dependence on the external field in the Green's function is contained in the operator \hat{S} . Hence, using

$$\frac{\delta \hat{S}}{\delta \phi(1)} = -i \hat{T} \left[\hat{S} \hat{\psi}_I^\dagger(1) \hat{\psi}_I(1) \right] \quad (2.18)$$

the functional derivative of the Green's function with respect to the external field is given by

$$\frac{\delta G(1, 2)}{\delta \phi(3)} = G_2(1, 2, 3, 3^+) - G(1, 2) G(3, 3^+) \quad (2.19)$$

where

$$G_2(1, 2, 3, 4) = - \frac{\langle \Psi_0^N | \hat{T} \left[\hat{S} \hat{\psi}_I(1) \hat{\psi}_I(3) \hat{\psi}_I^\dagger(4) \hat{\psi}_I^\dagger(2) \right] | \Psi_0^N \rangle}{\langle \Psi_0^N | \hat{S} | \Psi_0^N \rangle}. \quad (2.20)$$

By comparing Eq. 2.19 with the equation for the self-energy (Eq. 1.29) and using $\rho(1) = -iG(1, 1^+)$ one can identify

$$\int d1' \Sigma(1, 1') G(1', 2) = \underbrace{\int d3 v(1-3) \rho(3) G(1, 2)}_{V_H(1)} + i \int d3 v(1, 3) \frac{\delta G(1, 2)}{\delta \phi(3)}. \quad (2.21)$$

By evaluating $\frac{\delta}{\delta \phi} (G^{-1} G) = 0$ and reshuffling the terms, the functional derivative of G with respect to the external field can be rewritten as

$$\frac{\delta G}{\delta \phi} = -G \frac{\delta G^{-1}}{\delta \phi} G. \quad (2.22)$$

By inserting this identity in Eq. 2.21 and using the definition of the exchange-correlation self-energy $\Sigma^{xc} = \Sigma - V_H$

$$\Sigma^{xc}(1, 2) = -i \int d3d4v(1, 4)G(1, 3)\frac{\delta G^{-1}(3, 2)}{\delta \phi(4)}. \quad (2.23)$$

The vertex function (defined in Eq. 2.9) can be extracted from the right hand side by making use of the chain rule

$$v(1, 4)\frac{\delta G^{-1}(3, 2)}{\delta \phi(4)} = \int d5v(1, 4)\frac{\delta V(5)}{\delta \phi(4)} \underbrace{\frac{\delta G^{-1}(3, 2)}{\delta V(5)}}_{\Gamma(3, 2, 5)}. \quad (2.24)$$

This yields the Hedin equation for the self-energy (Eq. 2.10) with

$$W(1, 2) = \int d3v(1, 3)\underbrace{\frac{\delta V(2)}{\delta \phi(3)}}_{\epsilon^{-1}(2, 3)} \quad (2.25)$$

where we have defined the inverse dielectric function ϵ^{-1} as the change in the total potential with respect to the applied external field.

What is left is to relate the expression in Eq. 2.25 for the screened interaction to the corresponding Hedin equations for W and Π (Eqs. 2.7 - 2.8). Using the definition of $V = \phi + V_H$ the inverse dielectric function can be rewritten as

$$\begin{aligned} \epsilon^{-1}(1, 2) &= \frac{\delta V(1)}{\delta \phi(2)} = \delta(1 - 2) + \int d3v(1 - 3)\frac{\delta \rho(3)}{\delta \phi(2)} \\ &= \delta(1 - 2) + \int d3d4v(1 - 3)\frac{\delta \rho(3)}{\delta V(4)}\epsilon^{-1}(4, 2). \end{aligned} \quad (2.26)$$

Defining the polarization as the change in the density with respect to the total field, $\Pi = \frac{\delta \rho}{\delta V}$, and using the identity in Eq. 2.22 with V instead of ϕ and $\rho(1) = -iG(1, 1^+)$, the Hedin expression for the polarization (Eq. 2.8) is retrieved

$$\Pi(1, 2) = \frac{\delta \rho(1)}{\delta V(2)} = -i \int d(34)G(1, 3)\Gamma(3, 4, 2)G(4, 1^+). \quad (2.27)$$

Finally the Hedin equation for the screened interaction (Eq. 2.7) is retrieved by inserting Eqs. 2.27 and 2.26 into Eq. 2.25.

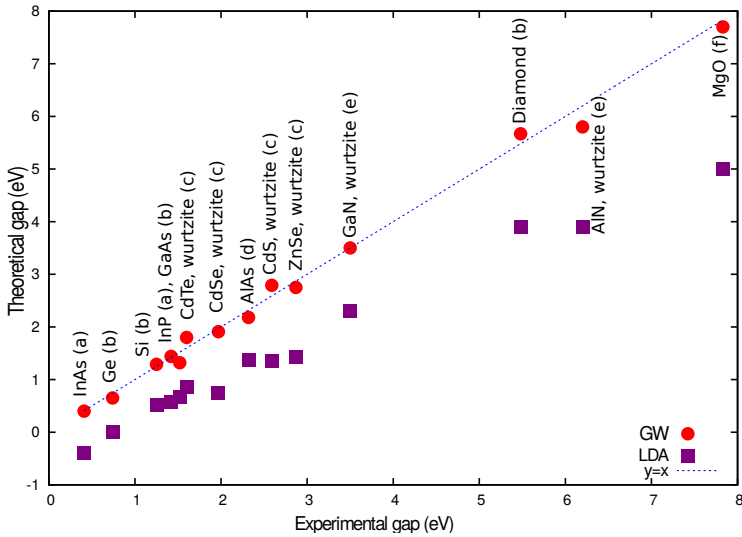


Figure 2.1: Minimum bandgaps calculated with the GW approximation and LDA for some semiconductors and insulators. The experimental data is taken from [69, 21, 190] and the GW and LDA data is taken from (a) [195], (b) [129], (c) [192], (d) [56], (e) [132], f [139]. The figure is reproduced from Paper V.

3 Implementations

Although the GW -equations in principle should be solved self-consistently, fully self-consistent calculations for real materials are rare. The reason for this is, partly that self-consistency is computationally expensive, but more importantly Holm and von Barth [73] showed that, for the electron gas, self-consistency yields a poor spectral function: The plasmon pole in W is flushed out and the quasiparticle peak is widened. The same failure was later observed for Aluminium [93]. For total energy calculations on the other hand self-consistency is essential [72, 93]. The standard GW -scheme for solids is instead the one-shot or G^0W^0 approximation. In this scheme the GW -self-energy is computed only once from the DFT (LDA) Green's function and used to obtain the spectral function. The G^0W^0 approximation has proved to be very successful for weakly correlated materials. A famous example is that it almost entirely cures the famous bandgap underestimation of the LDA for insulators and semiconductors with s or p valence electrons (Fig. 2.1) [78, 56]. However, the G^0W^0 approximation cannot account for the strong local correlations that e.g. drive the Mott-Hubbard metal to insulator transition and therefore qualitatively fails to describe many transition metal compounds, such as

the parent compounds of the cuprate superconductors. The G^0W^0 approximation also fails to describe the drastic reduction of quasiparticle weight in the Ce α - γ phase transition [137].

Another drawback with one-shot GW is the ambiguity in the starting Green's function. Different starting points will unavoidably give different results. To circumvent this problem, schemes based on quasiparticle self-consistency have recently been developed and shown to improve the one-shot results for a wide range of materials [33, 45, 34, 174, 35, 89] while it can also lead to an overestimation of the bandgaps [27]. However, these calculations are computationally expensive and still do not account for the strong local correlations present in many transition metal and lanthanide compounds.

A proper implementation of a fully self-consistent scheme in the full Hilbert space for real materials is a challenging and computationally demanding task. There are reports that self-consistency improves the bandgaps for Si and Ge semiconductors [92], although also contradictory results have been reported [140, 161]. However, as mentioned above, numerical studies for the electron gas and Aluminium indicate that self-consistency yields poor spectral functions. In Paper III and IV we show that this is also the case for the more strongly correlated $3d$ perovskites, SrVO_3 and SrMoO_3 , with a self-consistent GW -implementation where the self-consistency is restricted to the t_{2g} -subspace [25, 122]. For molecules, on the other hand, self-consistency generally improves total energies and yields ionization energies similar to or better than non-self-consistent calculations [154, 155, 91, 109, 131, 30, 29] but still gives worse spectra in many cases [109].

4 Matrix representation

With an appropriate choice of basis $\{\varphi_{i\mathbf{q}}(\mathbf{r})\}$ the GW -equations above can be expressed as matrix equations which at finite temperature and with summation over repeated indices are given by

$$\Sigma_{ik}(\mathbf{q}, \tau) = - \sum_{\mathbf{k}} G_{jl}(\mathbf{k}, \tau) W_{ijkl}(\mathbf{q} - \mathbf{k}, \tau), \quad (2.28)$$

$$G_{kl}(\mathbf{q}, i\nu_m) = G_{kl}^0(\mathbf{q}, i\nu_m) + G_{km}^0(\mathbf{q}, i\nu_m) \Sigma_{mn}(\mathbf{q}, i\nu_m) G_{nl}(\mathbf{q}, i\nu_m), \quad (2.29)$$

$$\Pi_{mm'nn'}(\mathbf{q}, \tau) = \sum_{\mathbf{k}} G_{mn}(\mathbf{k}, \tau) G_{n'm'}(\mathbf{k} - \mathbf{q}, -\tau), \quad (2.30)$$

$$W_{\alpha\beta}(\mathbf{q}, i\omega_n) = v_{\alpha\beta}(\mathbf{q}, i\omega_n) + v_{\alpha\gamma}(\mathbf{q}, i\omega_n) \Pi_{\gamma\eta}(\mathbf{q}, i\omega_n) W_{\eta\beta}(\mathbf{q}, i\omega_n). \quad (2.31)$$

where the product basis index $\alpha = \{ij\}$ and

$$W_{ijkl}(\mathbf{q} - \mathbf{k}, \tau) = \int d^3r d^3r' \varphi_{i\mathbf{q}}^*(\mathbf{r}) \varphi_{j\mathbf{k}}(\mathbf{r}) W(\mathbf{r}, \mathbf{r}', \tau) \varphi_{k\mathbf{q}}(\mathbf{r}') \varphi_{l\mathbf{k}}^*(\mathbf{r}'). \quad (2.32)$$

In practice the direct product basis is usually non-orthogonal and overcomplete and it could be useful to introduce an optimized orthogonalized product basis [9] as discussed in Ref. [48] for one of the implementations used in this work. However, as we discuss in detail in Paper IV, the mapping above in general does not require the use of an orthogonalized basis, and in certain cases it could be convenient to keep the direct product basis.

5 The screened interaction and the self-energy

To understand how correlation effects enter the self-energy through the screening it is instructive to have a closer look at W . In the $G^0 W^0$ approximation it follows from the spectral representations of G^0 and Σ that the imaginary part of the self-energy is directly related to the imaginary part of W [8]

$$\begin{aligned} |\text{Im}\Sigma(\mathbf{r}, \mathbf{r}', E)| = & \\ \begin{cases} \sum_i^{\text{occ}} \psi_i(\mathbf{r}) \psi_i^*(\mathbf{r}') \text{Im}W(\mathbf{r}, \mathbf{r}', \epsilon_i - E) \theta(\epsilon_i - E), & \text{if } E \leq \mu \\ \sum_i^{\text{unocc}} \psi_i(\mathbf{r}) \psi_i^*(\mathbf{r}') \text{Im}W(\mathbf{r}, \mathbf{r}', E - \epsilon_i) \theta(E - \epsilon_i), & \text{if } E > \mu \end{cases} \end{aligned} \quad (2.33)$$

Hence, a peak in $\text{Im}W$ at the energy E will produce a peak in $\text{Im}\Sigma$ at the energy $\epsilon_i - E$ for an occupied state and $\epsilon_i + E$ for an unoccupied state. The peak in $\text{Im}\Sigma$

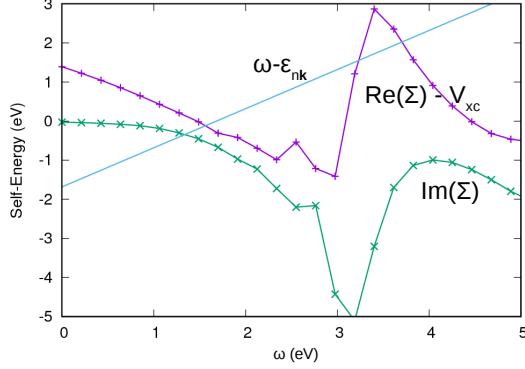


Figure 2.2: G^0W^0 self-energy for SrVO_3 at the R -point. The exchange-correlation potential has been subtracted from the real part. The peaks in the spectral function occurs at their crossings between $\text{Re}\Sigma - V_{xc}$ and the line $\omega - \epsilon_{n\mathbf{k}}$ when $\text{Im}\Sigma$ is small. $\epsilon_{n\mathbf{k}}$ is the LDA eigenvalue.

will produce a corresponding Kramer's Kronig feature in $\text{Re}\Sigma$. Further on, still considering a non-self-consistent calculation and assuming that the self-energy is diagonal in the single particle eigenstates, the spectral function of G is related to the self-energy as [64, 65]:

$$A(\omega) = \frac{1}{\pi} \sum_{\mathbf{k}} \sum_n \frac{|\text{Im}\Sigma_n(\mathbf{k}, \omega - \Delta)|}{(\omega - \epsilon_{\mathbf{k}n} - \text{Re}\Sigma_n(\mathbf{k}, \omega - \Delta) + V_n^{xc}(\mathbf{k}))^2 + (\text{Im}\Sigma_n(\mathbf{k}, \omega - \Delta))^2} \quad (2.34)$$

The shift $\Delta = E_F - \epsilon_F$ where E_F is the new Fermi energy and ϵ_F the Fermi energy of G^0 , assures that $\text{Im}\Sigma$ evaluated at the new Fermi level is zero. In Figure 2.2 we show the G^0W^0 self-energy of an unoccupied t_{2g} -state at the R -point for the cubic perovskite SrVO_3 . Assuming Δ to be negligible in Eq. 2.34 the peak in the spectral function will appear when $\omega - \epsilon_{\mathbf{k}n}$ crosses $(\text{Re}\Sigma_n(\mathbf{k}, \omega) - V_n^{xc}(\mathbf{k}))$ or when the difference between the two quantities is small and at the same time $\text{Im}\Sigma$ is small. In Figure 2.2 the first crossing will produce the quasiparticle peak and the third crossing will produce the satellite. The second crossing occurs roughly at the energy where we would expect the formation of a plasmon satellite. However, at this crossing the imaginary part of the self-energy is large and hence it will not produce any pronounced peak in $A(\omega)$. This kind of reasoning provides important insights about the GW approximation. Experimentally one can observe multiple plasmon satellites with decreasing intensities at the energies $\epsilon_{\mathbf{k}n} + m\omega_p$, where

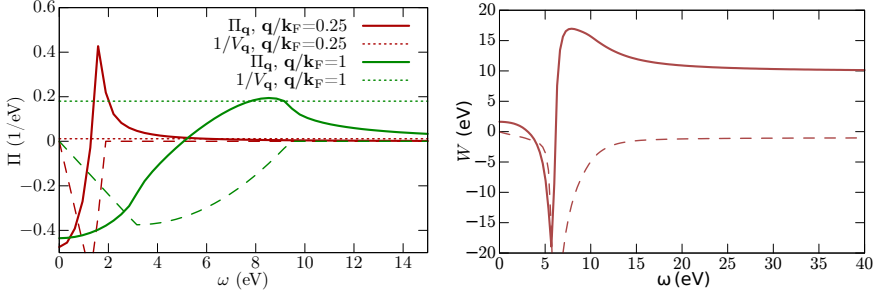


Figure 2.3: Left: The polarization for the non-interacting electron gas for two different \mathbf{q} points. The real part is shown with solid thick lines and the corresponding imaginary part with thin dashed lines. The Fermi energy was chosen to get a filling of $n = 1$ electron. $V_{\mathbf{q}}$ is the bare Coulomb interaction (denoted by $v(\mathbf{q})$ in the text). Right: “Local” projection of W for the electron gas. The real part is shown with solid thick lines and the corresponding imaginary part with thin dashed lines. The artificial unit cell was defined to be cubic with the same volume as the bcc unit cell for Na. With these definitions the local projection of W was defined as the \mathbf{q} sum of $W_{\mathbf{q}}$ in the first Brillouin zone. The figures are adapted from Paper IV.

ω_p is the plasma frequency and m an integer. The GW approximation will only yield a single satellite with an energy separation that is larger than ω_p from the quasiparticle peak. This deficiency with the GW approximation can be cured with the so called cumulant expansion of the Green’s function [11, 60], but the exact form of this expansion is outside the scope of this thesis.

To understand how the plasmon peaks appear in $\text{Im } W$ it is instructive to consider an electron-gas model. Eq. 2.31 can be rewritten as

$$W(\mathbf{q}, \omega) = \epsilon(\mathbf{q}, \omega)^{-1} v(\mathbf{q}), \quad (2.35)$$

where we have defined the dielectric function

$$\epsilon(\mathbf{q}, \omega) = 1 - v(\mathbf{q}) \Pi(\mathbf{q}, \omega). \quad (2.36)$$

Following the reasoning by Bohm and Pines [126] the poles of W will appear at the zeros of ϵ , that is when $\Pi(\mathbf{q}, \omega) = 1/v(\mathbf{q})$. In Figure 2.3 the polarization for the electron gas, calculated within the RPA, is shown together with the line $1/v(\mathbf{q})$. The condition $\Pi(\mathbf{q}, \omega) = 1/v(\mathbf{q})$ is fulfilled when the line $1/v(\mathbf{q})$ crosses $\text{Re}\Pi$ and $\text{Im}\Pi$ is zero. For the given \mathbf{q} -points $1/v(\mathbf{q})$ crosses $\text{Re}\Pi$ at two places. However, since $\text{Im}\Pi$ is large at the first crossing the plasmon pole will instead appear at the energy of the second crossing. For \mathbf{q} -points slightly larger than $q/k_F = 1$ there will not be any crossing and hence W will only have weak features for large \mathbf{q} -values. In the right panel of the same figure the \mathbf{q} -averaged W is shown. A clear

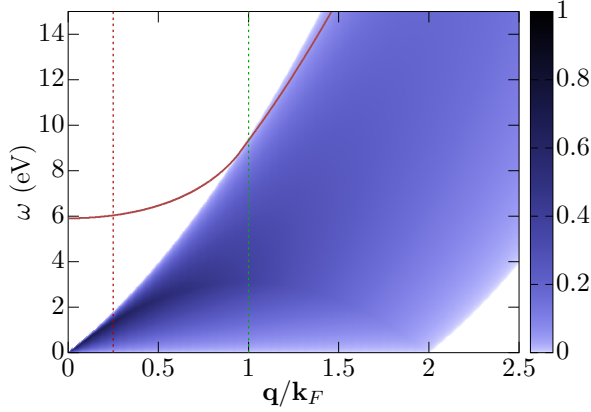


Figure 2.4: The dispersion of the plasma frequency defined by $\min\{|\Pi(\mathbf{q}, \omega) - 1/v(\mathbf{q})|\}$ (the solid red line) shown together with the imaginary part of the polarization for the noninteracting electron gas for different \mathbf{q} and ω values. The two vertical lines correspond to the two \mathbf{q} -points considered in Fig. 2.3. The Figure is similar to the one in Ref. [125] and is adapted from Paper IV.

plasmon peak is visible in $\text{Im}W$ and a corresponding Kramer's Kronig feature in the real part. There are two important conclusions that can be drawn from these considerations. First of all, since the small \mathbf{q} contribution to the plasmon dominates, plasmon excitations are highly nonlocal phenomena and cannot be captured properly by purely local or onsite approximations, such as DMFT. Secondly and related, the plasmon will have a dispersion. In Figure 2.4 the dispersion of the plasmon is shown together with the imaginary part of the polarization. Here it is evident that the plasmon will be damped for large \mathbf{q} since the imaginary part of Π is large for these \mathbf{q} -points.

3

The constrained Random-Phase Approximation (cRPA)

1 Defining a low-energy model

A route to include correlations beyond the GW approximation is to downfold the many-electron problem to a low-energy model that only includes the subspace in which the strongly correlated electrons reside. For transition metal compounds the low-energy model typically includes the $3d$ valence bands or a subset of these and correspondingly for lanthanide compounds the low energy model is typically spanned by the $4f$ valence states. Since the model includes much fewer bands than the complete problem it is possible to solve the downfolded model with more accurate methods.

In second quantized form the Hamiltonian in Eq. 1.3 can be expressed as:

$$\begin{aligned} \hat{H} = & \int dr \hat{\psi}^\dagger(r) \overbrace{\left(-\frac{\nabla^2}{2} + V_{\text{crys}}(\mathbf{r}) + V^{\text{MF}}(\mathbf{r}) \right)}^{H^{\text{MF}}(\mathbf{r})} \hat{\psi}(r) \\ & + \frac{1}{2} \int dr dr' \hat{\psi}^\dagger(r) \hat{\psi}^\dagger(r') \underbrace{\frac{1}{|\mathbf{r} - \mathbf{r}'|}}_{v(\mathbf{r}, \mathbf{r}')} \hat{\psi}(r') \hat{\psi}(r) - \int dr \hat{\psi}^\dagger(r) V^{\text{MF}}(\mathbf{r}) \hat{\psi}(r). \end{aligned} \quad (3.1)$$

In order to improve the single-particle starting point a mean-field potential $V^{\text{MF}}(\mathbf{r})$ has been added to the one-particle part of the Hamiltonian and correspondingly removed from the interaction part. If we now expand the field operators in the

eigenbasis of $H_{\text{MF}} (\{\phi_i\})$;

$$\hat{\psi}^\dagger(\mathbf{r}, \sigma) = \sum_i \phi_i^*(\mathbf{r}) \hat{a}_{i\sigma}^\dagger, \quad (3.2)$$

where $\hat{a}_{i\sigma}^\dagger$ creates an electron in state $|\phi_i\rangle$ with spin σ , the Hamiltonian becomes

$$\hat{H} = \sum_{ij\sigma} \hat{a}_{i\sigma}^\dagger H_{ij}^{\text{MF}} \hat{a}_{j\sigma} + \frac{1}{2} \sum_{ijkl\sigma\sigma'} \hat{a}_{i\sigma}^\dagger \hat{a}_{j\sigma'}^\dagger v_{ilkj} \hat{a}_{k\sigma'} \hat{a}_{l\sigma} - \sum_{ij\sigma} \hat{a}_{i\sigma}^\dagger V_{ij}^{\text{MF}} \hat{a}_{j\sigma}. \quad (3.3)$$

The Coulomb integral is defined as,

$$v_{ijkl} = \int d^3r d^3r' \phi_i^*(\mathbf{r}) \phi_j(\mathbf{r}) v(\mathbf{r}, \mathbf{r}') \phi_k(\mathbf{r}') \phi_l^*(\mathbf{r}'), \quad (3.4)$$

and we have for simplicity assumed a spin-independent single-particle basis.

Now we will consider the specific case of a material with a set of strongly correlated narrow bands around the Fermi energy, like many transition metal and lanthanide compounds. It is convenient to start from a density functional theory calculation, typically within the LDA, and choose $V^{\text{MF}} = V^H + V^{\text{xc}}$, where V^H is the Hartree potential and V^{xc} is the (converged) LDA exchange-correlation potential. Since the LDA cannot treat the strong local Coulomb correlations within the narrow bands these states are typically ill described by only the mean-field Hamiltonian H^{MF} . For the other states, on the other hand, the LDA works relatively well which implies that the double-counting term, $\sum_{ij} \hat{a}_i^\dagger V_{ij}^{\text{MF}} \hat{a}_j$, in Eq. 3.3 almost entirely cancels the contribution from the interaction term to the quasiparticle energies for these states. Hence, we only need to consider the interaction term explicitly for a low-energy model that includes the correlated orbitals, i.e

$$\begin{aligned} \hat{H}^{\text{model}} = & \sum_{\substack{ij \in \text{model} \\ \sigma}} \hat{a}_{i\sigma}^\dagger H_{ij}^{\text{MF}} \hat{a}_{j\sigma} + \frac{1}{2} \sum_{\substack{ijkl \in \text{model} \\ \sigma\sigma'}} \hat{a}_{i\sigma}^\dagger \hat{a}_{j\sigma'}^\dagger U_{ilkj} \hat{a}_{k\sigma'} \hat{a}_{l\sigma} \\ & - \sum_{\substack{ij \in \text{model} \\ \sigma}} \hat{a}_{i\sigma}^\dagger H_{ij}^{\text{DC}} \hat{a}_{j\sigma}. \end{aligned} \quad (3.5)$$

There are two subtleties that makes a downfolding to the low-energy model highly nontrivial:

1. Screening from outside the correlated subspace will reduce the effective Coulomb interaction within the subspace dramatically ($U \ll v$ in Eqs. 3.3-3.5).
2. Since the LDA exchange correlation functional is nonlinear in the density the double-counting term H^{DC} cannot be written as the projection of the mean-field potential on the correlated subspace and is in general ill-defined.

In this thesis we address both these issues. The constrained random-phase approximation, described in the next section, is a way to compute U from the mean-field bandstructure. The problem with the double-counting can be solved by changing the starting point from LDA to a Green's function theory, such as the GW approximation, which will be addressed in Chapter 5.

2 Keeping only the onsite interaction: The Hubbard model

In systems where the valence electrons are sufficiently localized the local, onsite Coulomb interaction will be much larger than the offsite components. It can then be justified to only treat the onsite Coulomb interaction explicitly in the model. This is the idea behind the Hubbard model [77], where the Hamiltonian is divided into a single electron hopping term and an onsite interaction term. In its simplest form, with only one orbital in the low-energy model, it takes the form

$$H = - \sum_{\mathbf{R} \neq \mathbf{R}', \sigma} t_{\mathbf{R}, \mathbf{R}'} \hat{c}_{\mathbf{R}\sigma}^\dagger \hat{c}_{\mathbf{R}'\sigma} + U \sum_{\mathbf{R}} \hat{n}_{\mathbf{R}\uparrow} \hat{n}_{\mathbf{R}\downarrow}, \quad (3.6)$$

where $\hat{c}_{\mathbf{R}\sigma}^\dagger$ creates an electron with spin σ on site \mathbf{R} and $\hat{n}_{\mathbf{R}\sigma} = \hat{c}_{\mathbf{R}\sigma}^\dagger \hat{c}_{\mathbf{R}\sigma}$ is the number operator on site \mathbf{R} .

However, in general we want to derive a Hubbard model for more than one band and also derive the parameters of the model from first principles. For a given model defined by an isolated set of bands, the hopping terms can be derived from the LDA bandstructure by expanding the LDA eigenfunctions in a localized basis (typically defined using maximally localized Wannier functions (MLWF:s) [110, 153, 136, 116] or linear muffin tin orbitals (LMTO:s) [5, 197]). In this work we use MLWF:s which are defined from a subset of the Bloch-eigenstates of the mean-

field (DFT) Hamiltonian ($\phi_{\alpha\mathbf{k}}(\mathbf{r})$) as

$$w_{\mathbf{R}\alpha}(\mathbf{r}) = \frac{V}{(2\pi)^3} \int_{BZ} d\mathbf{k} e^{-i\mathbf{k}\cdot\mathbf{R}} \sum_{\beta} U_{\alpha\beta}^{\mathbf{k}} \phi_{\beta\mathbf{k}}(\mathbf{r}). \quad (3.7)$$

Here $w_{\mathbf{R}\alpha}(\mathbf{r})$ is a Wannier function centred at \mathbf{R} , V is the volume of the unit cell and the integral is over the first Brillouin zone. We have made the Bloch form of the LDA eigenfunctions explicit by including wave-vector quantum number \mathbf{k} and orbital quantum number α separately. The spin has been omitted for simplicity and the orbital quantum number is assumed to span the range of correlated orbitals only. Hence, the number of Wannier functions on each site will be the same as the number of bands from which they are constructed. If the correlated bands are entangled with other crossing bands the procedure in Ref. [153] has to be used. The unitary transformation matrices $U_{mn}^{\mathbf{k}}$ are chosen to minimize the sum of the quadratic spread of the Wannier functions in their home unit cell around their centres (See Refs. [110, 153] for details). Eq. 3.7 can be inverted to yield the Bloch eigenstates as a function of the Wannier functions

$$\phi_{\alpha\mathbf{k}}(\mathbf{r}) = \sum_{\beta} \left(U^{\mathbf{k}} \right)_{\alpha\beta}^{-1} \sum_{\mathbf{R}} e^{i\mathbf{k}\cdot\mathbf{R}} w_{\beta\mathbf{R}}(\mathbf{r}). \quad (3.8)$$

By inserting this definition into the definition of the field operators in Eq. 3.2 and defining

$$\hat{c}_{\beta\mathbf{R}\sigma} = \sum_{\alpha\mathbf{k}} \left(U^{\mathbf{k}} \right)_{\alpha\beta}^{-1} e^{i\mathbf{k}\cdot\mathbf{R}} \hat{a}_{\alpha\mathbf{k}\sigma} \quad (3.9)$$

the Hamiltonian in Eq. 3.5 can be rewritten in a localized basis

$$\begin{aligned} \hat{H}^{\text{model}} = & \sum_{\alpha\beta\mathbf{R}\mathbf{R}'\sigma} \hat{c}_{\alpha\mathbf{R}\sigma}^{\dagger} \left(H_{\alpha\mathbf{R};\beta\mathbf{R}'}^{\text{MF}} - H_{\alpha\mathbf{R};\beta\mathbf{R}'}^{\text{DC}} \right) \hat{c}_{\beta\mathbf{R}'\sigma} \\ & + \frac{1}{2} \sum_{\substack{\alpha\alpha'\beta\beta' \\ \mathbf{R}_{\alpha}\mathbf{R}_{\alpha'}\mathbf{R}_{\beta}\mathbf{R}_{\beta'} \\ \sigma\sigma'}} \hat{c}_{\alpha\mathbf{R}_{\alpha}\sigma}^{\dagger} \hat{c}_{\beta'\mathbf{R}_{\beta'}\sigma'}^{\dagger} U_{\alpha\alpha'\beta\beta'}^{\mathbf{R}_{\alpha}\mathbf{R}_{\alpha'}\mathbf{R}_{\beta}\mathbf{R}_{\beta'}} \hat{c}_{\beta\mathbf{R}_{\beta}\sigma} \hat{c}_{\alpha'\mathbf{R}_{\alpha'}\sigma'}. \end{aligned} \quad (3.10)$$

The matrix elements of the interaction deserves a closer look. Similar to Eq. 3.4 we have

$$U_{\alpha\alpha'\beta\beta'}^{\mathbf{R}_{\alpha}\mathbf{R}_{\alpha'}\mathbf{R}_{\beta}\mathbf{R}_{\beta'}} = \int d^3r d^3r' w_{\alpha\mathbf{R}_{\alpha}}^*(\mathbf{r}) w_{\alpha'\mathbf{R}_{\alpha'}}(\mathbf{r}) U(\mathbf{r}, \mathbf{r}') w_{\beta\mathbf{R}_{\beta}}(\mathbf{r}') w_{\beta'\mathbf{R}_{\beta'}}^*(\mathbf{r}'). \quad (3.11)$$

If the basis functions are sufficiently localized the terms with $\mathbf{R}_\alpha \neq \mathbf{R}_{\alpha'}$ as well as $\mathbf{R}_\beta \neq \mathbf{R}_{\beta'}$ can be neglected since they contain products of Wannier functions localized on different sites. If further on, we assume that the interaction is very short-ranged one can neglect also the remaining intersite terms and keep only the onsite term with $\mathbf{R}_\alpha = \mathbf{R}_{\alpha'} = \mathbf{R}_\beta = \mathbf{R}_{\beta'}$. This approximation yields the multi-orbital Hubbard model:

$$\begin{aligned} \hat{H}^{\text{Hubbard}} = & \sum_{\alpha\beta\mathbf{R}\mathbf{R}'\sigma} \hat{c}_{\alpha\mathbf{R}\sigma}^\dagger (H_{\alpha\mathbf{R};\beta\mathbf{R}'}^{\text{MF}} - H_{\alpha\mathbf{R};\beta\mathbf{R}'}^{\text{DC}}) \hat{c}_{\beta\mathbf{R}'\sigma} \\ & + \frac{1}{2} \sum_{\substack{\alpha\alpha'\beta\beta' \\ \mathbf{R}\sigma\sigma'}} \hat{c}_{\alpha\mathbf{R}\sigma}^\dagger \hat{c}_{\beta'\mathbf{R}\sigma'}^\dagger U_{\alpha\alpha'\beta\beta'} \hat{c}_{\beta\mathbf{R}\sigma'} \hat{c}_{\alpha'\mathbf{R}\sigma}. \end{aligned} \quad (3.12)$$

While it is common practice to neglect the inter-site matrix elements of U this approximation can be dubious and lead to the wrong conclusions, as we will show in Chapter 5. The physical reason for this is that U in general does not contain metallic screening and hence is long-ranged and scales as $\propto \frac{1}{r}$ [46].

3 Effective Coulomb interaction

The constrained random-phase approximation (cRPA) [12] is a method to compute the effective Coulomb matrix elements in Eqs. 3.5 and 3.12 from first principles. The key idea behind the cRPA is to divide the polarization into the model polarization P_{model} and the rest P_{rest} ,

$$P = P_{\text{model}} + P_{\text{rest}}. \quad (3.13)$$

In Fig. 3.1 we illustrate the meaning of the two terms, P_{model} contains all screening from within the model subspace and P_{rest} includes screening from outside the model as well as screening involving transitions between the rest-subspace and the model subspace. We then define U as the partially screened Coulomb interaction (using matrix notation and omitting the \mathbf{k} -index for simplicity)

$$U(\omega) = (1 - P_{\text{rest}}(\omega)v)^{-1} v. \quad (3.14)$$

It can be readily shown that the fully screened interaction W is retrieved if U is further screened by the model polarization

$$W(\omega) = (1 - P_{\text{model}}(\omega)U(\omega))^{-1} U(\omega). \quad (3.15)$$

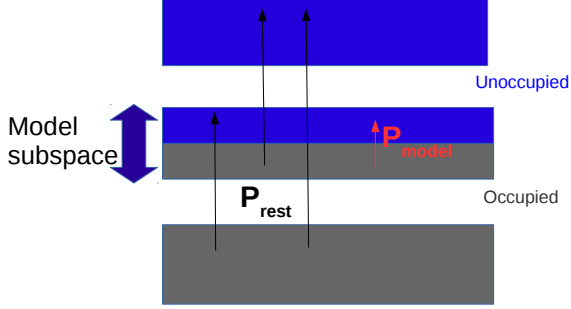


Figure 3.1: Schematic figure of the cRPA approach. The polarization is divided into that of the model (P_{model}) and the rest (P_{rest}).

Eq. 3.15 allows us to interpret $U(\omega)$ as the effective Coulomb interaction in the model subspace. The onsite component of $U(\omega)$ can thus be regarded as a frequency-dependent generalization of the Hubbard U .

While the equations above are exact, in practice the polarization is calculated within the random phase approximation, which for a given spin is given by

$$P(\mathbf{r}, \mathbf{r}'; \omega) = \sum_{\mathbf{k}n}^{\text{occ}} \sum_{\mathbf{k}'n'}^{\text{unocc}} \frac{\phi_{\mathbf{k}n}^*(\mathbf{r}) \phi_{\mathbf{k}'n'}(\mathbf{r}) \phi_{\mathbf{k}'n'}^*(\mathbf{r}') \phi_{\mathbf{k}n}(\mathbf{r}')}{\omega - \epsilon_{\mathbf{k}'n'} + \epsilon_{\mathbf{k}n} + i\delta} - \frac{\phi_{\mathbf{k}n}(\mathbf{r}) \phi_{\mathbf{k}'n'}^*(\mathbf{r}) \phi_{\mathbf{k}'n'}(\mathbf{r}') \phi_{\mathbf{k}n}^*(\mathbf{r}')}{\omega + \epsilon_{\mathbf{k}'n'} - \epsilon_{\mathbf{k}n} - i\delta}. \quad (3.16)$$

The total polarization is the sum over the spin channels and the single-particle orbitals $\{\phi_{\mathbf{k}n}(\mathbf{r})\}$ are usually taken from a DFT calculation within the LDA or Generalized Gradient Approximation GGA. The model polarization is obtained by restricting the sums in Eq. 3.16 to the model subspace.

4 cRPA for entangled bands

While for some materials it is possible to find an isolated set of bands that span the correlated subspace, this is not always the case. For both the lanthanides that we deal with in Paper I and the cuprates that we consider in Paper VI the correlated bands are entangled with other crossing broad bands of s or p character that correspond to extended states. These states are not necessary to include in the minimal

correlated model and therefore it is necessary to employ a method that separates the screening from within the correlated subspace and the rest. There are currently two different, well established ways to achieve this separation.

In the disentanglement method [113], which is the method mainly used in this thesis, the starting Hamiltonian is written on block diagonal form by simply approximating the hybridization between the model and the rest to be zero:

$$\tilde{H} = \begin{pmatrix} H_{\text{model}} & 0 \\ 0 & H_{\text{rest}} \end{pmatrix}.$$

The Wannier functions spanning the model subspace are then constructed to minimize the difference between \tilde{H} and the original Hamiltonian H . In practice this is achieved by choosing the parameters in the Wannier function construction so that the disentangled bandstructure resembles the original band structure as close as possible. Since the fully screened interaction can be computed for both the original (W_{orig}) and disentangled (W_{dis}) bandstructures a quantitative measure of how well the disentanglement method works for a given set of parameters can be obtained by comparing W_{dis} with W_{orig} . Ideally the two quantities should be identical.

Once \tilde{H} is defined the cRPA procedure is identical to the case where the bands are isolated. The main advantage with this approach is that it provides a consistent description of the hopping terms and the interaction terms in Eqs. 3.5 and 3.12 since they are both derived from the same mean-field Hamiltonian \tilde{H} . Also the disentanglement approach assures that all metallic screening from within the correlated bands is removed. In the next section we will consider explicit examples of the cRPA using the disentanglement approach for the lanthanides and the cuprates, however first we will briefly describe what we will call “the weighting approach”, which is a complementary method to treat entangled bands [79].

The weighting approach allows for calculations of U without disentanglement by defining P_{model} as

$$P_{\text{model}}(\mathbf{r}, \mathbf{r}'; \omega) = \sum_{\mathbf{k}n}^{\text{occ}} \sum_{\mathbf{k}'n'}^{\text{unocc}} \left(\frac{\phi_{\mathbf{k}n}^*(\mathbf{r}) \phi_{\mathbf{k}'n'}(\mathbf{r}) \phi_{\mathbf{k}'n'}^*(\mathbf{r}') \phi_{\mathbf{k}n}(\mathbf{r}')}{\omega - \epsilon_{\mathbf{k}'n'} + \epsilon_{\mathbf{k}n} + i\delta} - \frac{\phi_{\mathbf{k}n}(\mathbf{r}) \phi_{\mathbf{k}'n'}^*(\mathbf{r}) \phi_{\mathbf{k}'n'}(\mathbf{r}') \phi_{\mathbf{k}n}^*(\mathbf{r}')}{\omega + \epsilon_{\mathbf{k}'n'} - \epsilon_{\mathbf{k}n} - i\delta} \right) P_{\mathbf{k}n} P_{\mathbf{k}'n'}. \quad (3.17)$$

where $P_{\mathbf{k}n}$ is the probability that the electron in state $|\phi_{\mathbf{k}n}\rangle$ resides in the model subspace. These probabilities can be calculated directly from the Wannier transformation matrices. The advantage with the weighting approach is that it allows for calculations of U without altering the original bandstructure. It also opens up for the possibility of only including the interaction term in Eq. 3.12 for a subset of the orbitals of the Hamiltonian. However, a disadvantage is that, in general, not all metallic screening is removed from U which yields a smaller static value and could lead to an underestimation of the local correlations.

5 Results from Paper I: cRPA for the early lanthanides

In this paper we investigated the screened Coulomb interactions (U and W) for the early lanthanides (Ce-Gd). The lanthanides crystallize in close-packed, fcc or hcp structures. Apart for Eu and Gd, where the majority spin $4f$ -bands are filled and minority spin bands are empty, all materials considered in this paper exhibit a set of narrow, partially filled $4f$ bands in the LSDA bandstructure that hybridize with crossing $6s$ and $5d$ bands. Due to the very localized nature of the $4f$ -states these materials exhibit strong electron correlation effects. A clear example of this was provided in the last chapter, namely that the $G^0 W^0$ approximation is not sufficient to describe the Ce α - γ phase transition [137]. A route to treat the strong correlations is to downfold the problem to a low-energy model using e.g. the cRPA. However, due to the strong electron-electron correlation within the $4f$ -orbitals density functional theory within the LDA provides a rather poor starting point for these materials. On the other hand, in the cRPA the screening from within the $4f$ subspace is removed and thus as long as the LDA yields a good description of the r -subspace states (all states except the $4f$ bands) the method could provide reasonable estimates of U for the lanthanides albeit the poor starting point. Within the cRPA U depends on two factors:

1. The localization and shape of the Wannier basis functions.
2. The screening P_{rest} . However if the model subspace is not isolated, P_{rest} also implicitly depends on the Wannier functions, since these define the model subspace and hence also the the model polarization P_{model} .

The value of the bare Coulomb interaction, on the other hand, only depends on the localization and shape of the Wannier basis functions. More localized Wannier

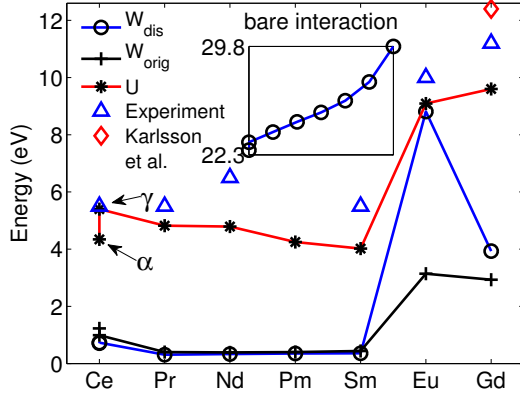


Figure 3.2: The static average direct diagonal matrix element of the fully screened interaction (W) and the partially screened interaction (U) for the Lanthanides. W was calculated both from the original bandstructure (W_{orig}) and the disentangled bandstructure (W_{dis}). The experimental data are estimations of U from XPS and BIS spectra, which is taken from ref. [70]. Karlsson et. al. calculated U using a cRPA based self consistent LDA+ U scheme [85]. The inset shows the average diagonal element of the bare interaction across the series. This figure was taken from Paper I.

functions typically yield a larger bare interaction and thereby also a larger static interaction U . If the model subspace is not isolated there exists a certain freedom in choosing the parameters for the Wannier function construction since, at each \mathbf{k} -point, it is not clear which states should be used to construct the Wannier functions. The more states that are used in the Wannier function construction, the larger the variational freedom and the more localized the Wannier functions. Which states that are used to construct the Wannier functions are determined by an energy window and a band-index range. Only states with an energy inside the energy window and a band index inside the band-index range are used in the Wannier function construction at each \mathbf{k} -point. Typically the parameters for the Wannier functions are chosen such that the disentangled bandstructure mimics the starting bandstructure as closely as possible. A good measure of this is to compare the fully screened interaction computed both for the original (W_{orig}) and disentangled bandstructures (W_{dis}).

To evaluate the accuracy of our cRPA+LDA calculations for these compounds we compared our results with experimental estimates in Ref. [70], where U was estimated from XPS/BIS spectra. For most materials considered in this work U was relatively insensitive to small variations in the parameters in the Wannier function construction and the static U was close to the experimental estimations, although

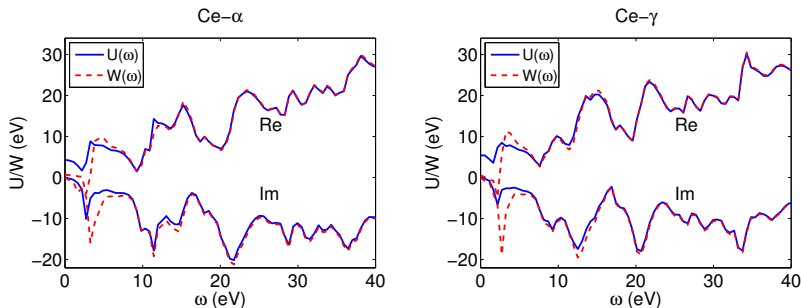


Figure 3.3: Frequency dependent U and W for the two phases of Ce . W was calculated using the disentangled band structure. The figures are adapted from Paper I.

consistently slightly smaller (Fig 3.2). However, especially for Eu the result varied substantially with respect to the energy window. A tight energy window in the Wannier function construction yielded a disentangled bandstructure that was close to the original one but a way too small value of U . On the other hand a large energy window yielded a good estimation of U but a large difference between W_{dis} and W_{orig} . The reason for this is simply that the LDA is not a sufficiently good starting point for Eu. In the LDA bandstructure the majority $4f$ bands are filled but close to the Fermi energy which yields a large hybridization between the $4f$ bands and the crossing $6s$ and $5p$ bands. Due to the large hybridization the Wannier functions become delocalized and the metallic screening is overestimated in P_{rest} , which yields a too small value of U . By the *ad hoc* choice of a large energy window the hybridization is reduced and U is increased to a value close to the experimental estimation. It is interesting to note the opposing trends in U compared to the bare interaction (inset in Figure 3.2). While the bare interaction increases monotonically throughout the series the static value decreases between Nd and Sm. This indicates that the screening from P_{rest} increases, due to the filling of the $4f$ bands, and thereby compensates for the increased bare interaction.

In Figure 3.3 the full frequency dependent U is shown together with the fully screened interactions for $Ce-\alpha$ and γ . Contrary to the electron gas, that only exhibits a single plasmon peak in $\text{Im } W$, the screened interaction for the lanthanides exhibits a rich frequency dependence with a number of subplasmons below and above the main plasmon peak. There are four main features that can be identified in U and W . First there is a low energy peak around 3-4 eV. In W this peak originates from low-energy transitions within the $4f$ -band as well as transitions from the $4f$ band to the crossing bands around the Fermi energy. The difference be-

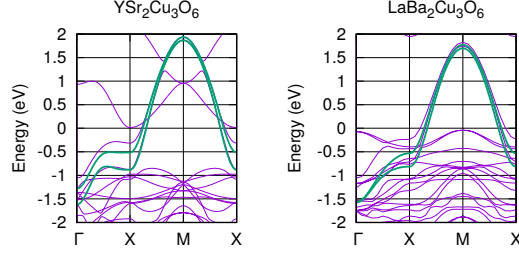


Figure 3.4: LDA and Wannier interpolated bandstructures of $\text{YSr}_2\text{Cu}_3\text{O}_6$ and $\text{LaBa}_2\text{Cu}_3\text{O}_6$. Taken from Paper VI.

tween U and W illuminates the effect of the $f \rightarrow f$ screening that is excluded in the former quantity. The next feature is a peak around 12 eV which corresponds to the main collective plasmon in the system. The energy of this plasmon can be estimated from an electron gas model as $\omega_p = \sqrt{4\pi\rho}$ where ρ is the valence electron density. This gives a value of approximately 13 eV for Ce in rough agreement with the peaks in W and U . The two subsequent pronounced peaks around 20 and 35 eV respectively originate from transitions from the shallow $5s$ and $5p$ core orbitals.

6 Results from Paper VI: cRPA for the cuprates

The crystal structure of all cuprates consist of the superconducting Cu-O layers separated by spacer layers. In most cuprates the in-plane Cu ions are located in an octahedral cage consisting of the four in-plane O ions as well as two apical O below and above the CuO plane. The crystal field splits the Cu $3d$ orbitals into the t_{2g} and e_g components, where the t_{2g} are lower in energy. Furthermore, due to the Jan-Teller distortion, the distance to the apical O is larger than the distance to the in-plane O. This lifts the cubic symmetry and the e_g manifold is split into the d_{z^2} and $d_{x^2-y^2}$ components. While the doped compounds are superconducting the parent compounds are insulating due to the large onsite Coulomb repulsion between the Cu $3d$ holes. However, since the LDA cannot capture the effect of the strong onsite Coulomb interactions the LDA bandstructure for the parent compound is metallic with a conduction band of $d_{x^2-y^2}$ symmetry, which consists of the antibonding combination of the Cu $d_{x^2-y^2}$ and O $p_{x/y}$ orbitals. The bonding and nonbonding bands, of mainly O $p_{x/y}$ -character are approximately 4-8 eV below the Fermi energy. The minimal low-energy model of the cuprates include only

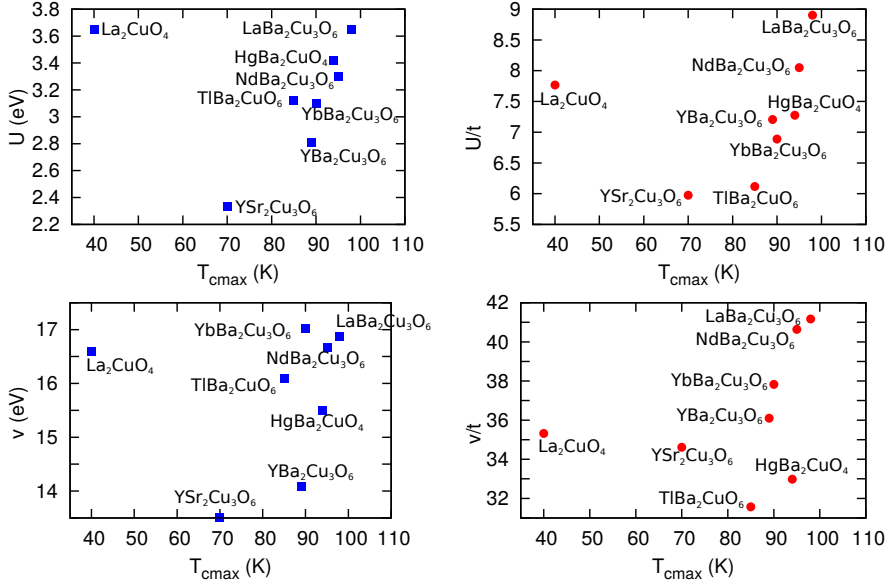


Figure 3.5: Top left: Static value of U in the one-band model for the parent compounds of hole-doped cuprates. Top right: The ratio U/t where t is the nearest neighbour hopping. Bottom left: The bare (unscreened) Coulomb interaction (v) in the one-band model. Bottom right: The ratio v/t . The figures are taken from Paper VI.

the antibonding conduction band (Fig. 3.4), and is therefore commonly referred to as the one-band model.

In Paper VI we compute the effective Coulomb interaction in the one-band model for the parent compounds of a number of hole-doped high- T_c cuprate superconductors using the cRPA. We consider the well-studied La_2CuO_4 as well as $\text{TlBa}_2\text{CuO}_6$, $\text{HgBa}_2\text{CuO}_4$ and the compounds $\text{R}(\text{Ba},\text{Sr})_2\text{Cu}_3\text{O}_6$ ($\text{R}=\text{Y}, \text{Yb}, \text{Nd}, \text{La}$). With the exception of La_2CuO_4 we find a trend between the maximum superconducting transition temperature $T_{c\max}$ and the onsite Coulomb repulsion U , as well as the ratio U/t where t is the nearest neighbour hopping (Fig. 3.5). The trend suggests that superconductivity is favoured by a large onsite Coulomb repulsion. However, that La_2CuO_4 does not follow the trend indicates that a large Coulomb repulsion cannot be the only important parameter to achieve high- T_c superconductivity, there are other mechanisms that hamper superconductivity in this compound. In Fig. 3.5 we show both the effective screened Coulomb interaction U and the corresponding matrix elements of the bare unscreened Coulomb interaction v . While the value of U depends both on the screening in the materials

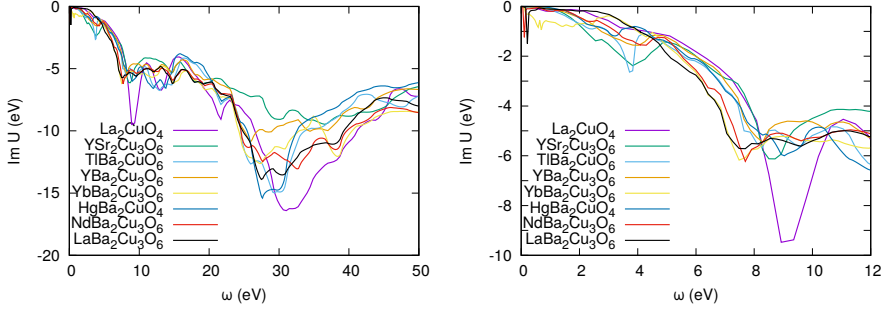


Figure 3.6: Imaginary part of the frequency dependent U for the different cuprates. The right panel shows a close-up on the low-frequency structure. The figures are reproduced from Paper VI.

and the Wannier basis functions, the value of the bare interaction only depends on the shape and extent of the Wannier basis functions. It is clear that ν does not show any clear correlation with $T_{c \max}$ and hence the trend is intimately related to the screening in the compounds.

We also analyse the different screening channels in the compounds by considering the full frequency dependent interaction $U(\omega)$ as well as by selectively removing different screening channels. Through this analysis we conclude that all low-energy screening channels collectively contribute to the trend. For La_2CuO_4 we show that the peak in $\text{Im}U(\omega)$ associated with the screening from the O_p orbitals to the conduction band (pd -screening) is at higher energy and also much more pronounced than in the other compounds (Fig. 3.6). The position of the peak is related to the distance between the O_p bands and the conduction band. Since this distance is larger in La_2CuO_4 than in the other compounds the pd -peak in $\text{Im}U$ also appears at higher energy.

To understand why La_2CuO_4 alludes the trend in U could yield important insights in the origin of the pairing mechanism. In Ref. [181] it was shown that $T_{c \max}$ shows an antilinear correlation with the charge-transfer energy $\epsilon_p - \epsilon_d$. This could provide an explanation of why La_2CuO_4 alludes the trend since this compound has an unusually large charge-transfer energy. Since both a large U and a small charge-transfer gap will push the lower Hubbard band below the p -states, and therefore support the charge-transfer rather than the Mott picture, we speculate that superconductivity may be favoured by having a pure charge-transfer insulating parent compound.

4

Dynamical Mean-Field Theory

I Self-consistent Anderson impurity model

Dynamical mean-field theory (DMFT) [52, 53] may be thought of as a mapping of the Hubbard model to an Anderson impurity model, that is an impurity model coupled to a bath, with the hybridization between the impurity and the bath determined self-consistently in such a way that the impurity Green's function equals the local (onsite) projection of the lattice Green's function. The key observation that makes this mapping possible is that the self-energy becomes local (onsite) in the limit of infinite dimensions ($\Sigma(\mathbf{k}, \omega) \rightarrow \Sigma(\omega)$) [112, 118]. The infinite dimensional case with a local self-energy can then be used as an approximation for solving the Hubbard model in finite dimensions.

For simplicity we will consider the single-band Hubbard model in Eq. 3.6. Assuming an onsite self-energy this Hamiltonian can be mapped to an Anderson impurity model

$$H_{AIM} = \underbrace{\sum_{k\sigma} \tilde{\epsilon}_k \hat{a}_{k\sigma}^\dagger \hat{a}_{k\sigma}}_{\text{bath}} - \underbrace{\mu \sum_{\sigma} \hat{c}_{0\sigma}^\dagger \hat{c}_{0\sigma} + U \hat{n}_{0\uparrow} \hat{n}_{0\downarrow}}_{\text{impurity}} + \underbrace{\sum_{k\sigma} (V_{k\sigma} \hat{a}_{k\sigma}^\dagger \hat{c}_{0\sigma} + V_{k\sigma}^* \hat{c}_{0\sigma}^\dagger \hat{a}_{k\sigma})}_{\text{coupling}}. \quad (4.1)$$

The impurity Green's function for the noninteracting Hamiltonian (i.e. with $U = 0$) is given by

$$\mathcal{G}_{0\sigma}^{-1}(i\omega_n) = i\omega_n + \mu - \Delta_{\sigma}(i\omega_n). \quad (4.2)$$

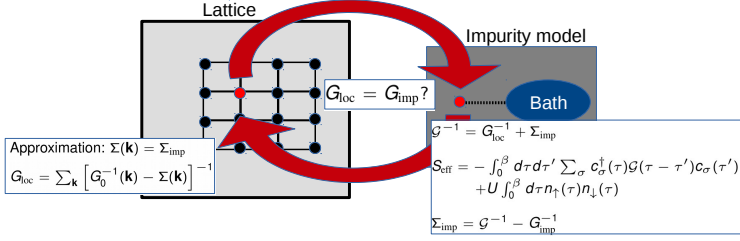


Figure 4.1: Schematic figure of the DMFT self-consistency loop. The effective impurity action in the figure is an example for a single band Hubbard model with static interaction. The figure is reproduced from Paper V.

The hybridization function, $\Delta_\sigma(i\omega_n)$, is defined as

$$\Delta_\sigma(i\omega_n) = \int_{-\infty}^{\infty} d\omega \frac{\Delta'_\sigma(\omega)}{i\omega_n - \omega}, \quad (4.3)$$

where

$$\Delta'_\sigma(\omega) = \sum_k |V_{k\sigma}|^2 \delta(\omega - \tilde{\varepsilon}_k). \quad (4.4)$$

The impurity Green's function for the interacting Hamiltonian is entirely determined by Δ (or equivalently \mathcal{G}), U and μ . In standard DMFT U is assumed to be a fixed parameter and Δ (or equivalently \mathcal{G}) is determined self-consistently so that the impurity Green's function equals the onsite projection of the lattice Green's function. The lattice Green's function can be computed from the impurity self-energy because of the assumption that the lattice self-energy is local. In that sense dynamical mean field theory can be regarded as a self-consistent Anderson-impurity model.

The full self-consistency cycle is depicted schematically in Fig 4.1 and takes the form (the spin index is omitted for readability):

1. Start with an initial guess for Σ^{imp} .
2. According to the DMFT approximation $\Sigma_{\mathbf{k}} = \Sigma^{\text{imp}}$.
3. Calculate $G^{\text{loc}} = \sum_{\mathbf{k}} \left(G_{\mathbf{k}}^{(0)-1} - \Sigma_{\mathbf{k}} \right)^{-1}$.

4. The effective impurity problem is defined by the dynamical Weiss field \mathcal{G} which is calculated by inverting the Dyson equation.

$$\mathcal{G} = \left(\Sigma^{\text{imp}} + \left(G^{\text{loc}} \right)^{-1} \right)^{-1}. \quad (4.5)$$

5. Numerically solve the impurity problem to obtain G^{imp} .
6. Use the current \mathcal{G} to calculate $\Sigma^{\text{imp}} = \mathcal{G}^{-1} - G^{\text{imp}-1}$.
7. Check if the self-consistency condition $G^{\text{imp}} = G^{\text{loc}}$ is fulfilled. If not go back to step 2.

As discussed in Chapter 4.1 the hopping terms can be derived from the LDA band structure. This provides a route to employ DMFT to realistic materials, the so-called LDA+DMFT approach [6, 103, 90, 67].

From the cRPA we know that the effective impurity interaction U for a down-folded model acquires a frequency dependence due to the dynamical screening from the degrees of freedom not accounted for within the model. One way to account for the frequency dependence is to introduce a continuum of additional bosonic fields explicitly in the Hamiltonian. The frequency dependence of the interaction is then represented by the coupling between the fermionic and bosonic fields. For the case with a single bosonic mode this mapping corresponds to the Hubbard-Holstein model [74, 77, 177].

Two approximate ways to solve the generalized Hubbard-Holstein model are the so called dynamic atomic-limit approximation (DALA) [31], which is exact in the limit of $\Delta \rightarrow 0$, and the Lang-Firsov approach. The Lang-Firsov approach relies on a Lang-Firsov transformation [97] that eliminates the electron-boson interaction in the Hubbard-Holstein Hamiltonian, however the solution of the transformed Hamiltonian still requires approximations. One commonly used is the Lang-Firsov approximation which is exact in the limit of infinite plasma frequency [182, 32]. A major advance towards truly first-principle calculations was made upon the introduction of the continuous time quantum Monte-Carlo method (CT-QMC) [184, 185, 186, 188, 58, 182], which provides a numerically exact solution of the impurity problem with a dynamical interaction. In this thesis we have used the hybridization expansion continuous time Monte-Carlo method (CT-hyb), which is a strong coupling approach that relies on an expansion in the

hybridization. The CT-hyb algorithm was originally derived for the Hubbard-Holstein model and then generalized to arbitrary $U(\omega)$, but in Ref. [13] it was derived directly from the imaginary time effective impurity action, which for the single orbital Hubbard model with dynamical interaction $U(\omega)$ is given by

$$S_{\text{eff}} = \sum_{\sigma} \int_0^{\beta} d\tau d\tau' c_{\sigma}^{\dagger}(\tau) \mathcal{G}_0^{-1}(\tau - \tau') c_{\sigma}(\tau') + \frac{1}{2} \int_0^{\beta} d\tau d\tau' n(\tau) U(\tau - \tau') n(\tau'), \quad (4.6)$$

where the fermionic degrees of freedom $\{c_{\sigma}\}$ are described by anticommuting Grassman fields [120]. Solving the impurity problem then means computing the impurity Green's function for the action in Eq. 4.6.

LDA+DMFT has been very successful in describing strongly correlated materials. A famous example is the α - γ isostructural phase-transition in Cerium at approximately 600 K. While both phases have fcc structures the γ phase has a larger volume than the α phase [4]. Experimentally a large reduction of the quasiparticle weight at the Fermi energy is observed in going from the smaller α to the larger γ phase. This reduction originates from an increase of the strong local correlations which is correctly captured by LDA+DMFT [68, 196, 63, 23], but cannot be described with the GW approximation or the LDA [137]. However, there are still a number of problems with LDA+DMFT.

First of all the nonlocal correlations are completely omitted. However, it is not clear for which materials this approximation is valid and for which materials the nonlocal correlations matter. This could potentially lead to misleading conclusions as was shown in Paper III for the cubic perovskite SrVO_3 . It is also worth noting that the frequency dependence of U and \mathbf{k} -dependence of U and Σ have opposing effects. The frequency dependence of U can be incorporated in an effective static value through a bandwidth renormalization. Hence the frequency dependence tend to increase the degree of local correlations by effectively reducing the bandwidth [32]. The \mathbf{k} -dependence of U and Σ , on the other hand, have the opposing effects. The \mathbf{k} -dependence of Σ effectively widens the bandwidth and consequently decrease the effective local correlations [114] and the nonlocal components of U yields a reduction of the effective onsite impurity interaction [141]. Hence there is an uncontrolled cancellation between the frequency dependence of

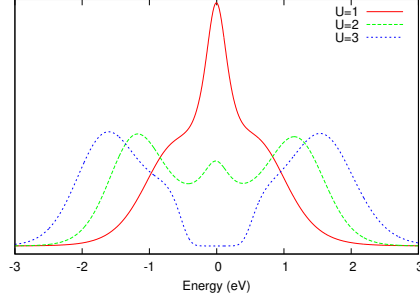


Figure 4.2: Spectral function of the 2D Hubbard model on a square lattice with nearest-neighbour hopping computed with DMFT. The hopping was defined as $t = 0.25$, to give a half-bandwidth of 1, and the calculations were performed for $\beta = 10$. The impurity problem was solved using the Alps CT-hyb impurity solver [3, 184, 185, 22, 61] and the analytic continuation was performed using the maximum entropy method.

U and \mathbf{k} -dependence of U and Σ . While for certain materials, such as La_2CuO_4 , the frequency dependent U is essential to get the correct gap in the spectral function, and therefore the cancellation by the \mathbf{k} -dependence appears to be small (see e.g. Paper II) in other materials the effect of the \mathbf{k} -dependence could be large. A proper treatment of both of these effects is therefore needed, which requires a treatment of both the local and nonlocal interaction and self-energy in the self-consistency cycle. Furthermore, as discussed in Chapter 3, the double-counting term in LDA+DMFT is ill-defined. These issues can be solved by combining DMFT with the GW approximation in the so called GW +EDMFT method [24] discussed in the next chapter. First, however, we will discuss a few basic properties of DMFT applied to simple models.

2 Hubbard bands: The physics of local correlations

2.1 Single-band Hubbard model

In Fig. 4.2 we show the spectral function for the one-band, half-filled, Hubbard model on a square lattice with nearest-neighbour hopping, for different values of the interaction, computed with DMFT. The bare dispersion of this model is given by

$$\epsilon(\mathbf{k}) = 2t(\cos(k_x) + \cos(k_y)) \quad (4.7)$$

For $U = 0$ the spectra is the bare DOS with a bandwidth given by $8t$. As U is increased the quasiparticle bandwidth is decreased and satellite structures appear above and below the quasiparticle peak, corresponding to the lower and upper Hubbard bands. When U reaches a critical value $U = U_c$ the quasiparticle disappears and the system becomes insulating.

In Fermi liquid theory [95, 96] the interacting Green's function for a state close to the Fermi level is assumed to have the form

$$G(i\nu_n, \mathbf{k}) \approx \underbrace{\frac{Z_{\mathbf{k}}}{i\nu_n - \epsilon_{\mathbf{k}}}}_{\text{coherent}} + \underbrace{G_{ic}(i\nu_n, \mathbf{k})}_{\text{incoherent}} \quad (4.8)$$

where the quasiparticle residue $Z_{\mathbf{k}} \leq 1$. Particle conservation then implies that the incoherent part is proportional to $1 - Z_{\mathbf{k}}$. Hence, from a Fermi-liquid theory perspective, increasing U yields a spectral weight transfer from the coherent to the incoherent part of the Green's function. For a large enough U the quasiparticle disappears which corresponds to a complete spectral transfer to the incoherent part. This metal-to-insulator transition, driven by the strong local Coulomb repulsion, is known as the Mott-Hubbard or simply Mott-transition.

To understand the origin of the satellites we will first consider the half-filled single Anderson impurity model in Eq. 4.1. Following the arguments in Ref. [44] we will consider three cases; (A) $U = 0$ but with finite Δ , (B) $\Delta = 0$ but with finite U as well as (C) the intermediate case with both quantities nonzero.

For both $U = 0$ and $\Delta = 0$ the spectra consists solely of a delta peak at the Fermi level corresponding to the impurity energy level. For $U = 0$ but with finite Δ (case A), the hybridization will give a Lorentzian broadening of width Δ of the impurity level at the Fermi energy. In the atomic limit, for zero hybridization on the other hand (case B), the spectra will have two delta-peaks separated by U , corresponding to the energy cost of double occupation. In the intermediate case, with both Δ and U nonzero both of these features will exist simultaneously, the quasiparticle feature at zero frequency with a reduced width compared to the noninteracting case and the two satellite features that are broadened by the hybridization. The width of the middle peak, corresponding to the Kondo resonance of the impurity model, will decrease as U increases. If the bare ($U = 0$) Green's function of the impurity model (\mathcal{G}) is metallic the Kondo resonance of the Anderson impurity model will be present for any finite value of U [119]. In DMFT, the hybridization

is determined self-consistently. The effect of self-consistency is to push the metal-to-insulator transition to a finite critical value of $U = U_c$.

It is interesting to note the different pictures that emerge depending on how the problem is approached. When the problem is approached from the impurity point of view the "quasi-particle" peak at the Fermi level is interpreted as a Kondo-resonance in between the upper and lower Hubbard band. This interpretation appears as a physically reasonable interpretation in the large- U limit where the majority of the spectral weight lies in the Hubbard bands. From a Fermi-liquid perspective the quasiparticle peak is interpreted as the coherent part of the Green's function originating from the non-interacting band structure from a tight-binding picture. This appears to be a physically reasonable interpretation in the small U regime. The self-consistency in DMFT provides a bridge between these two interpretations. By requiring that $G_{\text{loc}} = G_{\text{imp}}$ the Kondo resonance of the impurity problem is mapped to the \mathbf{k} -integrated quasiparticle peak of the lattice problem. In that sense the Kondo resonance can be interpreted as the quasiparticle of the impurity problem.

2.2 Multi-orbital models

For models with more than one orbital the situation becomes more complicated. To make a connection to our results for the cubic perovskites SrVO_3 and SrMoO_3 in paper III-IV we will consider a model with three equivalent orbitals and the Kanamori interaction

$$\begin{aligned}
H_K = & U \sum_a \hat{n}_{a\uparrow} \hat{n}_{a\downarrow} + \frac{1}{2} \sum_{a \neq b} \sum_{\sigma \sigma'} (U' - J \delta_{\sigma \sigma'}) \hat{n}_{a\sigma} \hat{n}_{b\sigma'} \\
& - \sum_{ab} J \underbrace{(\hat{c}_{a\uparrow}^\dagger \hat{c}_{a\downarrow} \hat{c}_{b\downarrow}^\dagger \hat{c}_{b\uparrow})}_{\text{spin-flip}} + \underbrace{(\hat{c}_{b\uparrow}^\dagger \hat{c}_{b\downarrow}^\dagger \hat{c}_{a\uparrow} \hat{c}_{a\downarrow})}_{\text{pair-hopping}}, \tag{4.9}
\end{aligned}$$

which is the form of the interaction for the low-energy t_{2g} orbitals of these systems. For a spherically symmetric system U' and the Hund's coupling J are related as $U' = U - 2J$. SrVO_3 and SrMoO_3 have cubic symmetry and therefore this relation does not exactly hold. However, while the deviation is large for $5d$ orbitals the deviation has been proven to be small for $3d$ orbitals [128] and therefore we will assume the spherically symmetric form of the interaction in the following analysis.

The gap in the spectral function, E_g , is given by the difference between the ionization energy, $E_I = E_0(N-1) - E_0(N)$ and electronic affinity, $E_A = E_0(N) - E_0(N+1)$,

$$E_g = E_0(N-1) + E_0(N+1) - 2E_0(N), \quad (4.10)$$

where $E_0(N)$ is the ground-state energy of the N -electron system. We will consider two cases, $J = 0$ and $J \neq 0$.

Case 1: $J = 0$

For the spherically symmetric parameters $J = 0$ also implies $U' = U$ and hence the intra- and inter-orbital interactions are the same. By considering the energy states of an isolated impurity, i.e. solving $H_K|N\rangle = E_0(N)|N\rangle$ where $|N\rangle$ is one of the degenerate ground states of the impurity occupied with N electrons, it is straightforward to see that

$$E_0(N) = U \frac{N!}{2(N-2)!} = \frac{U}{2} N(N-1). \quad (4.11)$$

Inserting this into Eq. 4.10 for the gap yields $E_g = U$ for all allowed occupations. Hence, the atomic gap is independent on the occupation if $J = 0$. The critical value U_c of the Mott-transition however will increase with the number of degenerate orbitals [59, 107] and the Hubbard bands will be broadened [62]. For a given number of orbitals U_c is maximum at half-filling. This is, in the above mentioned references, explained by an increase in the effective hopping through the orbital degeneracy.

Case 2: Finite J

The case with a finite J was studied extensively in Ref. [39]. It was shown that the Hund's coupling have different effects on U_c depending on the filling. For half-filled cases Hund's coupling enhances the correlations and U_c decreases with J (in agreement with the studies in Refs. [62, 86, 127, 187]) while at integer fillings away from half-filling it pushes the boundary for the Mott-transition to much higher values of U . Using similar arguments as in the $J = 0$ case above, although slightly

more complicated due to the more complicated atomic spectrum, it was shown in Ref. [39] that the gap for the isolated impurity with a finite value of J is given by:

$$E_g = \begin{cases} U - 3J, & \text{away from half filling} \\ U + (N - 1)J, & \text{at half-filling} \end{cases} \quad (4.12)$$

where it is clear that at half filling J works to increase the gap and hence the degree of correlation while away from half filling J has the opposite effect. It was also found that, with weak orbital hybridization (i.e. $t_{ij}^{mm'} \neq t_{ij}^{mm'} \delta_{mm'}$ where m and m' are orbital indices) and in non-degenerate systems, J enforces a decoupling of the bands. This yields a strong dependence on the details of the electronic structure and filling of the individual bands and different bands can display different degrees of electronic correlation.

3 Hubbard bands versus plasmons

Now we will return to the statement in Chapter 2, namely that the $G^0 W^0$ approximation cannot describe the Mott-metal to insulator transition. We will generalize this statement slightly to; 'No first-order approximation in W to the self-energy can yield a complete spectral weight transfer from the quasiparticle features to the incoherent features, like in the Mott-Hubbard metal-to insulator transition.' To prove this we will again consider Eq. 2.34. In order to achieve a complete spectral weight transfer for a state at the Fermi energy the imaginary part of the self-energy has to diverge at the Fermi energy. If we now consider Eq. 2.33 this would mean that $\text{Im} W$ must have a pole at zero frequency. However, from the antisymmetry of the spectral function of W it is evident that $\text{Im} W(\omega = 0) = 0$ [8], and hence the divergence in $\text{Im} \Sigma$ must originate from higher order self-energy diagrams (See Fig. 4.3), i.e. it cannot enter the first order self-energy diagram through W . This reasoning is equivalent to the statement in Ref. [19] that the Mott-transition is driven by the increase (and divergence) of the vertex-corrections.

Thus a practical way to distinguish between plasmons and Hubbard bands is that plasmons are features that enters the self-energy through $W(\omega)$ and Hubbard bands features that enter the self-energy through the higher order diagrams in W (or equivalently through the vertex in the Hedin equations). This definition agrees with the physical intuition that plasmons are long-ranged charge fluctuations, and hence should have a clear dispersion, while Hubbard bands originate mainly from

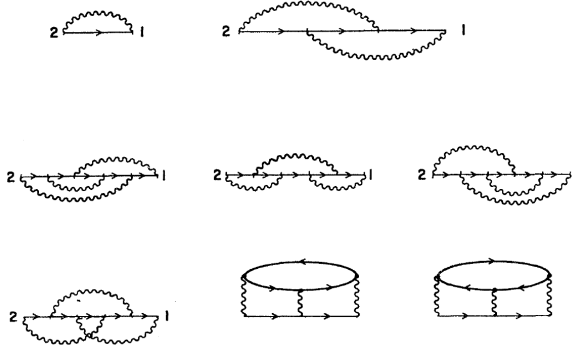


Figure 4.3: The first few diagrams of the self-energy expansion in W . The figure is reproduced from Ref. [64].

local correlations. In practice it means that satellites in the spectral function that can be identified as originating from features in $\text{Im } W$ can be identified as plasmons while features that originate from the onsite static Coulomb repulsion $U(\omega = 0)$ are identified as Hubbard bands.

4 Results from Paper II: LDA+DMFT for La_2CuO_4

A generic feature of the cuprate superconductors is that the crystal structure exhibits Cu-O sheets in between spacer layers of O and lanthanides (Fig. 4.4). While the parent compounds of the cuprates are antiferromagnetic Mott insulators the LDA-bandstructure is metallic with a conduction band of mainly $d_{x^2-y^2}$ symmetry. The most widely used low-energy models for these materials include the orbitals that span the CuO-planes, namely the Cu $d_{x^2-y^2}$ and O p_x/p_y orbitals. In the LDA the conduction band corresponds to the anti-bonding combination of these orbitals while the bonding and nonbonding combinations appear approximately 6 eV below the Fermi energy (right panel in Fig. 4.4).

In Paper II we computed the spectra of La_2CuO_4 , the parent compound of the prototypical high- T_c cuprate superconductor, using LDA+DMFT with *ab-initio* interaction parameters from cRPA. We considered two different models, a one-band model consisting only of the antibonding conduction band and a three band model that included also the bonding and nonbonding combinations (right panel in Fig. 4.4). In addition to the LDA and Wannier interpolated bandstructures in

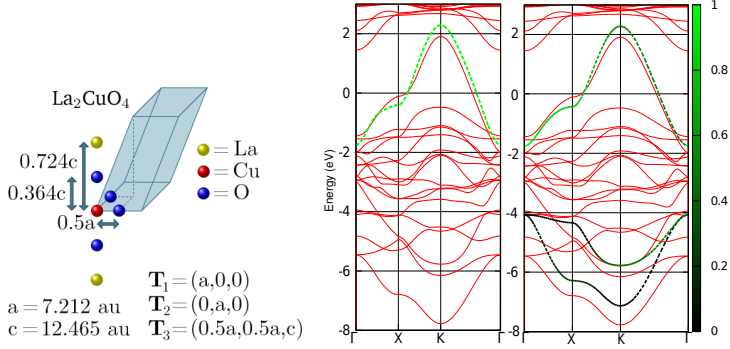


Figure 4.4: Reduced crystal structure (left) and LDA bandstructure (right) for La_2CuO_4 . The disentangled bandstructure is superimposed on top of the LDA bandstructure and the colour coding corresponds to the d -character of the bands which is defined by the projection on the d -like Wannier function. The left panel is taken from Ref [146] and the right panel from Paper II

Fig. 4.4 the colour coding shows the symmetry of the bands, as defined by the projection onto the corresponding Wannier functions. As can be seen, although the conduction band looks similar in the two models, the definition of the $d_{x^2-y^2}$ Wannier function is different. In the one-band model it is derived entirely from the conduction band while in the three band model it contains a small contribution from the two bands below E_F . Even though the main weight of the conduction band comes from the $d_{x^2-y^2}$ Wannier function the mixing yields a much more localized $d_{x^2-y^2}$ Wannier function in the three-band model.

While, in the one band model the definition of P_{rest} and hence $U(\omega)$ is unambiguous, for the three band model which screening channels that should be removed in P_{rest} depends on how the model is solved. A solution of the complete three band model would require us to consider a multi-site impurity problem with a dynamical interaction, including both the Cu and O sites. Since performing DMFT for such a problem was not possible at the time we only treated the d - d interactions within DMFT and the p - p and p - d interactions at the Hartree level. This meant that the p - d screening is not included in the solution of the model, and hence has to be included in $U(\omega)$. Since, as discussed above, the main d -weight is in the conduction band we simply removed the screening from within the conduction band when calculating P_{rest} . I will henceforth refer to this modified three-band model as the d - dp model. With this definition the difference between $U(\omega)$ in the one-band and d - dp models only comes from the Wannier basis functions. Since the $d_{x^2-y^2}$ Wannier function is more localized in the three-band case the corresponding matrix element of U will be larger. In the upper panel of Fig. 4.5 the

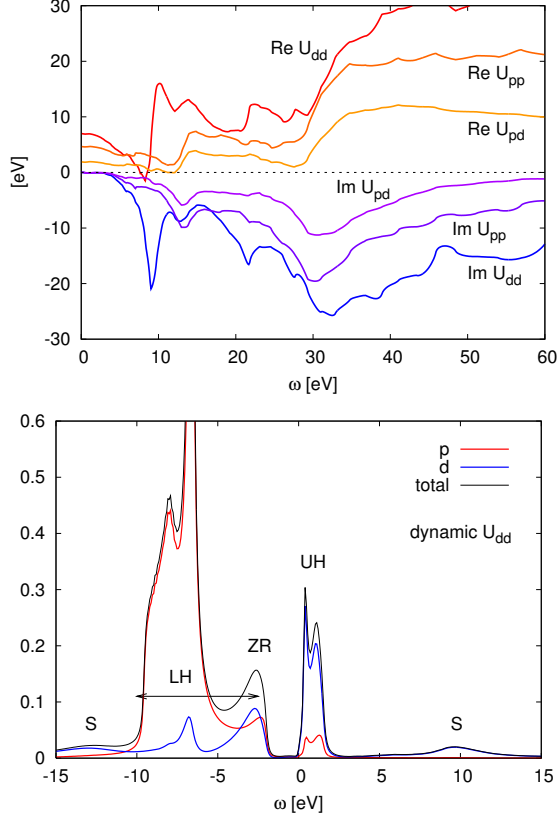


Figure 4.5: Top: Matrix elements of the dynamically screened Coulomb interaction for La_2CuO_4 in the d - dp model computed using the cRPA. Bottom: Spectral function computed within LDA+DMFT with the dynamic interaction $U(\omega)$ from the top panel and an additional Hartree treatment of the p -states (See text and Paper II for details). UH is the upper Hubbard band, ZR the Zhang-Rice singlet, LH the lower Hubbard band and S a plasmon satellite originating from the 9 eV peak in $\text{Im}U(\omega)$. The figures are taken from from Paper II.

matrix elements of $U(\omega)$ in the d - dp model are shown. The static value of U is approximately 7 eV, which is very much reduced compared to the bare interaction due to the large screening. The prominent peak around 9 eV in $\text{Im}U$ comes from transitions between the bonding/nonbonding valence bands and the antibonding conduction band. Since this peak only is present in U_{dd} and not U_{pd} or U_{pp} it has to be localized on the Cu site. This has later been confirmed by Sjöstrand *et al.* in a real-space calculation of U [146].

Traditionally the parent compounds of the cuprate superconductors are thought

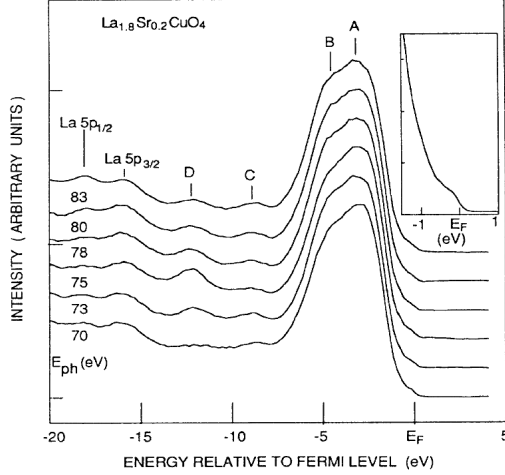


Figure 4.6: The experimental PES-spectra for $\text{La}_{1.8}\text{Sr}_{0.2}\text{CuO}_4$. The three features A B and D were deduced to be of $\text{Cu} 3d$ -character while the peak C is considered to be due to contamination. The data in the figure is for the hole-doped case but a similar result is obtained for the undoped case. The figure is reproduced from Ref. [143].

to be so called charge transfer insulators, with the occupied oxygen p -states in between the upper and lower Hubbard bands [42]. The charge transfer gap, i.e. the gap between the occupied p orbitals and the upper Hubbard band, has experimentally been estimated to around 2 eV using various techniques [55, 165, 41]. In Fig. 4.6 the experimental PES-spectra for La_2CuO_4 is shown. The three features A, B and D were in Ref. [143] deduced to be of $\text{Cu} 3d$ -character. The peak C is considered to be due to contamination and is also absent in more recent PES data [80]. In Ref. [143] the peak labelled D was identified as corresponding to the d^8 configuration and hence corresponding to the lower Hubbard band. This interpretation agrees with the calculations in Ref. [40] using DMFT with a static $U = 9$ eV but not with the LDA+DMFT calculations with a static $U = 8$ eV in Ref. [180] that places the lower Hubbard band closer to the Oxygen p -states.

Contrary to the above mentioned references we solve the impurity problem with a dynamic U computed from first principles within the cRPA. In order to understand the role of the frequency dependence of the interaction we computed the spectral function both with the static $U(\omega = 0)$ and the full dynamic U for both models. We found that the frequency dependence was essential in order to open up a gap in both cases. In the d - dp model (shown in the lower panel of Fig. 4.5) the

gap in the spectral function compared well with experiment but in the one-band case the gap was too small. This suggests that a pure one-band model might not be sufficient to describe the cuprates. The main features in our calculated spectra in Fig. 4.5 are:

- *UH*: The upper Hubbard band.
- *ZR*: A Zhang-Rice singlet of mixed p - d character corresponding to the d^8 ligand hole [193, 40].
- *LH*: A broad feature identified as the lower Hubbard band.
- *S*: A plasmon satellite shown to originate from the p - d peak in $\text{Im}U(\omega)$ at approximately 9 eV.

The position of the peak *S* agrees with the peak *D* in the PES-spectra. Hence our calculations yield a new interpretation of the electronic structure of La_2CuO_4 with the lower Hubbard band in the same energy range as the p -states and the feature below the p -states, found experimentally, explained as a plasmon satellite. The position of the p -states is slightly too low compared to experiment which indicates that the Hartree approximation employed for the p - d and p - p interactions might not be sufficient.

5

GW+EDMFT

As we discussed in the preceding chapters both the GW approximation and LDA+DMFT are successful methods to describe the electronic structure of materials with different degrees of correlation, but both methods suffer from inherent problems. The GW approximation breaks down for materials with strong local correlations and further on self-consistency worsens the spectra. Dynamical mean-field theory on the other hand captures the physics of strong local correlations but neglects the long-range correlations and also has a problem with double-counting. The combination of the GW approximation and dynamical mean-field theory, proposed by Ref. [24] in 2003, provides a suitable path to solve the issues present in the two methods separately, and thereby provides a path to a truly first-principle approach for strongly correlated materials.

I Basic theory

1.1 EDMFT

The combination of GW and dynamical mean-field theory requires the extension of DMFT to an extended framework (EDMFT)[144, 152, 37, 159], where not only the hybridization, but also the effective impurity interaction \mathcal{U} is determined self-consistently. This yields a set of equations for W , \mathcal{U} and the impurity polarization Π_{imp} that are analogous to those of G , \mathcal{G} and Σ_{imp} with an additional self-consistency condition, $W_{\text{imp}} = W_{\text{loc}}$, and an approximation that the polarization is local. Hence EDMFT is a way to account for nonlocal interactions with the approximation of a local polarization computed from the impurity problem. The

EDMFT self-consistency cycle takes the form:

1. Start with an initial guess for Σ^{imp} and Π^{imp} .
2. Use these for the local quantities $\Sigma^{\text{loc}} = \Sigma^{\text{imp}}$ and $\Pi^{\text{loc}} = \Pi^{\text{imp}}$ (EDMFT approximations) .
3. Use $\Sigma_{\mathbf{k}} = \Sigma^{\text{loc}}$ and $\Pi_{\mathbf{k}} = \Pi^{\text{loc}}$.
4. Calculate $G^{\text{loc}} = \sum_{\mathbf{k}} \left(G_{\mathbf{k}}^{(0)-1} - \Sigma_{\mathbf{k}} \right)^{-1}$ and $W^{\text{loc}} = \sum_{\mathbf{k}} (1 - \Pi_{\mathbf{k}} v_{\mathbf{k}})^{-1} v_{\mathbf{k}}$,
5. Use $G^{\text{imp}} = G^{\text{loc}}$ and $W^{\text{imp}} = W^{\text{loc}}$ (EDMFT self-consistency conditions).
6. Calculate the fermionic Weiss field

$$\mathcal{G} = \left(\Sigma^{\text{imp}} + (G^{\text{imp}})^{-1} \right)^{-1} \quad (5.1)$$

and the effective impurity interaction

$$\mathcal{U} = W^{\text{imp}} (1 + \Pi^{\text{imp}} W^{\text{imp}})^{-1} . \quad (5.2)$$

7. Numerically solve the impurity problem to obtain G^{imp} and the impurity charge susceptibility χ^{imp} .
8. Use the current \mathcal{G} and \mathcal{U} to calculate $\Sigma^{\text{imp}} = \mathcal{G}^{-1} - G^{\text{imp}-1}$ and $\Pi^{\text{imp}} = \chi^{\text{imp}} (\mathcal{U} \chi^{\text{imp}} - 1)^{-1}$. The fully screened interaction $W^{\text{imp}} = \mathcal{U} - \mathcal{U} \chi^{\text{imp}} \mathcal{U}$ only enters the calculations through the self-consistency condition in step 5.
9. Go back to step 2.

1.2 GW+EDMFT

EDMFT treats the onsite correlations nonperturbatively to all orders but the non-local correlations are omitted. Since the vertex function in the Hedin equations (Eq. 2.9) can be separated into the sum of the trivial vertex function used in

GW and the non-trivial vertex correction, the Hedin equations for the self-energy (Eq. 2.10) and the polarization (Eq. 2.8) also separate into two components:

$$\Sigma = \Sigma^{GW} + \Sigma^{vc}, \quad (5.3)$$

$$\Pi = \Pi^{GG} + \Pi^{vc}. \quad (5.4)$$

In GW +EDMFT the offsite components of Σ and Π are computed within the GW approximation and the local onsite components are computed to all orders within EDMFT. This is equivalent to approximating Σ^{vc} and Π^{vc} by their impurity counterparts in Eq. 5.4. The double counting is then well defined as the local projection of the GW self-energy and polarization,

$$\Sigma^{GW+EDMFT}(\mathbf{k}) = \Sigma^{GW}(\mathbf{k}) + \Sigma^{EDMFT} - \sum_{\mathbf{k}} \Sigma^{GW}(\mathbf{k}), \quad (5.5)$$

$$\Pi^{GW+EDMFT}(\mathbf{k}) = \Pi^{GG}(\mathbf{k}) + \Pi^{EDMFT} - \sum_{\mathbf{k}} \Pi^{GG}(\mathbf{k}). \quad (5.6)$$

The self-consistency cycle is equivalent to that of EDMFT but with $\Sigma(\mathbf{k})$ and $\Pi(\mathbf{k})$ in step 3 replaced by the corresponding quantities defined in Eqs. 5.5-5.6.

1.3 GW +EDMFT in model calculations

The effect of the long-range exchange and correlations within GW +EDMFT for model systems has been studied extensively in Refs. [19, 13, 75, 14, 15] for the one-band Hubbard model on the 2D square lattice with onsite interaction U , nearest neighbour interaction V and nearest neighbour hopping t . In Ref. [15] it was found that, especially the nonlocal exchange term had a substantial effect on the U - V phase-diagram, pushing the transition to the charge-ordered phase to smaller values of V . This effect was explained by an effective band-widening effect due to the nonlocal exchange term. If this term is neglected (which is the case in Refs. [19, 13, 75], see Refs [14, 15] for details) the phase-diagram is very similar to plain EDMFT. In the Mott-insulating phase the nonlocal screening was found to introduce high-energy satellites in the spectrum [13].

1.4 Functional derivation

The GW +EDMFT approach can, in its complete implementation, be derived from the free energy functional Ψ [24, 2, 37]. In Paper IV we provide a detailed derivation of the GW +EDMFT approach from a functional perspective following Refs. [24, 37, 13, 130]. In this section I will sketch the most important steps and discuss the physical consequences of the derivation. However, first I will discuss the functional derivation of plain DMFT loosely following Refs. [99, 17].

DMFT: Functional derivation

Dynamical mean-field theory can be derived by considering the Baym-Kadanoff functional of the Green's function

$$\Gamma[G] = \text{Tr}[\ln G] - \text{Tr}[(G_0^{-1} - G^{-1})G] + \Phi[G]. \quad (5.7)$$

The stationary point of Γ yields the exact Green's function of the system. The Φ -functional is the sum of all skeleton diagrams (closed, two-particle irreducible Feynman diagrams) constructed from the Green's function and bare Coulomb interaction of the system and G_0 is the noninteracting Green's function of the system. For the case of DMFT our system is represented by the generalized Hubbard Hamiltonian in Eq. 3.12. Since DMFT uses the Hubbard model as a reference system, in this case the interaction is restricted to onsite components. The functional derivative of Φ with respect to the Green's function yields the self-energy

$$\frac{\delta\Phi}{\delta G} = \Sigma. \quad (5.8)$$

Dynamical mean-field theory can be derived by making a local (onsite) projection of the Green's function, that is by expanding the Green's function in a localized basis $\{|w_{\mathbf{R}}^i\rangle\}$, where \mathbf{R} is a lattice vector and i an orbital index.

$$G_{\mathbf{R}\mathbf{R}} \equiv \sum_{ij} |w_{\mathbf{R}}^i\rangle \langle w_{\mathbf{R}}^i| G |w_{\mathbf{R}}^j\rangle \langle w_{\mathbf{R}}^j| \quad (5.9)$$

The DMFT Φ -functional is then defined as

$$\Phi^{\text{DMFT}} = \sum_{\mathbf{R}} \Phi(G_{\mathbf{R}\mathbf{R}}). \quad (5.10)$$

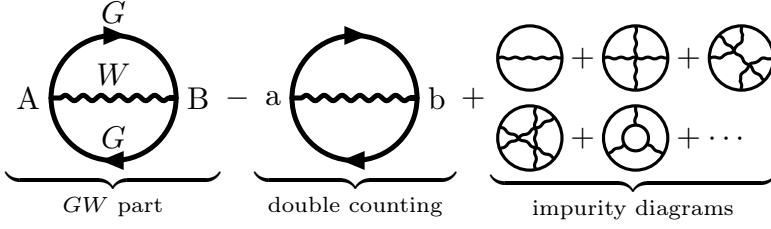


Figure 5.1: Diagrammatic representation of the first few terms in the $GW+EDMFT$ approximation to the Ψ functional. Lower case indices are restricted to the same site and thus correspond to the impurity contribution. Impurity indices for the higher order diagrams as well as combinatorial factors are omitted for readability. The figure is reproduced from Paper IV.

Since the interaction is assumed to be local so is $\Phi(G_{\mathbf{R}\mathbf{R}})$ and thus also the self-energy

$$\Sigma_{\mathbf{R}\mathbf{R}'}^{\text{DMFT}} = \frac{\delta \Phi^{\text{DMFT}}}{\delta G} = \Sigma_{\mathbf{R}\mathbf{R}'} \delta_{\mathbf{R}\mathbf{R}'} \quad (5.11)$$

The lattice model is mapped to an impurity model in Eq. 4.6 with effective bare propagator \mathcal{G} which is determined by the self-consistency condition

$$G_{\text{imp}} = G_{\mathbf{R}\mathbf{R}}. \quad (5.12)$$

Eq. 5.12 implies that the Φ -functional of the impurity problem (Φ^{imp}) also fulfils

$$\Phi^{\text{imp}} = \Phi(G_{\mathbf{R}\mathbf{R}}), \quad (5.13)$$

which together with Eq. 5.11 implies that

$$\Sigma^{\text{DMFT}} = \Sigma^{\text{imp}}. \quad (5.14)$$

GW+EDMFT: Functional derivation

$GW+EDMFT$ requires the generalized free energy functional [2, 37]

$$\begin{aligned} \Gamma[G, W] = & \text{Tr}[\ln(G)] - \text{Tr}[(G_H^{-1} - G^{-1})G] - \frac{\text{Tr}[\ln(W)]}{2} \\ & + \frac{\text{Tr}[(v^{-1} - W^{-1})W]}{2} + \Psi[G, W], \end{aligned} \quad (5.15)$$

which is a functional of both the Green's function G and screened interaction W of the solid. G_H is the Hartree Green's function of the solid and Ψ includes all two-particle irreducible diagrams constructed with G and W .

The Dyson equations,

$$G^{-1} = G_H^{-1} - \frac{\delta \Psi}{\delta G}, \quad (5.16)$$

$$W^{-1} = v^{-1} + 2 \frac{\delta \Psi}{\delta W}, \quad (5.17)$$

follow from requiring that Γ has a stationary point at the exact G and W . The self-energy and the polarization can then be defined as

$$\Sigma = \frac{\delta \Psi}{\delta G}, \quad (5.18)$$

$$\Pi = -2 \frac{\delta \Psi}{\delta W}. \quad (5.19)$$

Analogous to plain DMFT the EDMFT functional corresponds to making an onsite approximation to G and W

$$\Psi^{\text{EDMFT}} = \Psi[G_{\mathbf{RR}}, W_{\mathbf{RRRR}}]. \quad (5.20)$$

The GW approximation corresponds to keeping only the first-order contribution to Ψ in W :

$$\Psi^{GW} = -\frac{1}{2} \text{Tr}[GWG]. \quad (5.21)$$

This yields the full GW +EDMFT functional (schematically shown in Fig. 5.1):

$$\Psi^{GW+\text{EDMFT}}[G, W] = \Psi^{GW} + \Psi^{\text{EDMFT}} - \text{Tr}[G_{\mathbf{RR}} W_{\mathbf{RRRR}} G_{\mathbf{RR}}]. \quad (5.22)$$

The last term constitutes the double-counting term between the GW and EDMFT-functionals.

2 The multitier approach

In principle the GW +EDMFT equations should be solved self-consistently in the entire Hilbert space. However, there are a number of practical problems with this. First of all, it is computationally heavy. It is infeasible to solve a 200 orbital impurity problem, and even if the impurity problem would be restricted to a low-energy subspace (which in principle is allowed by the formalism by restricting the sum over orbitals in Eq. 5.9 to a subspace) self-consistent GW alone for real materials is computationally heavy. However, more importantly, as discussed in Chapter 2 self-consistent GW alone without vertex corrections from DMFT yields a poor spectral function.

In this thesis we have developed a multitier approach where the complete Hilbert space is divided into three subspaces, and each subspace is treated with an appropriate level of approximation. Previous GW +EDMFT calculations for real materials have been restricted to one-shot combinations, combining two separate GW and DMFT calculations [163, 138, 167, 172, 173, 38], and fully self-consistent calculations have only been performed for model systems [84, 13, 75, 171, 157, 15]. The multitier approach developed in Paper III and IV effectively bridges the gap between first-principle calculations and model calculations through a systematic down-folding procedure, therefore allowing for the first *ab initio* fully self-consistent GW +EDMFT calculations for real materials.

The idea behind the multitier approach is sketched in Figure 5.2. The aim with our first-principles approach is accurate descriptions of materials with strong local correlations but also non-negligible long-range correlations, with a reasonable computational cost. Typical examples of such materials are transition metal compounds such as transition metal oxides, transition metal based perovskites as well as cuprate or iron-based high T_c superconductors. To achieve this we employ a three-step procedure:

1. TIER III: First we perform a one-shot GW -calculation in the complete Hilbert space yielding a self-energy $\Sigma^{G^0 W^0}$. We then define an intermediate low-energy subspace, I , typically spanned by 3-10 bands around the Fermi energy. The effective interaction, U , on the intermediate subspace is computed using the cRPA. The $G^0 W^0$ self-energy contribution from within the intermediate subspace is removed from $\Sigma^{G^0 W^0}$ which yields an effective bare propagator on the intermediate subspace, G_k^0 . The construction

of $G_{\mathbf{k}}^0$ is a fermionic analogy of the cRPA construction of U .

2. TIER II: In the intermediate subspace the self-energy is calculated using a self-consistent GW -implementation. A correlated subspace C , which can be smaller or equal to the intermediate subspace, is defined. The local part of the GW self-energy and polarization from within the correlated subspace is subtracted.
3. TIER I: At each step of the self-consistency cycle local vertex corrections to the self-energy and polarization are computed using DMFT. Local vertex corrections are provided within the correlated subspace, which can be smaller or equal to the intermediate subspace.

Within this formalism all double-countings between the tiers are well-defined and the complete Green's function is given by:

$$G_{\mathbf{k}}^{-1} = \underbrace{i\omega_n + \mu - \varepsilon_{\mathbf{k}}^{\text{LDA}} + V_{\text{XC},\mathbf{k}}}_{G_{\text{Hartree},\mathbf{k}}^0} \underbrace{- \left(\Sigma_{\mathbf{k}}^{G^0 W^0} - \Sigma_{\mathbf{k}}^{G^0 W^0} \Big|_I \right)}_{-\Sigma_{\text{r},\mathbf{k}}} \underbrace{- \left(\Sigma_{\mathbf{k}}^{GW} \Big|_I - \Sigma^{GW} \Big|_{C,\text{loc}} + \Delta V_H \Big|_I \right)}_{\text{TIER II}} \underbrace{- \Sigma^{\text{EDMFT}} \Big|_{C,\text{loc}}}_{\text{TIER I}}. \quad (5.23)$$

The self-energies are assumed to only contain the exchange and correlation parts and $\Delta V_H|_I$ is the change of the Hartree potential within the intermediate subspace. A detailed account for how $\Delta V_H|_I$ is calculated is given in Paper IV. The notation $A|_I$ means that all internal sums when evaluating the quantity A are restricted to the subspace I .

The corresponding equation for W is

$$W_{\mathbf{q}}^{-1} = v_{\mathbf{q}}^{-1} \underbrace{- \left(\Pi_{\mathbf{q}}^{G^0 G^0} - \Pi_{\mathbf{q}}^{G^0 G^0} \Big|_I \right)}_{-\Pi_{\text{r},\mathbf{q}}} \underbrace{- \left(\Pi_{\mathbf{q}}^{GG} \Big|_I - \Pi^{GG} \Big|_{C,\text{loc}} \right)}_{\text{TIER II}} \underbrace{- \Pi^{\text{EDMFT}} \Big|_{C,\text{loc}}}_{\text{TIER I}}. \quad (5.24)$$

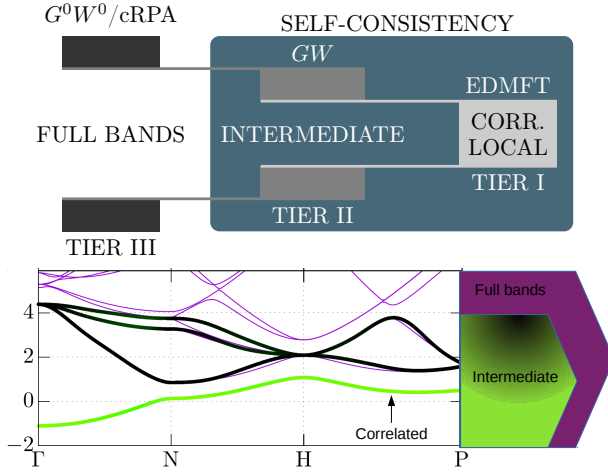


Figure 5.2: Top: A schematic illustration of the different tiers and their relation to the different subspaces, adapted from Paper III. Bottom: A schematic illustration of the different subspaces using the bandstructure of stretched sodium as an example (see section 4.2 for details). Tier III works on the full bands, Tier II on the intermediate subspace and TIER I on the local part of the correlated subspace.

3 Implementation

In Fig. 5.3 the flow of the calculations in our implementation is illustrated. The first step is a DFT calculation using the FLAPW-code FLEUR. [164]. From the DFT bandstructure the low-energy model is defined using MLWF [110, 116, 47, 136]. The interaction on the intermediate subspace and the G^0W^0 self-energy is then computed using the SPEX code [48, 164] which defines the bare propagators for the intermediate subspace [$G_{l,k}^0$ and $U_{l,q}^{-1}$ in Eqs. 5.23-5.24]. Using the initial assumptions

$$\Sigma^{\text{EDMFT}}|_{C,\text{loc}} = \Sigma^{\text{GW}}|_{C,\text{loc}}, \quad (5.25)$$

$$\Pi^{\text{EDMFT}}|_{C,\text{loc}} = \Pi^{\text{GG}}|_{C,\text{loc}}, \quad (5.26)$$

the Green's function and screened interaction can be calculated with Eqs. 5.23-5.24. Then the impurity self-energy ($\Sigma^{\text{EDMFT}}|_{C,\text{loc}}$) and polarization ($\Pi^{\text{EDMFT}}|_{C,\text{loc}}$) are computed using the ALPS CT-Hyb impurity solver [3, 184, 185, 22, 58, 61] which yields a new Green's function and screened interaction. The scheme is then iterated until the self-consistency conditions are fulfilled. The self-consistency cycle on TIERs II and I is implemented using the TRIQS framework [123] together with a customized finite temperature GW -implementation.

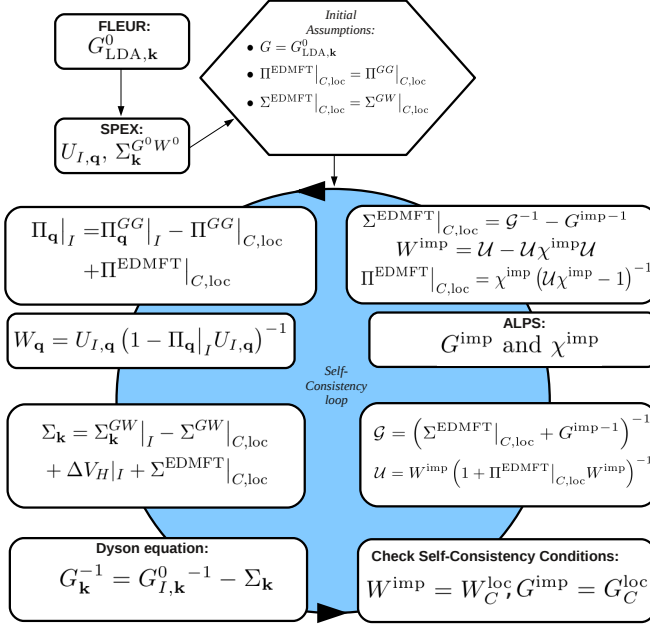


Figure 5.3: Schematic illustration of our implementation of the multitier self-consistent GW4EDMFT method, adapted from Paper IV. The self-energies only include the exchange and correlation parts.

4 Real Materials: A discussion of Paper III-V

4.1 The cubic perovskites SrVO_3 and SrMoO_3

In Paper III we applied our method to the cubic perovskite SrVO_3 and later in Paper IV to the related perovskite SrMoO_3 . However, it should be noted that at the time of writing Paper III, which only considers SrVO_3 , we had no knowledge of the recent experimental and theoretical findings for SrMoO_3 in Ref. [179] discussed below, and our conclusions for SrVO_3 were reached independently from SrMoO_3 . However, in this section I will take a bird's eye perspective and compare the two compounds directly, which I hope will provide a complementary angle to the ones presented in Paper III and IV.

SrVO_3 and SrMoO_3 crystallize in cubic perovskite structure with the V(Mo) atom

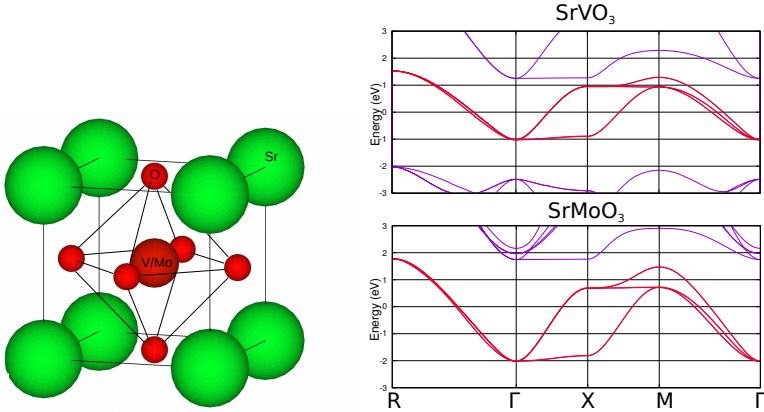


Figure 5.4: Left: Crystal structure (left) and LDA bandstructure (right) for SrVO_3 and SrMoO_3 . The red bands are the t_{2g} like bands.

trapped in an octahedral cage of O atoms (left panel in Figure 5.4). The crystal field splits the V (Mo) $3d$ ($4d$) states into the t_{2g} and e_g manifolds where the t_{2g} are lower in energy. The LDA bandstructure in both compounds exhibit partially filled isolated t_{2g} bands around the Fermi energy while the e_g bands are empty (right panel in Figure 5.4). The $3d$ orbitals in SrVO_3 have a filling of 1 electron per unit cell while the corresponding $4d$ orbitals of SrMoO_3 have a filling of 2 electrons per unit cell. Due to the more delocalized nature of the $4d$ orbitals compared to $3d$ orbitals the bandwidth of the t_{2g} bands in SrMoO_3 is larger than in SrVO_3 .

The experimental PES/IPES spectra of SrVO_3 exhibits a renormalized quasiparticle peak, a weak broad lower satellite feature at approximately -1.5 eV [115, 142, 160, 1, 20] and more pronounced upper satellite feature around 3 eV [115] (Figure 5.5). In the early studies the lower satellite feature was found to be more pronounced. The first data was obtained with low photon energies and Sekiyama *et al.* [142] showed that with higher photon energies the weight of the satellite decreases, indicating the importance of surface effects. Furthermore, the later studies by Backes *et al.* in [20] showed that a large part of the intensity of the lower satellite could be attributed to oxygen vacancies. The bottom of the t_{2g} -band is located around -0.7 eV [142, 20]. Compared to the LDA bandstructure this corresponds to an effective mass enhancement of approximately 2 [191], a number that also agrees with estimations from the specific heat coefficient [81].

While, to my knowledge, there is no IPES spectra for SrMoO_3 the PES spec-

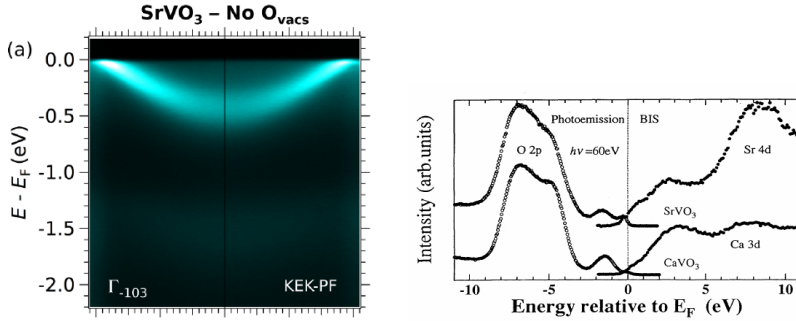


Figure 5.5: Experimental PES spectra of SrVO_3 . The left panel is taken from Ref. [20] and the right panel from [115].

tra exhibits a quasiparticle peak, only very slightly renormalized compared to the LDA bandstructure, and a shoulder structure around -2.5 eV, which indicates correlations effects beyond LDA [179].

Albeit the similarities between the two compounds the explanation of their electronic structure is traditionally different. For SrVO_3 the satellites are traditionally explained as Hubbard bands since they appear in LDA+DMFT calculations with a static effective interaction U [124, 121, 98, 20]. LDA+DMFT studies with a dynamical U computed from the cRPA offers the same explanation of the satellites but yields a too narrow quasiparticle band [138]. Furthermore all these studies place the upper satellite too close to the quasiparticle peak. If the nonlocal self-energy is included from a one-shot GW -calculation the quasiparticle band widens, which improves the agreement with experiment, but depending on if the G^0W^0 self energy is added before [166, 167] or after [138] the DMFT self-consistency cycle the upper satellite either merges with the quasiparticle peak or is placed at the wrong energy. In order to explain the disappearance of the upper satellite feature in Ref. [167] the upper satellite feature was instead reinterpreted as originating from the e_g states. In Paper V we provide a more detailed overview of different simplified GW +DMFT implementations and their results for SrVO_3 .

A different complementary view on the satellites was offered by Gatti *et al.* using a quasiparticle self-consistent GW approximation with the cumulant expansion for the Green's function [51]. While the quasiparticle renormalization in these calculations turned out to be too weak the position and weight of the satellites agrees with the experimental spectra. However, contrary to the DMFT based studies

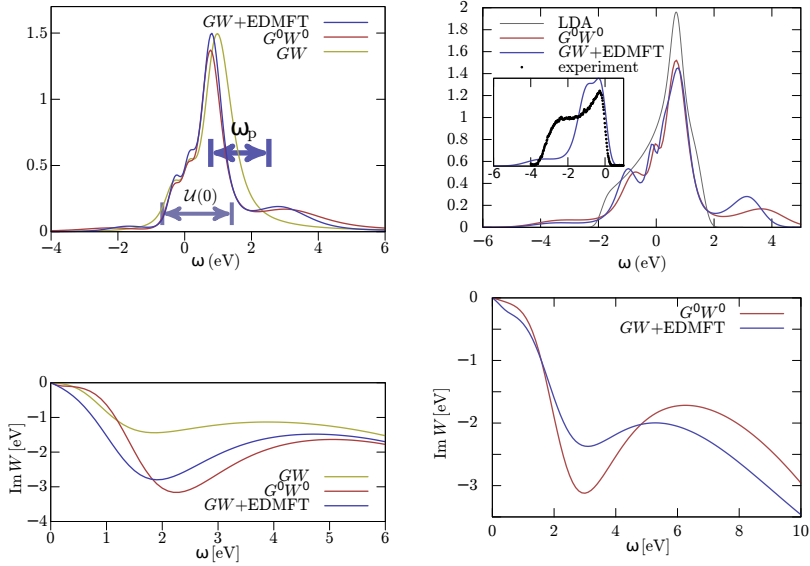


Figure 5.6: Spectral function and screened interaction for SrVO₃ (left) and SrMoO₃ (right). The inset in the top right figure shows the photoemission spectrum part of the GW+EDMFT spectral function and a Gaussian filter has been applied to match the experimental resolution. The experimental data in the inset is taken from Ref. [179]. The figures are adapted from Paper III-IV.

the satellites cannot be interpreted as Hubbard bands, since the strong local correlations that give rise to the formation of Hubbard bands are not accounted for within the theory. The satellites are instead interpreted as plasmons originating from long-ranged charge fluctuations. The DMFT based studies cited above do not account for long-range charge fluctuations that gives rise to plasmons since they lack a self-consistent feedback from the long-range screening to the effective impurity interaction. Hence, methods that only account for the strong local correlations yield an interpretation of the satellites as Hubbard bands while methods that only account for long-range charge fluctuations yields an interpretation of the satellites as plasmons. Since the multitier approach enables for a fully self-consistent GW+EDMFT calculation within the t_{2g} subspace it accounts for both kinds of excitations, and therefore provides the ideal tool to distinguish Hubbard bands from plasmons.

For SrMoO₃, on the other hand, the satellite, or shoulder structure, cannot be described within LDA+DMFT with any reasonable values of U [179]. Therefore, the satellites for this compound are thought to be plasmons.

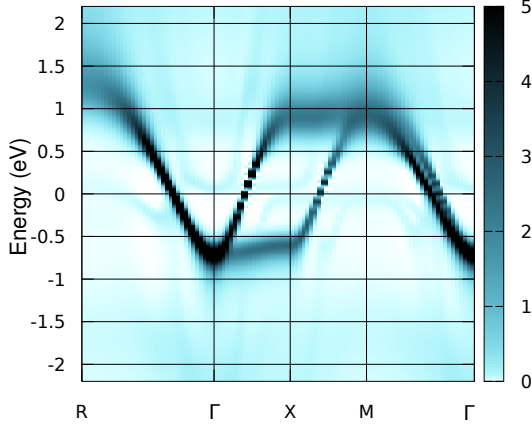


Figure 5.7: \mathbf{k} -resolved spectral function for SrVO_3 in $\text{GW}+\text{EDMFT}$.

In Paper III and IV we show that self-consistent $\text{GW}+\text{EDMFT}$ provides a coherent description of the satellite features as plasmons in both compounds. The long-range screening in SrVO_3 reduce the effective onsite Coulomb interaction \mathcal{U} and clear plasmonic modes appear in \tilde{W} for both compounds (Fig. 5.6). The static \mathcal{U} is too small in both compounds to account for the satellites as Hubbard bands, but the plasmon energy agrees well with the position of the satellites in the spectral function. *Hence, our results suggest that the satellites should be interpreted as plasmons in both SrVO_3 and SrMoO_3 .* Compared to G^0W^0 the satellites are pulled closer to the quasiparticle peak, in agreement with experiment and with the known overestimation of the plasmon binding energy in G^0W^0 .

Although the description of the satellites compare very well with the experimental spectra, for SrVO_3 the quasiparticle bandwidth is slightly overestimated compared to experiment. The $\text{GW}+\text{EDMFT}$ quasiparticle band for this compound closely resembles the G^0W^0 results and the bottom of the conduction band appears at roughly -0.7eV (Figure 5.7). The overestimation of the bandwidth for SrVO_3 can be related to the lack of nonlocal self-energy diagrams, beyond the GW -diagram. In the supplemental material for Paper III we simulate the effect of nonlocal vertex corrections by scaling the bandwidth, and show that our interpretation of the satellite features is not sensitive to the details of the quasiparticle bandstructure.

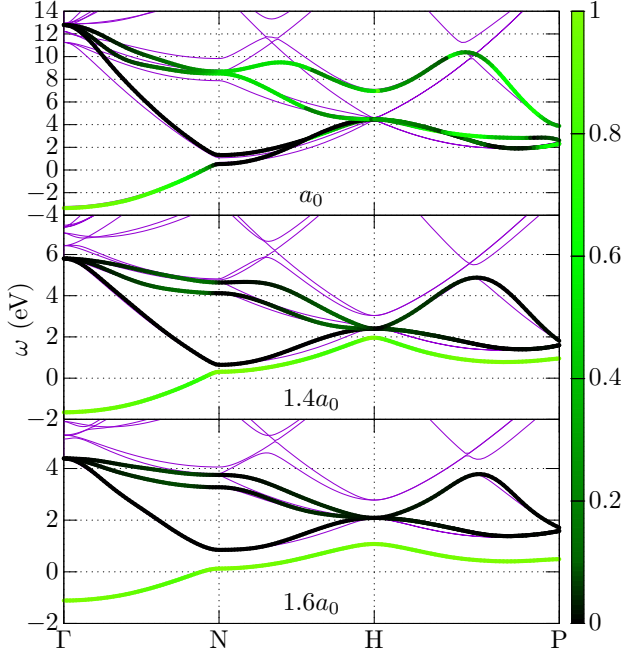


Figure 5.8: Interpolated band structures for Na with different lattice constants a_0 . The solid purple lines show the original LDA bandstructure and the colour coding shows the “ s character” of the bands as defined by the projection on the s -like Wannier function. The figures are taken from from Paper IV.

4.2 Sodium as a model

In order to investigate the performance of the GW +EDMFT method for realistic systems with different degrees of correlation we applied it to stretched sodium in Paper IV. Sodium is an electron-gas-like material with dominating long-ranged plasmonic correlations and is relatively well described within the GW approximation with the cumulant expansion. In Paper IV we used sodium as a starting point and successively increased the lattice constant and thereby effectively increased the degree of local correlations. Albeit there is no experimental data to compare to for the stretched systems, stretched sodium provides a convenient realistic model. Sodium crystallizes in bcc structure and the occupied $3s$ states mix with the unoccupied $3p$ states and form a broad conduction band. For these simulations we constructed the intermediate subspace from the $3s$ and $3p$ orbitals but restricted the correlated subspace to the s -like Wannier function, which is the dominant contribution to the conduction band (Figure 5.8). This allowed us to

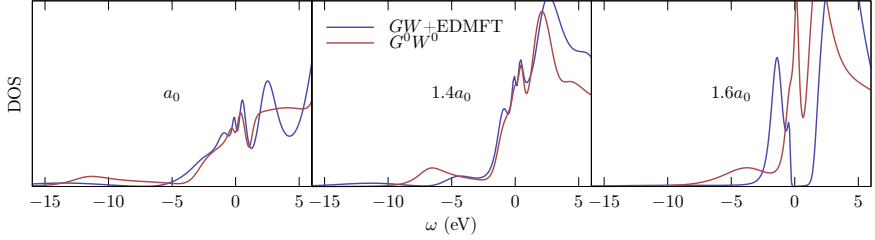


Figure 5.9: Spectral function of stretched sodium with different lattice constants (a_0) computed within $GW+EDMFT$ compared to one-shot GW . The figures are taken from from Paper IV.

explore the full capability of the multitier approach with tier I and tier II working on different subspaces. Our main findings in this investigation were:

1. *The $GW+EDMFT$ method breaks down for electron-gas like systems with weak but long-range correlations.* For elemental sodium with the experimental lattice constant $GW+EDMFT$ fails to describe the spectra (left panel in Fig. 5.9). Similar to $scGW$ the quasiparticle peak is widened and the satellite is almost flushed out and pushed to higher energies. This qualitative failure of the method is related to the lack of nonlocal self-energy and polarization diagrams beyond the first order diagrams included in GW . For systems where the nonlocal corrections become significant $GW+EDMFT$ will suffer from the same flaws as $scGW$, and hence the method breaks down. In the last section of Paper IV we analyse the effect of local approximations to the polarization in detail for an electron gas model.
2. *For moderately to strongly correlated compounds the method works well, and it can capture the Mott-Hubbard metal to insulator transition.* As the lattice constant is increased the nonlocal vertex corrections are expected to diminish and a clear plasmon appears in the spectra (middle panel in Fig 5.9). It is interesting to note that the satellite is pulled closer to the quasiparticle peak in the $GW+EDMFT$ results compared to G^0W^0 . As discussed in Chapter 2 the G^0W^0 approximation overestimates the plasmon energy in the spectral function since it only includes the first-order self-energy diagram in W . $GW+EDMFT$ includes all local self-energy diagrams and therefore does not suffer from this deficiency. For a large enough lattice constant the strong local correlations dominate and the system undergoes a Mott-Hubbard metal to insulator transition (right panel in Fig. 5.9).

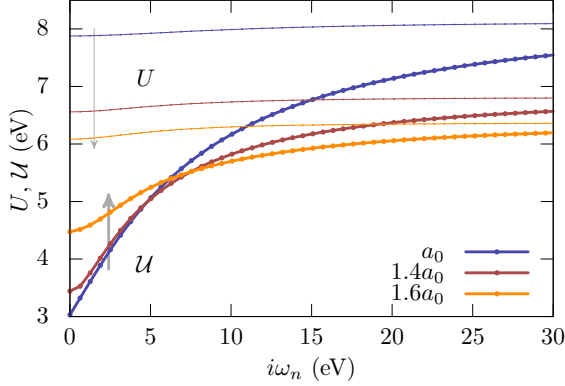


Figure 5.10: Effective impurity interaction \mathcal{U} compared to the cRPA U for stretched sodium with different lattice constants. The figure is taken from Paper IV.

3. *The long-range screening is essential to produce the correct trend in the effective impurity interaction.* In Fig. 5.10 the effective impurity interaction \mathcal{U} is compared to the cRPA U for the three different lattice constants. The cRPA interaction is almost static, implying that the dominating screening channels are included within the intermediate subspace. \mathcal{U} on the other hand has a static value that is significantly reduced compared to the bare high frequency limit due to the nonlocal screening. More importantly however is that U and \mathcal{U} follow opposing trends. While U decreases as the lattice constant is increased \mathcal{U} increases, reflecting the decreasing nonlocal screening in the latter case.

5 Comparison with related methods

GW +EDMFT is not the only path to a description of the solid beyond the local approximations in DMFT, even though it is the most tractable extension for real multi-orbital materials in terms of the computational cost. In this section I will compare GW +EDMFT with other methods to expand DMFT beyond a local approximation. This section is meant as a very brief overview over related methods and I refer to the relevant literature for more detailed descriptions.

There are (at least) two possible distinct paths to extend DMFT to effectively in-

clude nonlocal self-energies:

1. *Cluster extensions of DMFT*: In these methods the lattice problem is mapped onto a cluster of sites embedded in a dynamical bath. While correlations within the cluster are treated unpeturbatively correlations between the clusters are neglected and the exact solution is retrieved in the limit of infinite cluster size. However, the computational cost grows dramatically with increased cluster size and therefore cluster DMFT calculations are restricted to relatively small clusters of approximately 10×10 sites on a 2D lattice [130]. Cluster DMFT methods are reviewed in Ref. [108].

2. *Diagrammatic extensions of DMFT*: GW +EDMFT can be considered as a diagrammatic extension to DMFT, i.e. the local diagrams from DMFT are supplemented by a set of additional nonlocal diagrams which, in the particular case of GW +EDMFT, are computed within the GW approximation. There are alternative routes to diagrammatic extensions, reviewed in Ref. [130]. In this section I will very briefly describe some of these approaches and focus on their relation to GW +EDMFT.

5.1 Vertex Approximations

The vertex function

$$\Gamma(1, 2, 3) = \delta(1 - 2)\delta(2 - 3) + \int d(4567) \frac{\delta \Sigma(1, 2)}{\delta G(4, 5)} G(4, 6) G(7, 5) \Gamma(6, 7, 3)$$

is a central object in the Hedin equations (Eqs. 2.7-2.7). The vertex function can be divided into two parts, the trivial part $\delta(1 - 2)\delta(2 - 3)$, which is kept in the GW approximation, and the nontrivial remainder. In GW +EDMFT the self-energy and polarization are divided as

$$\begin{aligned} \Sigma &= \Sigma^{GW} + \Sigma^{vc} \\ \Pi &= \Pi^{GG} + \Pi^{vc} \end{aligned}$$

and the vertex corrections (vc), originating from the nontrivial part of the vertex function, are approximated by their impurity counterparts. If we now consider the self-energy term (the analogous argument can be made for the polarization),

$$\chi_{\sigma\sigma'}^{kk'q} = -\beta\delta_{kk'}\delta_{\sigma\sigma'} - \text{Diagram}$$

Figure 5.11: Definition of the generalized susceptibility $\chi_{\sigma\sigma'}^{kk'q}$ in terms of the two particle vertex function $F_{\sigma\sigma'}^{kk'q}$. The figure is adapted from Ref. [130].

the full expression for the self-energy is given by

$$\Sigma(1, 2) = iG(1, 2^+)W(1, 2) + i \int d(34)G(1, 3^+)W(1, 4)\Gamma^c(3, 2, 4) \quad (5.27)$$

where $\Gamma^c(1, 2, 3) = \Gamma(1, 2, 3) - \delta(1-2)\delta(2-3)$. Since the entire second term in the self-energy is approximated by its impurity counterpart it means that, in GW +EDMFT, the lattice G and W are used to compute the first part of the self-energy, $iG(1, 2^+)W(1, 2)$, while the impurity G , W and Γ are used in the second part, $i \int d(34)G(1, 3^+)W(1, 4)\Gamma^c(3, 2, 4)$. From a Hedin-equation perspective it might seem more consistent to use the lattice G and W for both terms of the self-energy and only approximate Γ^c by its impurity value (the trivial part of the vertex is local by construction). Such an approximation would also include much more nonlocal diagrams, beyond the GW approximation. This is exactly the approximation done in the so called Triply Irreducible Local Expansion (TRILEX) scheme [16]. In a recent generalization of TRILEX and GW +EDMFT for the 2D Hubbard model to describe superconducting paramagnetic phases within the Nambu formalism, both methods were shown to yield a superconducting dome of $d_{x^2-y^2}$ symmetry, in qualitative agreement with results of cluster DMFT calculations [178].

A more general scheme for vertex approximations is presented in the so called Dynamical Vertex Approximation (D Γ A) [168]. While DMFT assumes the locality of the self-energy, which is the one-particle irreducible vertex, in D Γ A this is generalized to the n -particle level; i.e. the fully n -particle irreducible n -particle vertex (Λ) is assumed to be local. This yields the exact solution of a model with local interaction (i.e. Hubbard model) in the limit $n \rightarrow \infty$. However, for practical calculations one is restricted to $n = 2$, which is called Parquet D Γ A since it relies on the solution of the Parquet equations [168, 130]. QUADRILEX [17]

provides an extension to the Parquet DΓA framework by requiring an additional self-consistency for the two-particle vertex, and is thereby derivable from a free-energy functional. Ladder DΓA is a simplification of DΓA which is necessary for real material calculations (in so called *ab initio* DΓA).

To understand the difference between the different versions of DΓA it is necessary to consider the decomposition of the generalized susceptibility into a disconnected part that describes the free propagation of a particle-hole pair and a connected part that includes all possible scattering processes between the electron and the hole

$$\chi_{\sigma\sigma'}^{kk'q} = -\beta G_k G_{k+q} \delta_{kk'} \delta_{\sigma\sigma'} - G_k G_{k+q} F_{\sigma\sigma'}^{kk'q} G_{k'} G_{k'+q} \quad (5.28)$$

Here $F_{\sigma\sigma'}^{kk'q}$ is the two-particle vertex function, $k = (\nu, \mathbf{k})$ etc. and it was assumed that $G_{k\uparrow\uparrow} = G_{k\downarrow\downarrow} = G_k$ (time and lattice translational invariance SU(2) symmetric and paramagnetic case). This decomposition is shown schematically in Fig. 5.11. The two particle vertex function $F_{\sigma\sigma'}^{kk'q}$ can be further decomposed into a sum of the set of diagrams which are two-particle fully irreducible $\Lambda_{\sigma\sigma'}^{kk'q}$ and the set of diagrams which are two particle reducible in a given channel $\Phi_{\sigma\sigma'}^{l, kk'q}$, l is equal to particle-hole (ph), vertical particle hole (\overline{ph}) or particle-particle (pp) channel,

$$F_{\sigma\sigma'}^{kk'q} = \Lambda_{\sigma\sigma'}^{kk'q} + \Phi_{\sigma\sigma'}^{ph, kk'q} + \Phi_{\sigma\sigma'}^{\overline{ph}, kk'q} + \Phi_{\sigma\sigma'}^{pp, kk'q}. \quad (5.29)$$

This decomposition is shown in Fig. 5.12. By selecting a certain channel (l) all diagrams that are irreducible in that channel can be grouped into the vertex $\Gamma_{\sigma\sigma'}^{l, kk'q}$, which gives the final decomposition of $F_{\sigma\sigma'}^{kk'q}$

$$F_{\sigma\sigma'}^{kk'q} = \Gamma_{\sigma\sigma'}^{l, kk'q} + \Phi_{\sigma\sigma'}^{l, kk'q}. \quad (5.30)$$

Parquet DΓA only assumes the locality $\Lambda_{\sigma\sigma'}^{kk'q}$ while ladder DΓA and *ab initio* DΓA assumes the locality of $\Gamma_{l, \sigma\sigma'}^{kk'q}$. Typically the particle-particle reducible channel is assumed to be local (i.e. $l = ph + \overline{ph}$). In Fig. 5.13 the self-consistency cycle for the different versions of DΓA are compared. It is noteworthy that, in ladder DΓA, first a complete DMFT self-consistency cycle is performed and then the DMFT Green's function and susceptibility is used as input for an additional post-processing step that accounts for the nonlocal corrections through the ladder DΓA flow. Hence, there is no feedback from the nonlocal vertex to the impurity problem.

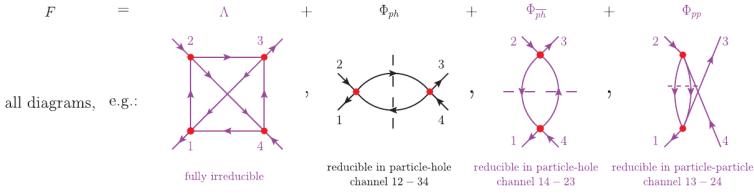


Figure 5.12: Division of $F_{\sigma\sigma'}^{kk'q}$ into into a sum of the set of diagrams which are two-particle fully irreducible $\Lambda_{\sigma\sigma'}^{kk'q}$ and the set of diagrams which are two particle reducible in a given channel $\Phi_{\sigma\sigma'}^{i, kk'q}$. The figure is adapted from Ref. [130]

ab initio D Γ A can be considered as an extension of ladder D Γ A to multi-orbital problems with nonlocal interactions. The nonlocal interaction is accounted for by the approximation of Γ by the corresponding local vertex plus the nonlocal Coulomb interaction.

ab initio D Γ A is of particular interest to this thesis, since similar to our multitier GW +EDMFT formulation it can be applied to real materials. In Ref. [49] the method was applied to SrVO_3 in a one-shot setup, with static onsite interaction and no offsite interaction. Due to the lack of self-consistency and long-range interactions these calculations do not include the plasmonic physics and therefore cannot make any statement about the nature of the satellites. It was found that, while the quasiparticle weight was essentially \mathbf{k} -independent and only slightly enhanced compared to the DMFT results, a large orbital and \mathbf{k} -dependence of the real part of the self-energy yielded a substantial quasiparticle band widening, compared to DMFT.

5.2 Dual expansions and Renormalization Group methods

Other ways to include diagrammatic extensions to DMFT include so called dual expansions of the action (dual fermion and dual boson method) [133, 134, 156] as well as renormalization group methods [111, 162]. Dual Fermion relies on a reformulation of the lattice action of the Hubbard model in dual variables. In practice dual fermion corresponds to a diagrammatic expansion around the DMFT and recovers DMFT as a zeroth order approximation. Similarly dual boson relies on the reformulation of the action of the extended Hubbard model with nonlocal interaction. This requires the introduction of an additional dual bosonic field which decouple the nonlocal interaction terms. The zeroth order approximation then

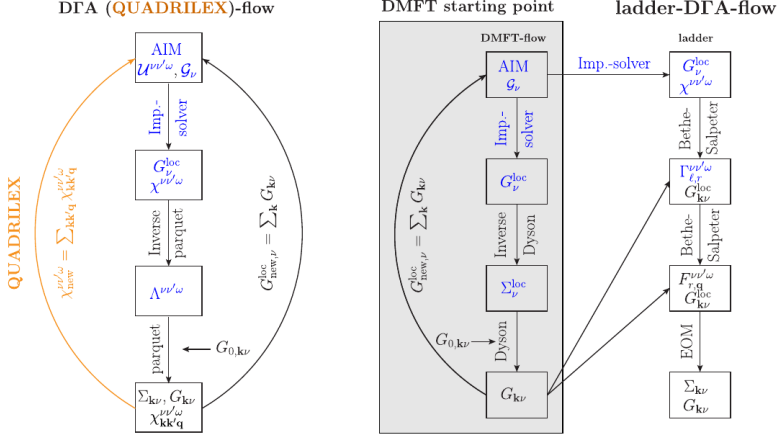


Figure 5.13: Comparison between the self-consistency cycles in Parquet DΓA, QUADRILEX and Ladder DΓA. In all figures four-vector notations were used, i.e. $k = (\nu, \mathbf{k})$. The figure is adapted from Ref. [130].

corresponds to EDMFT. Since none of these methods can be easily compared to our multitier formulation I will not go into further details here.

5.3 Comparison in a multitier context

It is useful to consider the multitier formulation as a more general scheme for *ab initio* calculations that is not restricted to the GW approximation for the nonlocal terms. The multitier formulation can both be used to compare existing schemes and as new methods are developed they can replace the corresponding approximations done on each tier in the multitier GW +EDMFT formulation. Table 5.1 lists and compares different methods that can be cast on a multitier form.

Table 5.1: Relation of existing formalisms to the multitier scheme. Methods which lack an approximation to the polarization Π in TIER II do not update the impurity interaction. The TIER I column lists the quantities that have to be measured in the impurity problem and enter the self-consistency on TIER II. It is implicit that the corresponding double-countings between the tiers are removed, which makes it necessary to add them back on TIER II in the case of $E_{\text{DFA}}^{\text{DFA}}$ and $E_{\text{SEX}}^{\text{DFA}}$, where the full LDA/SEX band values are used in the self-consistency. \emptyset indicates that the corresponding tier is empty. This table is adapted from Paper IV.

Colloquial name	non-sc		selfconsistent		References / Comments
	TIER III	TIER II	TIER II	TIER I used quantities	
model DMFT	Σ	Π	Σ	Σ	Ref. [53]
model EDMFT			local	Σ, Π	Ref. [37]
model DFA			local	Σ, γ^c	Ref. [168] (non-self-consistent)
model GW +EDMFT			SDE ^a /BSE ^b	Σ, Π	Refs. [159, 13, 73, 15]
model TRILEX			GW +imp	Σ, Π, Λ^d	Refs. [16, 18]
$G^0 W^0$			$GW\Lambda$ +imp	\emptyset	often referred to as GW . Ref. [10]
GW	$G^0 W^0$	$G^0 G^0$	\emptyset	\emptyset	rarely used. Refs. [73, 50, 91]
$Q\beta_{\text{sc}}GW$			GW	\emptyset	Refs. [174, 27, 51, 91]
LDA+DMFT			$G^{Qp} W^{Qp}$	\emptyset	Ref. [90]
LDA+DMFT+ $U(\omega)$	$E_{\text{xc}}^{\text{LDA}}$		$G^{Qp} W^{Qp}$	Σ	Ref. [183, 138, 189]
SEX+DMFT	$E_{\text{xc}}^{\text{LDA}}$	$G^0 G^0$	$E_{\text{xc}}^{\text{LDA}}$ +imp	Σ	Ref. [172] (BFA ^e for impurity)
GW +DMFT+ $U(\omega)$	$E_{\text{xc}}^{\text{SEX}}$	$G^0 G^0$	$E_{\text{xc}}^{\text{LDA}}$ +imp	Σ	Ref. [167] (BFA for impurity)
<i>ab initio</i> DFA	$E_{\text{xc}}^{\text{SEX}}$	$G^0 G^0$	$E_{\text{xc}}^{\text{SEX}}$ +imp	Σ	Refs. [169, 49] (non-self-consistent)
GW +EDMFT	$G^0 W^0$	$G^0 G^0$	$G^0 W^0$ +imp	Σ, γ	Refs. [24, 25]
	$E_{\text{xc}}^{\text{LDA}}$		$E_{\text{xc}}^{\text{LDA}}$ +SDE/BSE	Σ, Π	
	$G^0 W^0$	$G^0 G^0$	GW +imp		

^aSchwinger-Dyson equation

^bBethe-Salpeter equation

$c\gamma$ denotes the fully irreducible vertex of the impurity problem

^d Λ denotes the three-leg vertex

^eBFA stands for Bose Factorization Approach [31]

6

Summary and Outlook

The aim of this thesis is to provide accurate descriptions of strongly correlated materials, such as transition metal and lanthanide compounds, from first principles. Due to the localized nature of the $3d$ or $4f$ valence states in these compounds they exhibit strong electron-electron correlation effects. In practice this means that the onsite Coulomb repulsion between two electrons on the same site becomes comparable or larger than the kinetic energy of the electrons. Due to the strong onsite Coulomb interaction in these materials it is not clear that a mean-field treatment, such as a bandstructure calculation using density functional theory (DFT), or a perturbative treatment, such as the GW approximation, will work. In fact, for some of these compounds DFT with the local density approximation (LDA) and the GW approximation even gives qualitatively wrong results and predicts a metal when the actual system is insulating. Dynamical mean-field theory (DMFT) offers a route to treat the strong onsite correlations in a non-perturbative fashion but in turn neglects the correlation between electrons on different sites. In LDA+DMFT the complete problem is downfolded to a low energy problem that only includes the subspace where the strongly correlated electrons reside. The hopping parameters for the low-energy model can be computed directly from the LDA bandstructure and the interaction parameters can be computed using the constrained random-phase approximation. However, LDA+DMFT suffers from a double-counting problem, since it is not clear how to subtract the correlations that are already included in the LDA. Furthermore, the offsite correlations are neglected and it is not clear how these will influence the results. The combination of GW and DMFT into so called GW +DMFT or GW +EDMFT provides a way to include the nonlocal correlations perturbatively and also does not suffer from the double counting problem.

This thesis consists of two parts:

1. In Paper I and VI we use the cRPA to compute the effective Coulomb interaction $U(\omega)$ for a number of lanthanide and cuprate compounds. $U(\omega)$ can already tell us a lot about the materials, such as the degree of local correlations, and from the frequency dependence we can predict plasmon satellites in the spectral function. In Paper II we use the cRPA U in an LDA+DMFT calculation for the parent compound of the high- T_c cuprate superconductor La_2CuO_4 and show that a proper treatment of the frequency dependence is essential in order to reproduce the experimental spectral function. Actually the feature below the Oxygen p -states that is commonly interpreted as the lower Hubbard band turns out to be a plasmon satellite entering the spectral function through the frequency dependence of the effective Coulomb interaction $U(\omega)$.
2. In Paper III-V we develop and employ a multitier combination of GW and EDMFT (multitier GW +EDMFT). The multitier approach enables us to perform first-principle, self-consistent GW +EDMFT calculations for real materials. Our calculations are the first fully self-consistent GW +EDMFT calculations for real materials. We show that the effect of self-consistency can be large. The nonlocal screening effectively lowers the degree of local correlations and introduces plasmon satellites in the spectral function. Using our approach we show that, for SrVO_3 , the satellites that have previously been interpreted as Hubbard bands should in fact be interpreted as plasmons. For the related cubic perovskite SrMoO_3 where LDA+DMFT qualitatively fails to describe the spectral function, we show that the additional inclusion of the nonlocal correlations from GW improves the agreement with experiment substantially and contrary to LDA+DMFT our approach describes the experimentally observed satellites. We also investigate the range of applicability of the GW +EDMFT method using stretched sodium as a model system and discuss different technical aspects of the method in Paper IV.

The multitier GW +EDMFT approach developed in this thesis works well and provides new insights on the electronic structure of the compounds considered in this work. However, the method is still relatively untested and need to be applied to more materials before we can make a final statement on the usefulness of the approach. To be able to compete with the standard approaches such as LDA+DMFT

and apply it larger systems it would be good to improve the parallelization of the code. At the moment the GW part is parallelized with OpenMP, and hence the computations are restricted to single nodes with shared memory.

For SrVO_3 in Paper III it was observed that GW +EDMFT overestimates the quasiparticle bandwidth slightly due to the lack of nonlocal contributions beyond GW . Diagrammatic extensions to DMFT that go beyond GW for the nonlocal terms were briefly discussed in Chapter 5.6 and include Dynamical vertex approximation, TRILEX, QUADRILEX and dual boson/fermion. These methods are promising candidates for descriptions that go beyond GW for the nonlocal terms but, due to the complexity of the problem, have not yet been implemented in a self-consistent fashion for real materials. Cluster extensions to DMFT provides a different path for a non-perturbative treatment of nonlocal correlations.

Acronyms

DFT	Density Functional Theory
LDA	Local Density Approximation
DMFT	Dynamical Mean Field Theory
PES	Photo-Emission Spectroscopy
IPES	Inverse Photo-Emission Spectroscopy
ARPES	Angle-resolved PES
BIS	Bremsstrahlung Isochromate Spectroscopy
CT-QMC	Continuous-time Quantum Monte-Carlo
CT-hyb	Hybridization expansion continuous time Monte-Carlo

I References

- [1] S. Aizaki, T. Yoshida, K. Yoshimatsu, M. Takizawa, M. Minohara, S. Ideta, A. Fujimori, K. Gupta, P. Mahadevan, K. Horiba, H. Kumigashira, and M. Oshima. Self-energy on the low- to high-energy electronic structure of correlated metal SrVO_3 . *Physical Review Letters*, 109:056401, 2012.
- [2] C. O. Almbladh, U. von Barth, and R. van Leeuwen. Variational total energies from ϕ - and ψ - derivable theories. *International Journal of Modern Physics B*, 13:535–541, 1999.
- [3] ALPS collaboration. ALPS project. <http://alps.comp-phys.org>.
- [4] B. Amadon, S. Biermann, A. Georges, and F. Aryasetiawan. The α - γ transition of Cerium is entropy driven. *Physical Review Letters*, 96:066402, 2006.
- [5] O. K. Andersen. Linear methods in band theory. *Physical Review B*, 12:3060–3083, Oct 1975.
- [6] V. I. Anisimov, A. I. Poteryaev, M. A. Korotin, A. O. Anokhin, and G. Kotliar. First-principles calculations of the electronic structure and spectra of strongly correlated systems: dynamical mean-field theory. *Journal of Physics: Condensed Matter*, 9:7359, 1997.
- [7] ARPESgeneral. (<https://commons.wikimedia.org/wiki/File:ARPESgeneral.png>), marked as public domain.
- [8] F. Aryasetiawan. The GW approximation. In V. I. Anisimov, editor, *Strong Coulomb correlations in electronic structure calculations . Beyond the local density approximation*, pages 1–95. Gordon and Breach, 2000.
- [9] F. Aryasetiawan and O. Gunnarsson. Product-basis method for calculating dielectric matrices. *Physical Review B*, 49:16214–16222, 1994.
- [10] F. Aryasetiawan and O. Gunnarsson. The GW method. *Reports on Progress in Physics*, 61:237, 1998.
- [11] F. Aryasetiawan, L. Hedin, and K. Karlsson. Multiple plasmon satellites in Na and Al spectral functions from ab initio cumulant expansion. *Physical Review Letters*, 77:2268–2271, 1996.

- [12] F. Aryasetiawan, M. Imada, A. Georges, G. Kotliar, S. Biermann, and A. I. Lichtenstein. Frequency-dependent local interactions and low-energy effective models from electronic structure calculations. *Physical Review B*, 70:195104, 2004.
- [13] T. Ayral, S. Biermann, and P. Werner. Screening and nonlocal correlations in the extended Hubbard model from self-consistent combined GW and dynamical mean field theory. *Physical Review B*, 87:125149, 2013.
- [14] T. Ayral, S. Biermann, and P. Werner. Erratum: Screening and nonlocal correlations in the extended Hubbard model from self-consistent combined GW and dynamical mean field theory [Physical Review B 87, 125149 (2013)]. *Physical Review B*, 94:239906, 2016.
- [15] T. Ayral, S. Biermann, P. Werner, and L. Boehnke. Influence of Fock exchange in combined many-body perturbation and dynamical mean field theory. *Physical Review B*, 95:245130, 2017.
- [16] T. Ayral and O. Parcollet. Mott physics and spin fluctuations: A unified framework. *Physical Review B*, 92:115109, 2015.
- [17] T. Ayral and O. Parcollet. Mott physics and collective modes: An atomic approximation of the four-particle irreducible functional. *Physical Review B*, 94:075159, 2016.
- [18] T. Ayral and O. Parcollet. Mott physics and spin fluctuations: A functional viewpoint. *Physical Review B*, 93:235124, 2016.
- [19] T. Ayral, P. Werner, and S. Biermann. Spectral properties of correlated materials: Local vertex and nonlocal two-particle correlations from combined GW and dynamical mean field theory. *Physical Review Letters*, 109:226401, 2012.
- [20] S. Backes, T. C. Rödel, F. Fortuna, E. Frantzeskakis, P. Le Fèvre, F. Bertran, M. Kobayashi, R. Yukawa, T. Mitsuhashi, M. Kitamura, K. Horiba, H. Kumigashira, R. Saint-Martin, A. Fouchet, B. Berini, Y. Dumont, A. J. Kim, F. Lechermann, H. O. Jeschke, M. J. Rozenberg, R. Valentí, and A. F. Santander-Syro. Hubbard band versus oxygen vacancy states in the correlated electron metal SrVO₃. *Physical Review B*, 94:241110, 2016.

- [21] G. Baldini and B. Bosacchi. Optical properties of Na and Li Halide crystals at 55 °K. *Physica Status Solidi (B)*, 38:325–334, 1970.
- [22] B. Bauer, L. D. Carr, H. G. Evertz, A. Feiguin, J. Freire, S. Fuchs, L. Gamper, J. Gukelberger, E. Gull, S. Guertler, A. Hehn, R. Igarashi, S. V. Isakov, D. Koop, P. N. Ma, P. Mates, H. Matsuo, O. Parcollet, G. Pawłowski, J. D. Picon, L. Pollet, E. Santos, V. W. Scarola, U. Schollwöck, C. Silva, B. Surer, S. Todo, S. Trebst, M. Troyer, M. L. Wall, P. Werner, and S. Wessel. The ALPS project release 2.0: open source software for strongly correlated systems. *Journal of Statistical Mechanics: Theory and Experiment*, 2011:P05001, 2011.
- [23] J. Bieder and B. Amadon. Thermodynamics of the α - γ transition in Cerium from first principles. *Physical Review B*, 89:195132, 2014.
- [24] S. Biermann, F. Aryasetiawan, and A. Georges. First-principles approach to the electronic structure of strongly correlated systems: Combining the GW approximation and dynamical mean-field theory. *Physical Review Letters*, 90:086402, 2003.
- [25] L. Boehnke, F. Nilsson, F. Aryasetiawan, and P. Werner. When strong correlations become weak: Consistent merging of GW and DMFT. *Physical Review B*, 94:201106, 2016.
- [26] Lewin Boehnke. Bryan MaxEnt analytical continuation. <http://www.bitbucket.com/lewinboehnke/maxent>.
- [27] F. Bruneval, N. Vast, and L. Reining. Effect of self-consistency on quasi-particles in solids. *Physical Review B*, 74:045102, 2006.
- [28] R. K. Bryan. Maximum entropy analysis of oversampled data problems. *European Biophysics Journal*, 18:165–174, 1990.
- [29] F. Caruso, P. Rinke, X. Ren, A. Rubio, and M. Scheffler. Self-consistent GW: All-electron implementation with localized basis functions. *Physical Review B*, 88:075105, 2013.
- [30] F. Caruso, P. Rinke, X. Ren, M. Scheffler, and A. Rubio. Unified description of ground and excited states of finite systems: The self-consistent GW approach. *Physical Review B*, 86:081102, 2012.

- [31] M. Casula, A. Rubtsov, and S. Biermann. Dynamical screening effects in correlated materials: Plasmon satellites and spectral weight transfers from a Green's function ansatz to extended dynamical mean field theory. *Physical Review B*, 85:035115, 2012.
- [32] M. Casula, P. Werner, L. Vaugier, F. Aryasetiawan, T. Miyake, A. J. Millis, and S. Biermann. Low-Energy Models for Correlated Materials: Bandwidth Renormalization from Coulombic Screening. *Physical Review Letters*, 109:126408, 2012.
- [33] S. A. Chambers, T. Droubay, T. C. Kaspar, M. Gutowski, and M. van Schilfgaarde. Accurate valence band maximum determination for SrTiO_3 (0 0 1). *Surface Science*, 554:81–89, 2004.
- [34] A. N. Chantis, M. van Schilfgaarde, and T. Kotani. Ab initio prediction of conduction band spin splitting in zinc blende semiconductors. *Physical Review Letters*, 96:086405, 2006.
- [35] A. N. Chantis, M. van Schilfgaarde, and T. Kotani. Quasiparticle self-consistent GW method applied to localized $4f$ electron systems. *Physical Review B*, 76:165126, 2007.
- [36] J. T. Chayes, L. Chayes, and Mary Beth Ruskai. Density functional approach to quantum lattice systems. *Journal of Statistical Physics*, 38:497–518, 1985.
- [37] R. Chitra and Gabriel Kotliar. Effective-action approach to strongly correlated fermion systems. *Physical Review B*, 63:115110, 2001.
- [38] S. Choi, A. Kutepov, K. Haule, M. van Schilfgaarde, and G. Kotliar. First-principles treatment of Mott insulators: linearized QSGW+DMFT approach. *Npj Quantum Materials*, 1:16001, 2016.
- [39] L. de' Medici. Hund's coupling and its key role in tuning multiorbital correlations. *Physical Review B*, 83:205112, 2011.
- [40] L. de' Medici, X. Wang, M. Capone, and A. J. Millis. Correlation strength, gaps, and particle-hole asymmetry in high- T_c cuprates: A dynamical mean field study of the three-band copper-oxide model. *Physical Review B*, 80:054501, 2009.

- [41] D. S. Ellis, J. P. Hill, S. Wakimoto, R. J. Birgeneau, D. Casa, T. Gog, and Young-June Kim. Charge-transfer exciton in La_2CuO_4 probed with resonant inelastic x-ray scattering. *Physical Review B*, 77:060501, 2008.
- [42] V. J. Emery. Theory of high- T_c superconductivity in oxides. *Physical Review Letters*, 58:2794–2797, 1987.
- [43] Lei Zhang et. al. Correlated metals as transparent conductors. *Nature Physics*, 15:204–210, 2016.
- [44] M. Fabrizio. Kondo physics and the Mott transition. In E. Pavarini, E. Koch, D. Vollhardt, and A. Lichtenstein, editors, *The physics of correlated insulators, metals and superconductors*. Forschungszentrum Jülich GmbH, Institute for Advanced Simulation, 2017.
- [45] S. V. Faleev, M. van Schilfhaarde, and T. Kotani. All-electron self-consistent GW approximation: Application to Si, MnO, and NiO. *Physical Review Letters*, 93:126406, 2004.
- [46] A. L Fetter and J. D Walecka. *Quantum Theory of Many-Particle Systems*. Dover, Mineola, New York, 2003.
- [47] F. Freimuth, Y. Mokrousov, D. Wortmann, S. Heinze, and S. Blügel. Maximally localized Wannier functions within the FLAPW formalism. *Physical Review B*, 78:035120, 2008.
- [48] C. Friedrich, S. Blügel, and A. Schindlmayr. Efficient implementation of the GW approximation within the all-electron FLAPW method. *Physical Review B*, 81:125102, 2010.
- [49] A. Galler, P. Thunström, P. Gunacker, J. M. Tomczak, and K. Held. Ab initio dynamical vertex approximation. *Physical Review B*, 95:115107, 2017.
- [50] P. García-González and R. W. Godby. Self-consistent calculation of total energies of the electron gas using many-body perturbation theory. *Physical Review B*, 63:075112, 2001.
- [51] M. Gatti and M. Guzzo. Dynamical screening in correlated metals: Spectral properties of SrVO_3 in the GW approximation and beyond. *Physical Review B*, 87:155147, 2013.

- [52] A. Georges and G. Kotliar. Hubbard model in infinite dimensions. *Physical Review B*, 45:6479–6483, 1992.
- [53] A. Georges, G. Kotliar, W. Krauth, and M. J. Rozenberg. Dynamical mean-field theory of strongly correlated fermion systems and the limit of infinite dimensions. *Review of Modern Physics*, 68:13–125, 1996.
- [54] T. L. Gilbert. Hohenberg-Kohn theorem for nonlocal external potentials. *Physical Review B*, 12:2111–2120, 1975.
- [55] J. M. Ginder, M. G. Roe, Y. Song, R. P. McCall, J. R. Gaines, E. Ehrenfreund, and A. J. Epstein. Photoexcitations in La_2CuO_4 : 2-eV energy gap and long-lived defect states. *Physical Review B*, 37:7506–7509, 1988.
- [56] R. W. Godby, M. Schlüter, and L. J. Sham. Self-energy operators and exchange-correlation potentials in semiconductors. *Physical Review B*, 37:10159–10175, 1988.
- [57] J. E. Gubernatis, Mark Jarrell, R. N. Silver, and D. S. Sivia. Quantum Monte Carlo simulations and maximum entropy: Dynamics from imaginary-time data. *Physical Review B*, 44:6011–6029, 1991.
- [58] E. Gull, A. J. Millis, A. I. Lichtenstein, A. N. Rubtsov, M. Troyer, and P. Werner. Continuous-time Monte Carlo methods for quantum impurity models. *Review of Modern Physics*, vol. 83, Issue 2, pp. 349–404, 83:349–404, 2011.
- [59] O. Gunnarsson, E. Koch, and R. M. Martin. Mott transition in degenerate Hubbard models: Application to doped fullerenes. *Physical Review B*, 54:R11026–R11029, 1996.
- [60] M. Guzzo, G. Lani, F. Sottile, P. Romaniello, M. Gatti, J. J. Kas, J. J. Rehr, M. G. Silly, F. Sirotti, and L. Reining. Valence electron photoemission spectrum of semiconductors: Ab initio description of multiple satellites. *Physical Review Letters*, 107:166401, 2011.
- [61] H. Hafermann, P. Werner, and E. Gull. Efficient implementation of the continuous-time hybridization expansion quantum impurity solver. *Comput. Phys. Commun.*, 184:1280 – 1286, 2013.

- [62] J. E. Han, M. Jarrell, and D. L. Cox. Multiorbital Hubbard model in infinite dimensions: Quantum Monte Carlo calculation. *Physical Review B*, 58:R4199–R4202, 1998.
- [63] K. Haule, V. Oudovenko, S. Y. Savrasov, and G. Kotliar. The $\alpha \rightarrow \gamma$ transition in Ce: A theoretical view from optical spectroscopy. *Physical Review Letters*, 94:036401, 2005.
- [64] L. Hedin. New method for calculating the one-particle Green’s function with application to the electron-gas problem. *Physical Review*, 139:A796–A823, 1965.
- [65] L. Hedin. On correlation effects in electron spectroscopies and the GW approximation. *Journal of Physics: Condensed Matter*, 11:R489, 1999.
- [66] L. Hedin and J. D. Lee. Sudden approximation in photoemission and beyond. *Journal of electron spectroscopy and related phenomena*, 124:289–315, 2002.
- [67] K. Held. Electronic structure calculations using dynamical mean field theory. *Advances in Physics*, 56:829–926, 2007.
- [68] K. Held, A. K. McMahan, and R. T. Scalettar. Cerium volume collapse: Results from the merger of dynamical mean-field theory and local density approximation. *Physical Review Letters*, 87:276404, 2001.
- [69] K-H Hellwege and O. Madelung, editors. *Numerical Data and Functional Relationships in Science and Technology*. Landolt-Börnstein, New Series, Group III, Vols. 17a and 22a (Springer, Berlin), 1982.
- [70] J. F. Herbst and J. W. Wilkins. Chapter 68 calculation of 4f excitation energies in the metals and relevance to mixed valence systems. In *High Energy Spectroscopy*, volume 10 of *Handbook on the Physics and Chemistry of Rare Earths*, pages 321 – 360. Elsevier, 1987.
- [71] P. Hohenberg and W. Kohn. Inhomogeneous electron gas. *Physical Review*, 136:B864–B871, 1964.
- [72] B. Holm. Total energies from GW calculations. *Physical Review Letters*, 83:788, 1999.

- [73] B. Holm and U. von Barth. Fully self-consistent GW self-energy of the electron gas. *Physical Review B*, 57:2108–2117, 1998.
- [74] T. Holstein. Studies of polaron motion: Part i. the molecular-crystal model. *Annals of Physics*, 8:325–342, 1959.
- [75] L. Huang, T. Ayral, S. Biermann, and P. Werner. Extended dynamical mean-field study of the Hubbard model with long-range interactions. *Physical Review B*, 90:195114, 2014.
- [76] J. Hubbard. The description of collective motions in terms of many-body perturbation theory. *Proceedings of the Royal Society of London A*, 240:539–560, 1957.
- [77] J. Hubbard. Electron correlations in narrow energy bands. *Proceedings of the Royal Society of London A: Mathematical, Physical and Engineering Sciences*, 276:238–257, 1963.
- [78] M. S. Hybertsen and S. G. Louie. Electron correlation in semiconductors and insulators: Band gaps and quasiparticle energies. *Physical Review B*, 34:5390–5413, 1986.
- [79] E. Şaşıoğlu, C. Friedrich, and S. Blügel. Effective coulomb interaction in transition metals from constrained random-phase approximation. *Physical Review B*, 83:121101, 2011.
- [80] A. Ino, T. Mizokawa, K. Kobayashi, A. Fujimori, T. Sasagawa, T. Kimura, K. Kishio, K. Tamasaku, H. Eisaki, and S. Uchida. Doping dependent density of states and pseudogap behavior in $\text{La}_{2-x}\text{Sr}_x\text{CuO}_4$. *Physical Review Letters*, 81:2124–2127, 1998.
- [81] I. H. Inoue, O. Goto, H. Makino, N. E. Hussey, and M. Ishikawa. Bandwidth control in a perovskite-type $3d^1$ -correlated metal $\text{Ca}_{1-x}\text{Sr}_x\text{VO}_3$. i. evolution of the electronic properties and effective mass. *Physical Review B*, 58:4372–4383, 1998.
- [82] M. Jarrell. The maximum entropy method: Analytic continuation of qmc data. In E. Pavarini, E. Koch, F. Anders, and M. Jarrell, editors, *Correlated electrons: From models to materials*. Verlag des Forschungszentrum Julich, 2012.

- [83] M. Jarrell and J. E. Gubernatis. Bayesian inference and the analytic continuation of imaginary-time quantum Monte-Carlo data. *Physics Reports*, 269:133 – 195, 1996.
- [84] K. Karlsson. Self-consistent GW combined with single-site dynamical mean field theory for a Hubbard model. *Journal of Physics: Condensed Matter*, 17:7573, 2005.
- [85] K. Karlsson, F. Aryasetiawan, and O. Jepsen. Method for calculating the electronic structure of correlated materials from a truly first-principles LDA + U scheme. *Physical Review B*, 81:245113, 2010.
- [86] A. Koga, Y. Imai, and N. Kawakami. Stability of a metallic state in the two-orbital Hubbard model. *Physical Review B*, 66:165107, 2002.
- [87] W. Kohn. v -representability and density functional theory. *Physical Review Letters*, 51:1596–1598, 1983.
- [88] W. Kohn and L. J. Sham. Self-Consistent Equations Including Exchange and Correlation Effects. *Physical Review*, 140:A1133, 1965.
- [89] T. Kotani, M. van Schilfgaarde, and S. V. Faleev. Quasiparticle self-consistent GW method: A basis for the independent-particle approximation. *Physical Review B*, 76:165106, 2007.
- [90] G. Kotliar, S. Y. Savrasov, K. Haule, V. S. Oudovenko, O. Parcollet, and C. A. Marianetti. Electronic structure calculations with dynamical mean-field theory. *Review of Modern Physics*, 78:865–951, 2006.
- [91] P. Koval, D. Foerster, and D. Sánchez-Portal. Fully self-consistent GW and quasiparticle self-consistent GW for molecules. *Physical Review B*, 89:155417, 2014.
- [92] W. Ku and A. G. Eguiluz. Band-gap problem in semiconductors revisited: Effects of core states and many-body self-consistency. *Physical Review Letters*, 89:126401, 2002.
- [93] A. Kutepov, S. Y. Savrasov, and G. Kotliar. Ground-state properties of simple elements from GW calculations. *Physical Review B*, 80:041103, 2009.

- [94] N. Labhasetwar, G. Saravanan, S. Kumar Megarajan, N. Manwar, R. Khorragade, P. Doggali, and F. Grasset. Perovskite-type catalytic materials for environmental applications. *Science and Technology of Advanced Materials*, 16:036002, 2015.
- [95] L. D. Landau. The theory of a fermi liquid. *Soviet Physics JETP-USSR*, 3:920–925, 1957.
- [96] L. D. Landau. On the theory of the fermi liquid. *Soviet Physics JETP-USSR*, 8:70, 1959.
- [97] I. G. Lang and Yu A. Firsov. Kinetic theory of semiconductors with low mobility. *Soviet Physics JETP-USSR*, 16:1301, 1963.
- [98] F. Lechermann, A. Georges, A. Poteryaev, S. Biermann, M. Posternak, A. Yamasaki, and O. K. Andersen. Dynamical mean-field theory using Wannier functions: A flexible route to electronic structure calculations of strongly correlated materials. *Physical Review B*, 74:125120, 2006.
- [99] J. Lee and K. Haule. Diatomic molecule as a testbed for combining DMFT with electronic structure methods such as GW and DFT. *Physical Review B*, 95:155104, 2017.
- [100] M. Levy. Universal variational functionals of electron densities, first-order density matrices, and natural spin-orbitals and solution of the v-representability problem. *Proceedings of the National Academy of Sciences of the United States of America*, 76:6062–6065, 1979.
- [101] M. Levy. Electron densities in search of Hamiltonians. *Physical Review A*, 26:1200–1208, 1982.
- [102] M. Levy, J. P. Perdew, and V. Sahni. Exact differential equation for the density and ionization energy of a many-particle system. *Physical Review A*, 30:2745–2748, 1984.
- [103] A. I. Lichtenstein and M. I. Katsnelson. Ab initio calculations of quasiparticle band structure in correlated systems: LDA++ approach. *Physical Review B*, 57:6884–6895, 1998.
- [104] E. H. Lieb. Density functionals for Coulomb systems. In A Shimony and H Feshbach, editors, *Physics as Natural Philosophy*, page 111. MIT press Cambridge, 1982.

- [105] E. H. Lieb. Density functionals for Coulomb systems. *International Journal of Quantum Chemistry*, 24:243–277, 1983.
- [106] I. L. M. Locht. *Theoretical methods for the electronic structure and magnetism of strongly correlated materials*. PhD thesis, Uppsala University, Materials Theory, 2017.
- [107] J. P. Lu. Metal-insulator transitions in degenerate Hubbard models and A_xC_{60} . *Physical Review B*, 49:5687–5690, 1994.
- [108] T. Maier, M. Jarrell, T. Pruschke, and M. H. Hettler. Quantum cluster theories. *Review of Modern Physics*, 77:1027–1080, 2005.
- [109] N. Marom, F. Caruso, X. Ren, O. T. Hofmann, T. Körzdörfer, J. R. Chelikowsky, A. Rubio, M. Scheffler, and P. Rinke. Benchmark of GW methods for azabenzenes. *Physical Review B*, 86:245127, 2012.
- [110] N. Marzari and D. Vanderbilt. Maximally localized generalized Wannier functions for composite energy bands. *Physical Review B*, 56:12847–12865, 1997.
- [111] W. Metzner, M. Salmhofer, C. Honerkamp, V. Meden, and K. Schönhammer. Functional renormalization group approach to correlated fermion systems. *Review of Modern Physics*, 84:299–352, 2012.
- [112] W. Metzner and D. Vollhardt. Correlated lattice fermions in $d = \infty$ dimensions. *Physical Review Letters*, 62:324–327, 1989.
- [113] T. Miyake, F. Aryasetiawan, and M. Imada. Ab initio procedure for constructing effective models of correlated materials with entangled band structure. *Physical Review B*, 80:155134, 2009.
- [114] T. Miyake, C. Martins, R. Sakuma, and F. Aryasetiawan. Effects of momentum-dependent self-energy in the electronic structure of correlated materials. *Physical Review B*, 87:115110, 2013.
- [115] K. Morikawa, T. Mizokawa, K. Kobayashi, A. Fujimori, H. Eisaki, S. Uchida, F. Iga, and Y. Nishihara. Spectral weight transfer and mass renormalization in Mott-Hubbard systems $SrVO_3$ and $CaVO_3$: Influence of long-range Coulomb interaction. *Physical Review B*, 52:13711–13714, 1995.

- [116] A. A. Mostofi, J. R. Yates, Y-S Lee, I. Souza, D. Vanderbilt, and N. Marzari. Wannier90: A tool for obtaining maximally-localised Wannier functions . *Computer Physics Communications* , 178:685–699, 2008.
- [117] J. A. Moyer, C. Eaton, and R. Engel-Herbert. Highly conductive SrVO_3 as a bottom electrode for functional perovskite oxides. *Advanced Materials*, 25:3578–3582, 2013.
- [118] E. Müller-Hartmann. Correlated fermions on a lattice in high dimensions. *Zeitschrift für Physik B Condensed Matter*, 74:507–512, 1989.
- [119] E. Müller-Hartmann. The Hubbard model at high dimensions: some exact results and weak coupling theory. *Zeitschrift für Physik B Condensed Matter*, 76:211–217, 1989.
- [120] J. W. Negele and H. Orland. *Quantum Many-Particle Systems*. Advanced Book Classics. Westview Press, Boulder, CO, 1988.
- [121] I. A. Nekrasov, K. Held, G. Keller, D. E. Kondakov, Th. Pruschke, M. Kollar, O. K. Andersen, V. I. Anisimov, and D. Vollhardt. Momentum-resolved spectral functions of SrVO_3 calculated by LDA+DMFT. *Physical Review B*, 73:155112, 2006.
- [122] F. Nilsson, L. Boehnke, P. Werner, and F. Aryasetiawan. Multitier self-consistent GW+EDMFT. *Physical Review Materials*, 1:043803, 2017.
- [123] O. Parcollet, M. Ferrero, T. Ayrál, H. Hafermann, I. Krivenko, L. Messio, and P. Seth. TRIQS: a toolbox for research on interacting quantum systems. *Computer Physics Communications*, 196:398 – 415, 2015.
- [124] E. Pavarini, S. Biermann, A. Poteryaev, A. I. Lichtenstein, A. Georges, and O. K. Andersen. Mott Transition and Suppression of Orbital Fluctuations in Orthorhombic $3d^1$ Perovskites. *Physical Review Letters*, 92:176403, 2004.
- [125] D. Pines. *Elementary Excitations in Solids*. Lecture notes and supplements in physics. Benjamin, 1963.
- [126] D. Pines and D. Bohm. A collective description of electron interactions: II. collective vs individual particle aspects of the interactions. *Physical Review*, 85:338–353, 1952.

- [127] Th. Pruschke and R. Bulla. Hund’s coupling and the metal-insulator transition in the two-band Hubbard model. *The European Physical Journal B - Condensed Matter and Complex Systems*, 44:217–224, 2005.
- [128] T. Ribic, E. Assmann, A. Tóth, and K. Held. Cubic interaction parameters for t_{2g} Wannier orbitals. *Physical Review B*, 90:165105, 2014.
- [129] M. Rohlfing, P. Krüger, and J. Pollmann. Quasiparticle band-structure calculations for C, Si, Ge, GaAs, and SiC using Gaussian-orbital basis sets. *Physical Review B*, 48:17791–17805, 1993.
- [130] G. Rohringer, H. Hafermann, A. Toschi, A. A. Katanin, A. E. Antipov, M. I. Katsnelson, A. I. Lichtenstein, A. N. Rubtsov, and K. Held. Diagrammatic routes to nonlocal correlations beyond dynamical mean field theory. *Review of Modern Physics*, 90:025003, 2018.
- [131] C. Rostgaard, K. W. Jacobsen, and K. S. Thygesen. Fully self-consistent GW calculations for molecules. *Physical Review B*, 81:085103, 2010.
- [132] A. Rubio, J. L. Corkill, M. L. Cohen, E. L. Shirley, and S. G. Louie. Quasi-particle band structure of AlN and GaN. *Physical Review B*, 48:11810–11816, 1993.
- [133] A. N. Rubtsov, M. I. Katsnelson, and A. I. Lichtenstein. Dual fermion approach to nonlocal correlations in the hubbard model. *Physical Review B*, 77:033101, 2008.
- [134] A. N. Rubtsov, M. I. Katsnelson, and A. I. Lichtenstein. Dual boson approach to collective excitations in correlated fermionic systems. *Annals of Physics, Volume 327, Issue 5, p. 1320-1335.*, 327:1320–1335, 2012.
- [135] E. Runge and E. K. U. Gross. Density-functional theory for time-dependent systems. *Physical Review Letters*, 52:997–1000, 1984.
- [136] R. Sakuma. Symmetry-adapted Wannier functions in the maximal localization procedure. *Physical Review B*, 87:235109, 2013.
- [137] R. Sakuma, T. Miyake, and F. Aryasetiawan. Self-energy and spectral function of Ce within the GW approximation. *Physical Review B*, 86:245126, 2012.

- [I38] R. Sakuma, P. Werner, and F. Aryasetiawan. Electronic structure of SrVO_3 within GW+DMFT. *Physical Review B*, 88:235110, 2013.
- [I39] U. Schönberger and F. Aryasetiawan. Bulk and surface electronic structures of MgO . *Physical Review B*, 52:8788–8793, 1995.
- [I40] W-D Schöne and A. G. Eguiluz. Self-consistent calculations of quasiparticle states in metals and semiconductors. *Physical Review Letters*, 81:1662, 1998.
- [I41] M. Schüler, M. Rösner, T. O. Wehling, A. I. Lichtenstein, and M. I. Katsnelson. Optimal Hubbard models for materials with nonlocal coulomb interactions: Graphene, Silicene, and Benzene. *Physical Review Letters*, 111:036601, 2013.
- [I42] A. Sekiyama, H. Fujiwara, S. Imada, S. Suga, H. Eisaki, S. I. Uchida, K. Takegahara, H. Harima, Y. Saitoh, I. A. Nekrasov, G. Keller, D. E. Kondakov, A. V. Kozhevnikov, Th. Pruschke, K. Held, D. Vollhardt, and V. I. Anisimov. Mutual experimental and theoretical validation of bulk photoemission spectra of $\text{Sr}_{1-x}\text{Ca}_x\text{VO}_3$. *Physical Review Letters*, 93:156402, 2004.
- [I43] Zhi-xun Shen, J. W. Allen, J. J. Yeh, J. S. Kang, W. Ellis, W. Spicer, I. Lindau, M. B. Maple, Y. D. Dalichaouch, M. S. Torikachvili, J. Z. Sun, and T. H. Geballe. Anderson Hamiltonian description of the experimental electronic structure and magnetic interactions of copper-oxide superconductors. *Physical Review B*, 36:8414–8428, 1987.
- [I44] Q. Si and J. L. Smith. Kosterlitz-thouless transition and short range spatial correlations in an extended Hubbard model. *Physical Review Letters*, 77:3391–3394, 1996.
- [I45] M. Sing. Introduction to photoemission spectroscopy. In E. Pavarini, E. Koch, D. Vollhardt, and A. Lichtenstein, editors, *DMFT at 25: Infinite Dimensions*, pages 14.2–14.17. Forschungszentrum Jülich GmbH, Institute for Advanced Simulation, 2014.
- [I46] T. J. Sjöstrand, F. Nilsson, and F. Aryasetiawan. Position representation of effective electron-electron interactions in solids. *To be published*, 2018.
- [I47] J. Skilling. Classic maximum entropy. In J. Skilling, editor, *Maximum Entropy and Bayesian Methods*. Kluwer Academic, Dordrecht, 1989.

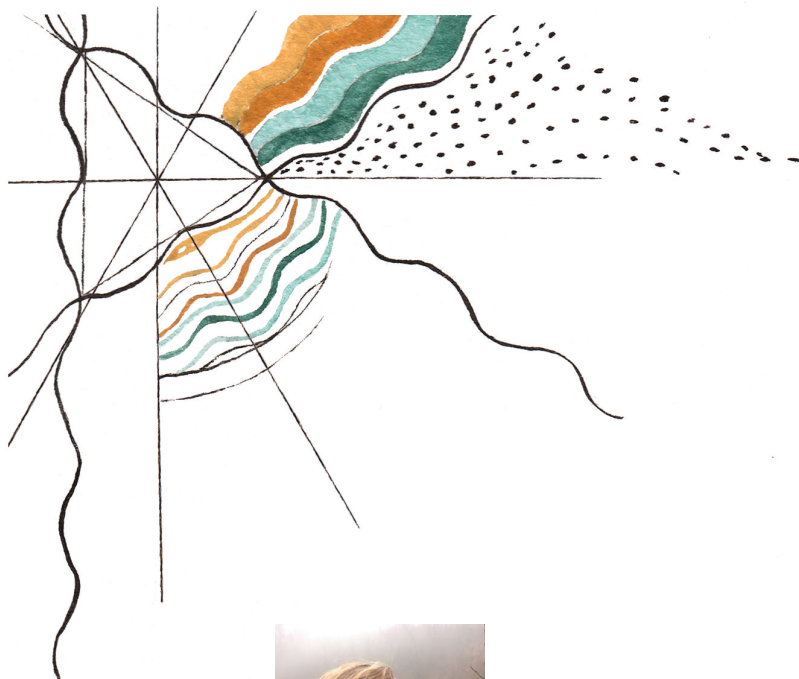
- [148] J. C. Slater. Magnetic effects and the Hartree-Fock equation. *Physical Review*, 82:538–541, 1951.
- [149] J. C. Slater. A simplification of the Hartree-Fock method. *Physical Review*, 81:385–390, 1951.
- [150] J. C. Slater. A generalized self-consistent field method. *Physical Review*, 91:528–530, 1953.
- [151] James Slezak. Cornell Laboratory of Atomic and Solid State Physics (https://commons.wikimedia.org/wiki/File:BI2223-piece3_001.jpg), „BI2223-piece3_001“, <https://creativecommons.org/licenses/by-sa/3.0/legalcode>.
- [152] J. L. Smith and Q. Si. Spatial correlations in dynamical mean-field theory. *Physical Review B*, 61:5184–5193, 2000.
- [153] I. Souza, N. Marzari, and D. Vanderbilt. Maximally localized Wannier functions for entangled energy bands. *Physical Review B*, 65:035109, 2001.
- [154] A. Stan, N. E. Dahlen, and R. van Leeuwen. Fully self-consistent GW calculations for atoms and molecules. *Europhysics Letters*, 76:298, 2006.
- [155] A. Stan, N. E. Dahlen, and R. Van Leeuwen. Levels of self-consistency in the GW approximation. *The Journal of Chemical Physics*, 130:114105, 2009.
- [156] E. A. Stepanov, A. Huber, E. G. C. P. van Loon, A. I. Lichtenstein, and M. I. Katsnelson. From local to nonlocal correlations: The dual boson perspective. *Physical Review B*, 94:205110, 2016.
- [157] E. A. Stepanov, E. G. C. P. van Loon, A. A. Katanin, A. I. Lichtenstein, M. I. Katsnelson, and A. N. Rubtsov. Self-consistent dual boson approach to single-particle and collective excitations in correlated systems. *Physical Review B*, 93:045107, 2016.
- [158] M. Stone. *The Physics of Quantum Fields*. Springer-Verlag, New York, 2000.
- [159] P. Sun and G. Kotliar. Extended dynamical mean-field theory and GW method. *Physical Review B*, 66:085120, 2002.

- [160] M. Takizawa, M. Minohara, H. Kumigashira, D. Toyota, M. Oshima, H. Wadati, T. Yoshida, A. Fujimori, M. Lippmaa, M. Kawasaki, H. Koinuma, G. Sordi, and M. Rozenberg. Coherent and incoherent d -band dispersions in SrVO_3 . *Physical Review B*, 80:235104, 2009.
- [161] D. Tamme, R. Schepe, and K. Henneberger. Comment on “Self-Consistent calculations of quasiparticle states in metals and semiconductors”. *Physical Review Letters*, 83:241, 1999.
- [162] C. Taranto, S. Andergassen, J. Bauer, K. Held, A. Katanin, W. Metzner, G. Rohringer, and A. Toschi. From infinite to two dimensions through the functional renormalization group. *Physical Review Letters*, 112:196402, 2014.
- [163] C. Taranto, M. Kaltak, N. Parragh, G. Sangiovanni, G. Kresse, A. Toschi, and K. Held. Comparing quasiparticle GW+DMFT and LDA+DMFT for the test bed material SrVO_3 . *Physical Review B*, 88:165119, 2013.
- [164] The FLEUR group. The FLEUR project. <http://www.flapw.de>.
- [165] Y. Tokura, S. Koshihara, T. Arima, H. Takagi, S. Ishibashi, T. Ido, and S. Uchida. Cu-O network dependence of optical charge-transfer gaps and spin-pair excitations in single- CuO_2 -layer compounds. *Physical Review B*, 41:11657–11660, 1990.
- [166] J. M. Tomczak, M. Casula, T. Miyake, F. Aryasetiawan, and S. Biermann. Combined GW and dynamical mean-field theory: Dynamical screening effects in transition metal oxides. *Europhysics Letters*, 100:67001, 2012.
- [167] J. M. Tomczak, M. Casula, T. Miyake, and S. Biermann. Asymmetry in band widening and quasiparticle lifetimes in SrVO_3 : Competition between screened exchange and local correlations from combined GW and dynamical mean-field theory GW+DMFT. *Physical Review B*, 90:165138, 2014.
- [168] A. Toschi, A. A. Katanin, and K. Held. Dynamical vertex approximation: A step beyond dynamical mean-field theory. *Physical Review B*, 75:045118, 2007.
- [169] A. Toschi, G. Rohringer, A.A. Katanin, and K. Held. Ab initio calculations with the dynamical vertex approximation. *Annalen der Physik*, 523:698–705, 2011.

- [170] R. van Leeuwen. Density functional approach to the many-body problem: key concepts and exact functionals. *Advances in Quantum Chemistry*, 43:25–94, 2003.
- [171] E. G. C. P. van Loon, F. Krien, H. Hafermann, E. A. Stepanov, A. I. Lichtenstein, and M. I. Katsnelson. Double occupancy in dynamical mean-field theory and the dual boson approach. *Physical Review B*, 93:155162, 2016.
- [172] A. van Roekeghem, T. Ayrál, J. M. Tomczak, M. Casula, N. Xu, H. Ding, M. Ferrero, O. Parcollet, H. Jiang, and S. Biermann. Dynamical correlations and screened exchange on the experimental bench: Spectral properties of the cobalt pnictide BaCo_2As_2 . *Physical Review Letters*, 113:266403, 2014.
- [173] A. van Roekeghem and S. Biermann. Screened exchange dynamical mean-field theory and its relation to density functional theory: SrVO_3 and SrTiO_3 . *EPL (Europhysics Letters)*, 108:57003, 2014.
- [174] M. van Schilfgaarde, T. Kotani, and S. Faleev. Quasiparticle self-consistent GW theory. *Physical Review Letters*, 96:226402, 2006.
- [175] H. J. Vidberg and J. W. Serene. Solving the Eliashberg equations by means of N-point Padé approximants. *Journal of Low Temperature Physics*, 29:179–192, 1977.
- [176] U. von Barth and L. Hedin. A local exchange-correlation potential for the spin polarized case. i. *Journal of Physics C: Solid State Physics*, 5:1629, 1972.
- [177] W. von der Linden, E. Berger, and P. Valášek. The hubbard-holstein model. *Journal of Low Temperature Physics*, 99:517–525, 1995.
- [178] J. Vučičević, T. Ayrál, and O. Parcollet. TRILEX and GW+EDMFT approach to *d*-wave superconductivity in the Hubbard model. *Physical Review B*, 96:104504, 2017.
- [179] H. Wadati, J. Mravlje, K. Yoshimatsu, H. Kumigashira, M. Oshima, T. Sugiyama, E. Ikenaga, A. Fujimori, A. Georges, A. Radetnac, K. S. Takahashi, M. Kawasaki, and Y. Tokura. Photoemission and DMFT study of electronic correlations in SrMoO_3 : Effects of Hund’s rule coupling and possible plasmonic sideband. *Physical Review B*, 90:205131, 2014.

- [180] C. Weber, K. Haule, and G. Kotliar. Optical weights and waterfalls in doped charge-transfer insulators: A local density approximation and dynamical mean-field theory study of $\text{La}_{2-x}\text{Sr}_x\text{CuO}_4$. *Physical Review B*, 78:134519, 2008.
- [181] C. Weber, C. Yee, K. Haule, and G. Kotliar. Scaling of the transition temperature of hole-doped cuprate superconductors with the charge-transfer energy. *EPL (Europhysics Letters)*, 100:37001, 2012.
- [182] P. Werner and M. Casula. Dynamical screening in correlated electron systems—from lattice models to realistic materials. *Journal of Physics: Condensed Matter*, 28:383001, 2016.
- [183] P. Werner, M. Casula, T. Miyake, F. Aryasetiawan, A. J. Millis, and S. Biermann. Satellites and large doping and temperature dependence of electronic properties in hole-doped BaFe_2As_2 . *Nature Physics*, 8:331–337, 2012.
- [184] P. Werner, A. Comanac, L. de’ Medici, M. Troyer, and A. J. Millis. Continuous-time solver for quantum impurity models. *Physical Review Letters*, 97:076405, 2006.
- [185] P. Werner and A. J. Millis. Hybridization expansion impurity solver: General formulation and application to kondo lattice and two-orbital models. *Physical Review B*, 74:155107, 2006.
- [186] P. Werner and A. J. Millis. Efficient dynamical mean field simulation of the Holstein-Hubbard model. *Physical Review Letters*, 99:146404, 2007.
- [187] P. Werner and A. J. Millis. High-spin to low-spin and orbital polarization transitions in multiorbital mott systems. *Physical Review Letters*, 99:126405, 2007.
- [188] P. Werner and A. J. Millis. Dynamical screening in correlated electron materials. *Physical Review Letters*, 104:146401, 2010.
- [189] P. Werner, R. Sakuma, F. Nilsson, and F. Aryasetiawan. Dynamical screening in La_2CuO_4 . *Physical Review B*, 91:125142, 2015.
- [190] R. C. Whited, C. J. Flaten, and W. C. Walker. Exciton thermorefectance of MgO and CaO . *Solid State Communications*, 13:1903 – 1905, 1973.

- [191] T. Yoshida, M. Hashimoto, T. Takizawa, A. Fujimori, M. Kubota, K. Ono, and H. Eisaki. Mass renormalization in the bandwidth-controlled Mott-Hubbard systems SrVO_3 and CaVO_3 studied by angle-resolved photoemission spectroscopy. *Physical Review B*, 82:085119, 2010.
- [192] O. Zakharov, A. Rubio, X. Blase, M. L. Cohen, and S. G. Louie. Quasi-particle band structures of six II-VI compounds: ZnS , ZnSe , ZnTe , CdS , CdSe , and CdTe . *Physical Review B*, 50:10780–10787, 1994.
- [193] F. C. Zhang and T. M. Rice. Effective Hamiltonian for the superconducting Cu oxides. *Physical Review B*, 37:3759–3761, 1988.
- [194] Z. Zhong, M. Wallerberger, J. M. Tomczak, C. Taranto, N. Parragh, A. Toschi, G. Sangiovanni, and K. Held. Electronics with correlated oxides: $\text{SrVO}_3/\text{SrTiO}_3$ as a Mott transistor. *Physical Review Letters*, 114:246401, 2015.
- [195] X. Zhu and S. G. Louie. Quasiparticle band structure of thirteen semiconductors and insulators. *Physical Review B*, 43:14142–14156, 1991.
- [196] M. B. Zöhlfl, I. A. Nekrasov, Th. Pruschke, V. I. Anisimov, and J. Keller. Spectral and magnetic properties of α - and γ -Ce from dynamical mean-field theory and local density approximation. *Physical Review Letters*, 87:276403, 2001.
- [197] E. Zurek, O. Jepsen, and O. K. Andersen. Muffin-tin orbital Wannier-like functions for insulators and metals. *ChemPhysChem*, 6:1934–1942, 2005.



This is a thesis about electrons in solids and how to describe the electronic structure of materials with strong electron-electron correlations without adjustable parameters.

The work was performed at the Division of Mathematical Physics at Lund University and defended the 30:th of January 2019.



Lund University
Faculty of Science
Department of Physics
Division of Mathematical Physics
ISBN 978-91-7753-918-6

